UNIVERSITÀ POLITECNICA DELLE MARCHE

FACULTY OF ENGINEERING

Master's Degree course in **Environmental Engineering**

The effects of downstream boundary conditions on the hydraulic modelling of the flooding of estuarine cities: the Misa River (Senigallia, Italy)

Supervisor:

Prof. **Matteo Postacchini**

Candidate:

Yohannes Aklil Getachew

Co-supervisor

Dr. **Eleonora Perugini**

A.Y. 2025/2026

Contents

Abstract

This thesis investigates the influence of downstream boundary conditions on the hydraulic modelling of flood events in estuarine environments, with specific reference to the Misa River (Italy). Estuarine systems are governed by the interaction between fluvial discharge and marine forcing, which jointly control hydrodynamics, sediment transport, and erosion processes, particularly in the vicinity of hydraulic structures. The study focuses on the downstream reach of the river, where tidal dynamics play a key role in modulating flow behaviour. A one-dimensional hydraulic model was developed using HEC-RAS and calibrated against observed hydrometric and tidal data. A total of 26 numerical simulations were carried out, including 18 steady-state scenarios and 8 unsteady scenarios based on different combinations of upstream flood hydrographs and downstream tidal boundary conditions. The results show that, while tidal influence on water levels is limited during the most intense flood events, it significantly affects flow velocities in the downstream reach. In particular, low-tide conditions enhance flow velocities near the river mouth, increasing the potential for local erosion around bridge structures. Velocity variations associated with flood and ebb tidal phases are also evident under moderate flow conditions. These findings indicate that intermediate discharge events, often neglected in flood assessments, can play a critical role in sediment dynamics and local erosion when combined with unfavourable tidal conditions. Overall, the study highlights the importance of accurately representing downstream boundary conditions in hydraulic models of estuarine systems, even in microtidal environments. The results contribute to a better understanding of river–sea interactions and support improved flood risk assessment and management. Future work should consider fully coupled hydromorphodynamic modelling approaches to capture the feedback between flow and sediment processes.

1. Introduction

Hydraulic modelling is widely used to analyse river flow behaviour and flood propagation under different hydraulic conditions. In estuarine environments, water levels are influenced not only by upstream forcing but also by downstream conditions at the river mouth, where tidal dynamics and sea-level variations play a crucial role in controlling the hydraulic response of the system.

The transition zone between the river channel and the coastal area is a highly complex setting in which multiple hydrodynamic processes coexist and interact. In these areas, the interaction between river discharge and marine forcing can significantly exacerbate flooding, particularly in urbanised estuarine regions. Recent studies have highlighted the increasing relevance of compound flooding, where extreme rainfall events coincide with high tides or storm surges, producing impacts greater than the sum of individual contributions (Camus et al., 2021).

In addition to large-scale processes, local hydraulic conditions can be strongly influenced by the presence of infrastructures such as bridges. Bridge piers interact with the flow, modifying velocity and water depth and promoting local scour and sediment transport processes (Postacchini et al., 2023). In estuarine reaches, tidal oscillations generate bidirectional currents that further complicate flow patterns around bridge structures, especially near the river mouth. Under extreme conditions, water levels may approach bridge deck elevations, increasing the likelihood of pressurised flow and potential structural vulnerability (Carnacina et al., 2019).

In this context, the evolution of water levels along the river depends not only on upstream conditions but also on downstream boundary conditions imposed by tidal dynamics. Different tidal states at the river mouth can significantly modify water levels along the downstream reach, influencing flood propagation and hydraulic behaviour. These effects may extend several kilometres upstream due to long-wave propagation, even in microtidal environments. Despite their importance, the role of downstream boundary conditions in estuarine urban rivers remains relatively understudied (Gaiolini et al., 2023).

The Misa River, which flows through the city of Senigallia before discharging into the Adriatic Sea, represents a typical example of such a system, where the interaction between river discharge, tidal forcing, and urban infrastructure plays a key role in determining hydraulic conditions along the downstream reach.

In this framework, hydraulic simulations were carried out using the HEC-RAS software, one of the most widely used tools for river analysis. A series of numerical simulations was performed by combining upstream water-level hydrographs with different downstream boundary conditions representing tidal variability.

The aim of this study is to evaluate how different downstream boundary conditions influence the hydraulic modelling of flood events in an estuarine urban river system. Particular attention is given to selected cross-sections located upstream of bridge structures, in order to assess how variations in downstream forcing affect local hydraulic conditions in the presence of bridge piers. By analysing variations in water levels, flow depth, and velocity along the river, this work contributes to a better understanding of river–sea interactions and supports more reliable hydraulic modelling approaches for flood risk assessment.

The thesis is organised as follows: after the Introduction and the theoretical background, Chapter 3 describes the study area. Chapter 4 presents the materials and methods adopted in the study, including the modelling approach and data processing. Chapter 5 presents the results of the hydraulic simulations, while Chapter 6 provides a discussion and interpretation of the results. Finally, Chapter 7 summarises the main outcomes of the work and highlights the key conclusions.

2. Theoretical Background

The hydraulic behaviour of estuarine rivers results from the interaction between fluvial and marine processes. River discharge, tidal oscillations, channel morphology, and hydraulic structures jointly influence water levels, flow velocities, sediment transport, and flood propagation within the downstream reach of a river. Understanding these processes is essential for analysing the effects of downstream boundary conditions on river hydraulics and for interpreting the response of estuarine systems under different hydrological and tidal scenarios.

Since the present study focuses on the influence of downstream boundary conditions on the hydraulic behaviour of the Misa River estuary, this chapter presents the theoretical concepts relevant to the analysis. Particular attention is given to estuarine hydraulics and to the influence of bridge structures on flow dynamics, as these elements play a fundamental role in the propagation of water levels and velocities within the study reach.

2.1. Estuarine hydraulics

In coastal environments, two main types of river mouths can be identified, depending on how the river interacts with the sea: estuaries and deltas. Focusing on the former, an estuary can be defined as “a partially enclosed coastal body of brackish water with one or more rivers or streams flowing into it, and with a free connection to the open sea” (Pritchard, D. W. 1967). Figure 1 shows an example of such a system, namely the Misa River estuary.

Figure 1. The Misa River estuary top view

Estuarine environments are dynamically complex, with the hydrodynamics being triggered by many factors, such as nonlinear interactions between the bathymetry, the river current and many sea forcing actions. The sediment transport and related morphodynamics derives from such complexity and act in the estuarine region by shaping the riverbed and sometimes leading to interesting morphological features, like river mouth bars that, after being generated, migrate and evolve in proximity of the river mouth (Baldoni et al., 2021).

2.1.1. Types of Estuaries

Estuaries can be classified based on the balance between river discharge and tidal forcing. In "salt-wedge estuaries", river flow is dominant and a clear stratification between freshwater and seawater is maintained. In contrast, "well-mixed estuaries" are characterised by strong tidal action, leading to a nearly uniform vertical structure. Between these two conditions, partially "mixed estuaries" exhibit intermediate behaviour, where both stratification and mixing processes are relevant (Valle-Levinson, 2011).

This classification is not fixed, as estuarine conditions may vary over time depending on seasonal changes in river discharge and tidal intensity.

In addition, estuaries can be classified according to tidal range as micro-tidal (less than 2 m), meso-tidal (2–4 m), and macro-tidal (greater than 4 m). In Mediterranean environments, micro-tidal estuaries are the most common and are generally characterised by limited tidal influence and longer water residence times (Postacchini et al., 2023).

2.1.2. Circulation Patterns

The hydrodynamics of estuaries are governed by the interaction between freshwater inflow and saline water intrusion. A typical feature is the development of a two-layer circulation pattern, where freshwater flows seaward near the surface, while denser seawater moves landward along the bed, as illustrated in Figure 2.

This circulation is influenced by several factors, including river discharge, tidal forcing, and channel geometry, and can vary significantly over time. Under strong tidal conditions, vertical mixing increases and the flow tends to become more homogeneous. Conversely, when river discharge dominates, stratification becomes more pronounced, with a clearer separation between freshwater and seawater layers.

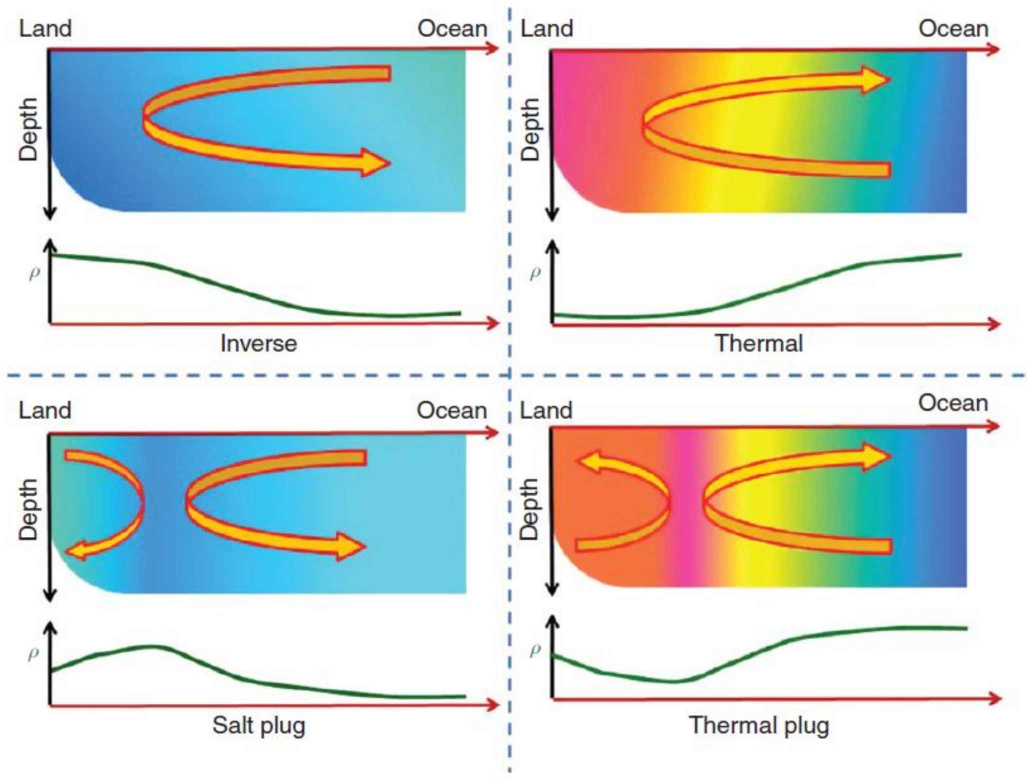

Figure 2. Types of estuaries according to their water balance (low-inflow estuaries). (Valle-Levinson, 2011)

Figure 2 shows four circulation patterns that may develop in low-inflow estuaries. In an inverse estuary, evaporation exceeds freshwater inflow, leading to increasing salinity toward the upstream reach and generating a circulation pattern opposite to that of a classical estuary. A thermal estuary develops when density gradients are controlled mainly by temperature differences rather than salinity variations. In salt-plug estuaries, a salinity maximum forms within the central part of the basin, modifying water exchange and circulation patterns. Similarly, thermal-plug estuaries are characterised by a temperature-induced density maximum that affects mixing and flow circulation. These examples illustrate how different density gradients can generate distinct circulation regimes within estuarine environments (Valle-Levinson, 2011).

2.2. Bridge Influence on Estuarine Flow

Bridges located within estuarine reaches, such as those in the final urban stretch of the Misa River, introduce significant hydraulic vulnerabilities. Unlike inland crossings, these structures are subjected to combined forcing from upstream river discharge and downstream tidal oscillations, resulting in highly variable hydraulic conditions.

The interaction between bridge piers and these complex flow conditions alter local velocities and water depths. As illustrated in the plan view (Figure 3), the presence of piers and abutments induces a contraction of the flow area, forcing streamlines to converge. This constriction leads to increased velocities and turbulence, enhancing sediment transport processes and promoting the development of local scour around bridge foundations (Lu et al., 2004).

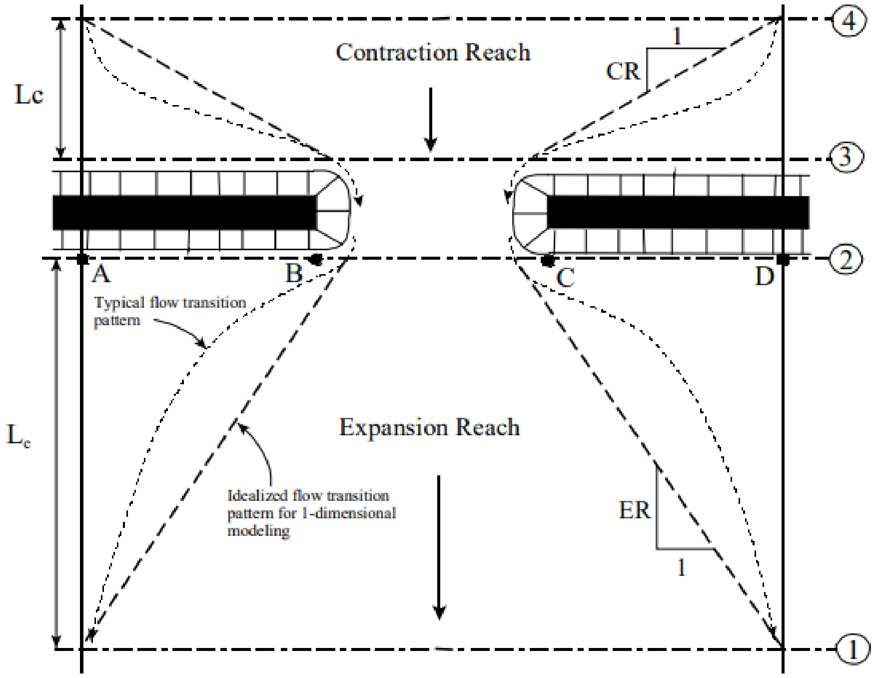

Figure 3. Contraction and expansion of the flow area through a bridge opening. Source: USACE (2020)

In HEC-RAS bridge modelling, a series of cross-sections is typically used to represent the hydraulic transition through a bridge opening. As shown in Figure 4, the longitudinal profile includes four cross-sections that define the contraction and expansion reaches associated with the structure. The bridge cross-section is positioned on the natural ground profile, while ineffective flow areas may be specified near the bridge abutments under low-flow conditions. These elements allow the hydraulic effects of bridge crossings, including flow contraction, expansion, and the associated energy losses, to be represented correctly (USACE, 2020).

In addition to horizontal flow contraction, the hydraulic response is also evident in the longitudinal water surface profile. Energy losses associated with the bridge structure generate an upstream increase in water level , modifying the flow regime across the structure. In estuarine environments, this effect is further complicated by tidal forcing. The alternation of flow direction produces unsteady and bidirectional currents, which influence both contraction and expansion processes near the bridge.

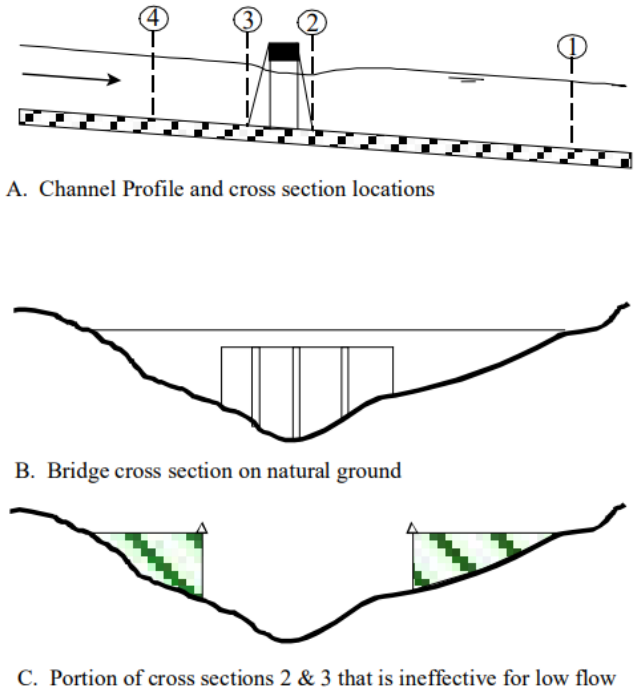

Figure 4. Cross section near Bridges

Under high tide conditions, the downstream boundary may limit the expansion of flow, amplifying backwater effects and increasing upstream water levels. In extreme events, water levels may approach the bridge deck, potentially leading to pressurised flow conditions. These conditions significantly increase hydraulic loads on the structure and represent a critical factor in flood risk, particularly in urban areas such as Senigallia (Carnacina et al., 2019).

In addition to the increase in water levels, bridge crossings are often affected by local scour processes generated by the interaction between the flow and structural elements such as piers and abutments. The acceleration of the flow around these obstacles increases bed shear stresses and promotes sediment removal from the riverbed, potentially compromising foundation stability. Hydraulic loads acting on bridge components are also influenced by variations in water depth and flow velocity, particularly during flood events. In estuarine environments, where river discharge and tidal forcing interact, the combined effects of changing water levels and flow velocities may further modify local scour potential and the hydraulic loading conditions around bridge structures (Carnacina et al., 2019).

3. Description of the study area

The Misa River, approximately 45 km long, is entirely located within the Province of Ancona. Its catchment covers an area of about 383 km², with estimated discharges of approximately 400, 450, and 600 m³/s associated with return periods of 100, 200, and 500 years, respectively (Brocchini et al., 2017).

The Misa River flows into the Adriatic Sea through the city of Senigallia and forms an estuarine environment that, according to the circulation classification described in the previous section, can be considered a salt-wedge estuary. The geographical location of the Misa River within the Marche Region and its position in central Italy are shown in Figure 5.

Figure 5. Location of the Misa River within the Marche Region, Italy. Source: adapted from Ilari (2020/2021)

The Misa River catchment is shown in Figure 6. The basin is bounded by the Cesano watershed to the north-west, the Esino River watershed to the south-east, and the Sentino sub-basin to the south. The watershed is characterised by a predominantly hilly morphology and drains toward the Adriatic Sea through the urban area of Senigallia.

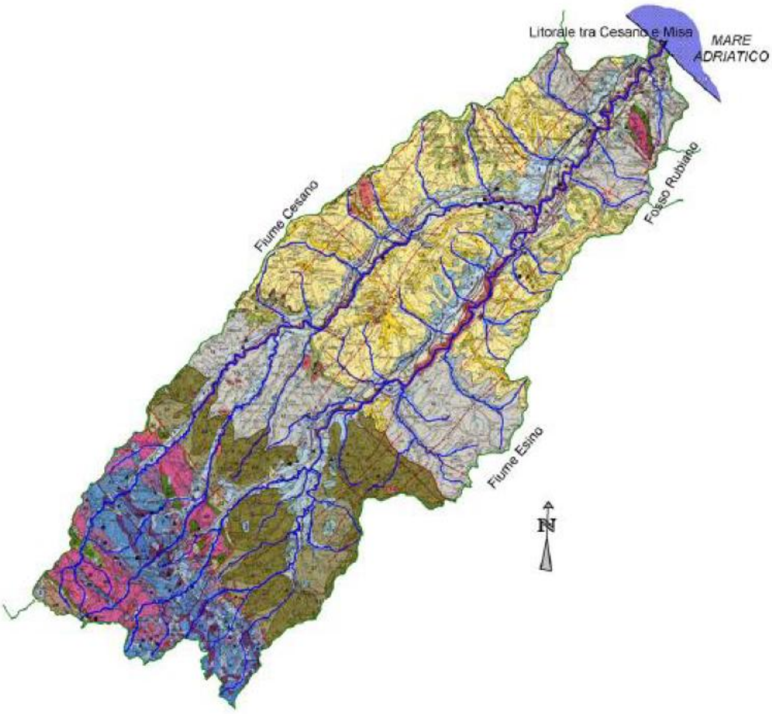

Figure 6. Misa River catchment and watershed boundaries. Source: adapted from Ilari (2020/2021)

The Misa River watershed is enclosed between the following municipalities: Arcevia, Barbara, Belvedere Ostrense, Castelleone di Suasa, Corinaldo, Genga, Mergo, Montecarotto, Ostra, Ostra Vetere, Poggio San Marcello, Rosora, Sassoferrato, Senigallia, Serra dei Conti, Serra San Quirico, Trecastelli (Castelcolonna and Ripe).

The Misa River, of Apennine origin, rises on the south-west slopes of the Arcevia's anticlinal, more precisely in Colle Ameno (793 m.a.s.l.) close to San Donnino village in Genga municipality. It travels through Genga, Arcevia, Serra De'Conti, Ostra Vetere, Ostra and lastly Senigallia in SW-NE direction, and flows into the Adriatic Sea within an estuary bounded by two reinforced concrete jetties, which stick out on the shoreline longitudinal profile for about 250 – 300 m.

The main Misa River left tributary is the Nevola River, which, in turn, generates from the confluence between the Fenella stream and the Acquaviva one, and joins the Misa River at about 9 km before its end, thus ensuring a remarkable increase of both solid and liquid flows. The Nevola River, along with the Acquaviva stream, point in the same direction as the Misa River (SW-NE) (Regione Marche, 2016).

The Misa River, as the vast majority of the Marche Region rivers, is characterized by a torrential regime, i.e. with poor or null flows during dry periods and very high flows (in the order of magnitude of hundreds of cubic meters per second) during rainy periods depending on the geological, geomorphological, lithological and climatic characteristics of the watershed. The Misa River basin is composed of around 85% of clayey rocks, thus owning a low permeability degree, whereas, for what concerns the most inner area, is made up of calcareous rocks having a secondary permeability deriving from the rocks fracturing. This lithology leads to a fairly high runoff coefficient, from which the poor subsoil infiltration derives from and that allows for very fast meteoric water discharges along the slopes and relatively short times of concentration (Regione Marche, 2016).

The natural Misa River, at times, is characterized by a meander-like shape flow path and it is strongly influenced by a remarkable number of anthropic structures, in particular by several roads which cross the river channel transversally. Moreover, the Misa River is also crossed by numerous transversals and longitudinal river bank protections. For what concerns the former, they include 23 bridles and 2 traverses, the vast majority of whom are located upstream of Pianello di Ostra, thus implying a strong vertical erosion. As regards the latter, they consist of 2,337 m of protecting walls (including stone gabions, concrete cubes, concrete slabs, reinforced concrete Jersey barriers), 318 m of bank strengthening using soft approaching (bioengineering) and 403 m of cliffs (gigantic calcareous boulders, concrete hexapods and tetrapod) (Regione Marche, 2016).

The Misa River hydrographic basin is significantly asymmetric, and the left tributaries, which are more developed than the right ones, predominantly participate to the river discharge.

The geomorphology of the watershed is characterized by narrow and deep valleys in the upstream sections of the river and by an enlargement of the latter moving downstream where there is also the presence of alluvial terraces. Also in this case, the alluvial terraces are greatly developed on the hydrographic left than on the hydrographic right.

The Misa River features a riverbed which flows within its own terraces that are characterized by different width and order. From a geological-sedimentological point of view, the alluvial terraces in the middle section of the catchment are made of gravel and calcareous boulders intertwined with gravelly-sandy lenses. On the other side, for what regards the alluvial deposits, they are characterized by an increased clayey fraction (Regione Marche, 2016).

At its mouth, the Misa River interacts with the Adriatic Sea, where both tidal and wave forcing contribute to the hydrodynamic behaviour of the estuarine area. The coastal environment is characterised by a microtidal regime, with relatively limited tidal amplitudes compared to oceanic coasts. Nevertheless, tidal oscillations can influence water levels in the downstream river reach, particularly during moderate-flow conditions. In addition, wave action generated within the Adriatic basin may affect the river mouth, especially during storm events. The combined action of river discharge, tides, and waves plays an important role in controlling water circulation and sediment dynamics within the estuarine environment (Melito et al., 2020).

4. Materials and Methods

The analysis carried out in the present work is divided into three main phases.

The first phase was focused on the collection and analysis of hydrometric and tidal data of the Misa River. Upstream water level data were obtained from the Bettolelle station through the SIRMIP system, while downstream tidal levels were derived from the tide gauge located at Ancona harbour, managed by ISPRA. These datasets were processed to define the boundary conditions of the hydraulic model, including both time-dependent series and representative constant values.

This is followed by the implementation of the data in an existing hydraulic model developed in HEC-RAS for the study reach. The model geometry and parameters were retained, while the boundary conditions were updated according to the selected datasets. A set of simulations was defined under both unsteady and steady flow conditions. Unsteady simulations were carried out by imposing time-varying downstream tidal levels (max high tide, max low tide, min high tide, min low tide), whereas steady simulations were performed using constant downstream water levels representative of characteristic hydraulic conditions.

Finally, the results of the hydraulic simulations were analysed with particular attention to the downstream reach of the river. Three specific bridge locations, namely Ponte Garibaldi, Ponte II. Giugno, and Ponte Statale, were selected due to their relevance in influencing local hydraulic conditions. For each bridge, a monitoring cross-section was defined upstream in order to evaluate variations in water depth and flow velocity under different boundary condition scenarios. The results were then compared to assess the influence of downstream forcing on the hydraulic behaviour of the system.

4.1. Available data

4.1.1. Hydrometric data acquisition

The SIRMIP (Sistema Informativo Regionale Meteo-Idro-Pluviometrico) is a database belonging to the Centro Funzionale Multirischi of the Civil Protection of the Marche Region, where it is possible to have access to different hydro-meteorological data, including hydrometry, pressure, precipitation, humidity, temperature, snow, solar radiation and wind data. The main interface of the platform is shown in Figure 7.

Figure 7. SIRMIP website main window

These data, which were originally managed by the Servizio Idrografico e Mareografico Nazionale (SIMN) and only later by the Civil Protection (2002), are based on two distinct networks, a mechanical and a telemetric one.

The mechanical network was developed by the SIMN in the 1916 and owned thermometers, pluviometers and hydrometers as sensors. Further, when these tasks were addressed to the Civil Protection, 21 thermometers and 83 pluviometers were in operation.

For what concerns the telemetric network, following the strengthening program for the weather, hydro, pluviometric monitoring stations, the Marche Region were equipped with a telemetric monitoring system, consisting of 53 thermometers, 77 pluviometers, 13 anemometers, 15 barometers, 30 hygrometers, 7 snow-meters and 70 hydrometers along with a hydrometric rod for the calibration measures. In January 2019 the telemetric network fully replaced the mechanical one and both the number and the types of the sensor increased. Since the 2005, on some hydrometric stations, the discharges are continuously estimated.

Through the use of this database, the data for the hydraulic analysis of the Misa River have been downloaded: in particular, data of the hydrometric level and relative rating curves have been selected and organized in excel files.

The stations selected for this work are displayed in Figure 8. As shown in Figure 9, on the SIRMIP website, there is the possibility of choosing either the basin and/or the province and/or the municipality where the data acquisition is required. Subsequently, it is possible to select the needed sensors (the place of the stations) together with the type of data to download. In particular, the data that have been downloaded are those regarding the stage, the rating curves, the coordinates of the stations and the hydrological characteristics, which can be directly downloaded in both text and excel format, depending on their availability.

Figure 8. Location of Bettolelle (RG2) and Ponte Garibaldi (RG1) hydrometric stations within the Misa River (adapted from Melito et al., 2020)

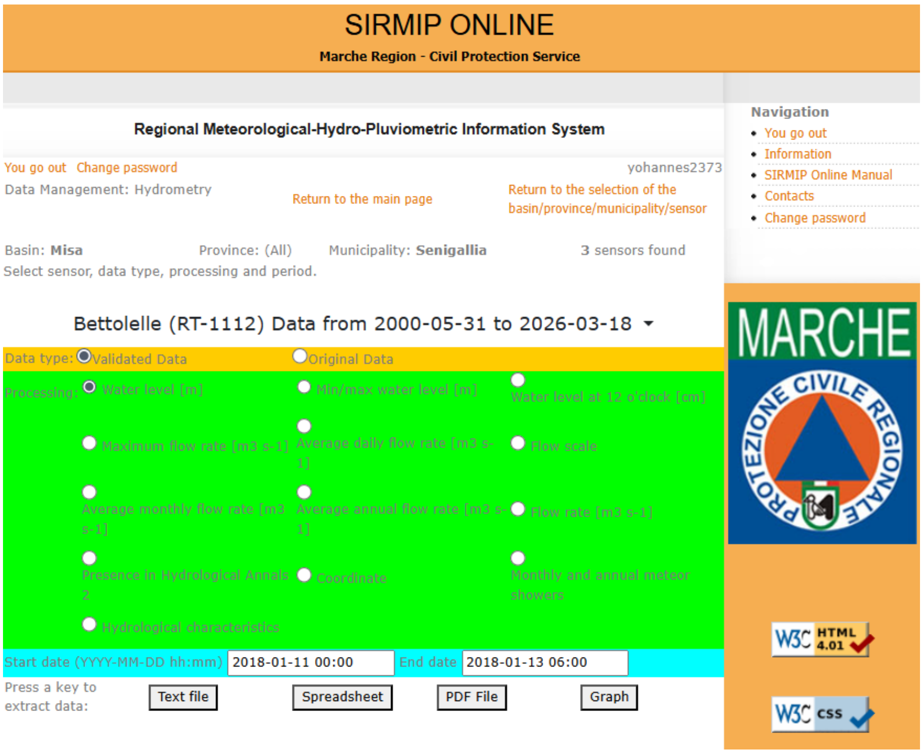

Figure 9. SIRMIP window for stages downloading

From the website, different data regarding both the Bettolelle and the Ponte Garibaldi stations have been extracted. For what concerns the former, the downloaded data regarded both the stage levels and the rating curves, whereas the data downloaded from the Ponte Garibaldi River station were only referred to the stage values, since no rating curve is currently available. The extracted data were subsequently used to define the hydraulic boundary conditions adopted in the HEC-RAS simulations and to support the analysis of the river response under the investigated scenarios.

As shown in figure 10, the first column of the downloaded excel files identifies the sensor (1112 stays for Bettolelle sensor), the subsequent five columns identify the date and the time of data acquisition, the seventh column reports the water level, whereas the last two columns refer to the interpolated water-level flag and the station code, respectively.

Codice sensore	Data: Ann	Mese	Giorno	Ora	Minuto	Livello idrometrico [m]	Livello idrometrico interpolato [0/1]	Codice stazione
1112	2018	1	11	0	30	1.16	0	26
1112	2018	1	11	1	0	1.16	0	26
1112	2018	1	11	1	30	1.16	0	26
1112	2018	1	11	2	0	1.15	0	26
1112	2018	1	11	2	30	1.16	0	26
1112	2018	1	11	3	0	1.15	0	26
1112	2018	1	11	3	30	1.15	0	26
1112	2018	1	11	4	0	1.15	0	26
1112	2018	1	11	4	30	1.15	0	26
1112	2018	1	11	5	0	1.15	0	26
1112	2018	1	11	5	30	1.15	0	26
1112	2018	1	11	6	0	1.15	0	26
1112	2018	1	11	6	30	1.15	0	26
1112	2018	1	11	7	0	1.15	0	26
1112	2018	1	11	7	30	1.15	0	26
1112	2018	1	11	8	0	1.16	0	26
1112	2018	1	11	8	30	1.16	0	26
1112	2018	1	11	9	0	1.17	0	26
1112	2018	1	11	9	30	1.16	0	26
1112	2018	1	11	10	0	1.15	0	26
1112	2018	1	11	10	30	1.15	0	26
1112	2018	1	11	11	0	1.15	0	26
1112	2018	1	11	11	30	1.15	0	26
1112	2018	1	11	12	0	1.15	0	26
1112	2018	1	11	12	30	1.14	0	26
1112	2018	1	11	13	0	1.14	0	26
1112	2018	1	11	13	30	1.14	0	26
1112	2018	1	11	14	0	1.15	0	26
1112	2018	1	11	14	30	1.15	0	26
1112	2018	1	11	15	0	1.14	0	26
1112	2018	1	11	15	30	1.15	0	26

Figure 10. Example of SIRMIP downloaded data

Then, the rating curves, only available for Bettolelle station, have been downloaded and reported in Table 1.

Table 1. Bettolelle station rating curves with relative range of validity

Starting validity	Ending validity	Stage interval(m)	Rating curve equation
1/1/2011 00:01	1/3/2011 10:30	0.77<H<9999	$Q=11.4929*[\ H-(0.76)]^{1.8516}$
5/3/2011 00:01	23/5/2015 06:30	0.55<H<4.39	$Q=6.195*[\ H-(0.517)\ ]^{2.576}+0$
5/3/2011 00:01	23/5/2015 06:30	4.4<H<6.35	$Q=185.568*[H-(4.39)\ ]^{1.138}+202.776$
23/5/2015 00:01	7/3/2017 6:30	0.2<H<1.51	Q=5.9*[H-(0.148)]2.934+0
23/5/2015 00:01	7/3/2017 6:30	1.52<H<3.01	$Q=27.549*[H-(1.51)\ ]^{1.188}+14.609$
23/5/2015 00:01	7/3/2017 6:30	3.02<H<6.5	$Q=101.284*[H-(3.01)\ ]^{1.061}+59.209$
7/3/2017 16:01	5/3/2018 00:00	0.95<H<3.02	$Q=14.388*[H-(0.942)\ ]^{1.974}+0$
7/3/2017 16:01	5/3/2018 00:00	3.03<H6.5	$Q=100.396*[H-(3.02]^{1.068}+60.954$
15/12/2019 00:00	1/1/2030 00:00	0.85<H<1.03	$Q=2.33*[H-(0.84)^{0.79}+0$
15/12/2019 00:00	1/1/2030 00:00	1.04<H<2.1	$Q=19.68*[H-(1.03)]^{1.24}+0.6$
15/12/2019 00:00	1/1/2030 00:00	2.11<H<3.8	$Q=64.05*[H-(2.1]^{1.26}+22.01$
15/12/2019 00:00	1/1/2030 00:00	3.81<H<5.5	$Q=155.87*[H-(3.8)]^{1.16}+146.7$

Each equation reported is referred to a specific range of validity, in terms of both time (i.e. initial and ending date of validity) and space (i.e. the hydrometric level range of validity). The reason why there are a number of different equations is that they are strictly dependant on the geometry of the cross-section.

4.1.2. Tidal stage data acquisition

Extensive in-situ measurement campaigns have been conducted in the Misa River estuary within the EsCoSed and MORSE projects, (http://www.morse.univpm.it/en/), including tidal observations. However, the tidal records collected within the estuary were not used in the present study because the available time series contain temporal gaps and do not provide continuous data suitable for the analysed simulations (Postacchini et al., 2025).

For the implementation of tidal stages, data recorded by the tide gauge located 30 km from Senigallia, at Ancona harbour, have been considered. For the purposes of this work, tidal ranges from different time periods at the Ancona station have been used. The choice of the Ancona station is due to the absence of a tidal station in Senigallia and to the negligible differences in tide elevation between the two locations.

The Servizio Mareografico Nazionale (SMN) of the Higher Institute for Environmental Protection and Research (the Istituto Superiore per la Protezione e la Ricerca Ambientale) (ISPRA) is responsible for monitoring marine climate, coastal conditions, and sea levels, providing observed and processed data together with cartography, standards, and acquisition methods. In the marine environment, the SMN manages the National Wave Gauge Network (Rete Ondametrica Nazionale, RON), which contributed to the development of the National Tide Gauge Network (Rete Mareografica Nazionale, RMN).

The RMN replaces the previous oceanographic monitoring system and is composed of 36 measuring stations, evenly distributed along the national territory and mainly located within port facilities. For almost all RMN stations, the hydrometric level is monitored using a microwave (radar) sensor with millimetric accuracy, coupled with a floating gauge, while the historical ultrasound sensor is still in operation. By comparing the outputs from these three sensors, with the ultrasound sensor used for verification, ISPRA is able to calibrate the radar sensor and ensure high accuracy in stage measurements.

Each sensor records water levels with respect to an oceanographic reference rod, whose elevation is linked to the Istituto Geografico Militare (IGM) altimetric network through the closest IGM benchmark. The stations are also equipped with anemometric sensors measuring wind direction and velocity at 10 m above ground level, as well as barometric, air temperature, water temperature, and relative humidity sensors. Furthermore, 10 stations are equipped with a multiparametric probe for water quality monitoring, measuring parameters such as water temperature, pH, conductivity, and redox.

All stations are provided with local systems for data management and storage, along with transmission systems (UMTS) directly connected to the SMN headquarters in Rome. In addition, 9 stations, identified as strategic for specific phenomena (e.g., rogue waves), are equipped with a secondary satellite transmission system to ensure data transmission in case of UMTS failure.

All data collected by the SMN are publicly available and can be downloaded from the ISPRA website.

The Ancona station is located at latitude 43°37’29.16’’ and longitude 13°30’23.46’’, specifically inside the S. Primiano harbour. The station is equipped with altimetric benchmarks referenced to the mean sea level measured in Genova by the historical Thomson tide gauge.

In order to download the data, after selecting the station on the ISPRA website, it is possible to access the available submenus, as shown in Figure 11.

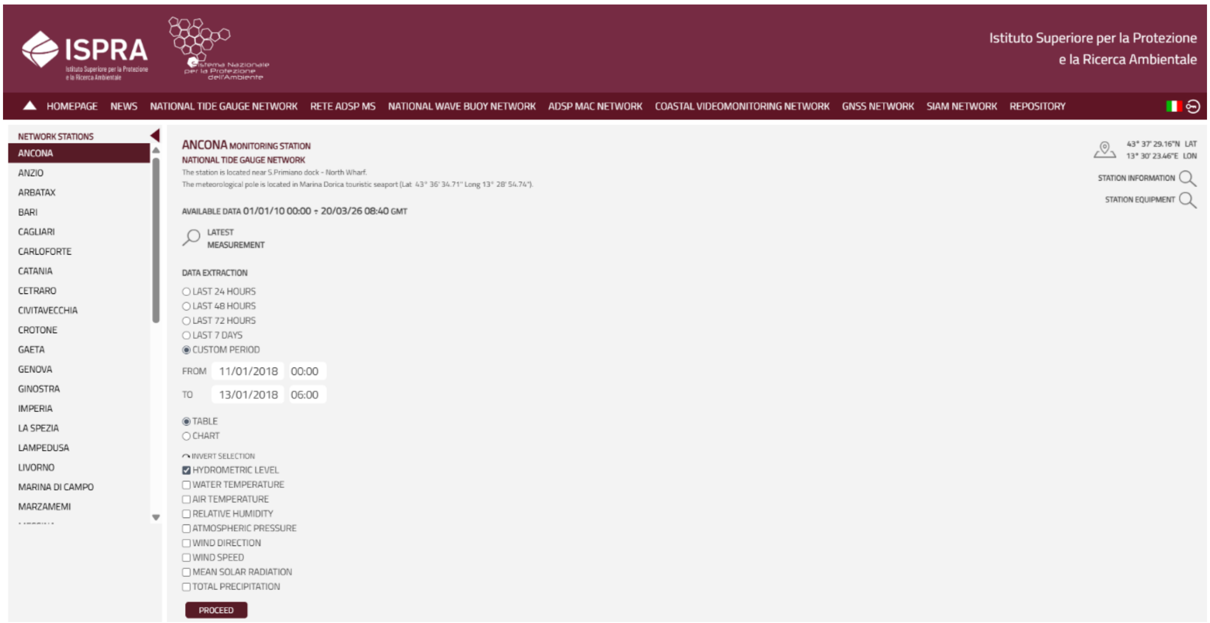

Figure 11. National Tide gauge Network main window

4.2. Boundary Conditions and Data Processing

As described earlier the boundary conditions used in the numerical simulations were defined based on hydrometric and tidal data obtained from the SIRMIP and ISPRA databases. The raw datasets were pre-processed to ensure consistency with the vertical reference system of the numerical model and to extract representative conditions for the simulations.

At the upstream boundary, water level data recorded at the Bettolelle hydrometric station were used. The original measurements refer to the hydrometer zero level; therefore, an offset of 19.18 m above mean sea level was added to express the data in the same elevation reference system as the model geometry. From the available time series, two flood events were selected, corresponding to the years 2018 and 2023. The 2018 event represents a typical condition and was used for model calibration, with a peak discharge of approximately 158 m³/s. In contrast, the 2023 event was chosen to represent a more extreme scenario, reaching a peak discharge of approximately 300 m³/s, consistent with the maximum discharge capacity of the river. As shown in Figure 12, the 2023 hydrograph exhibits significantly higher peak values compared to the 2018 event, highlighting the difference between typical and extreme flow conditions.

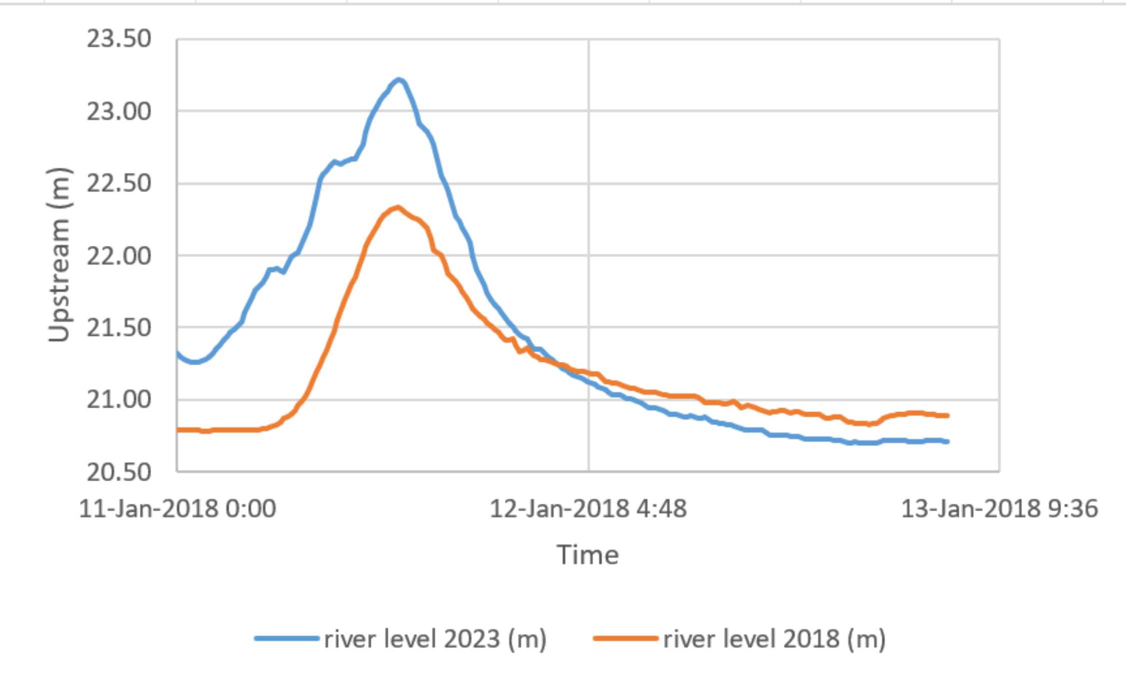

Figure 12. Upstream boundary condition: river level hydrograph referenced to mean sea level.

At the downstream boundary, tidal data recorded at the Ancona tide gauge were considered. The raw data refer to the local gauge zero level and were adjusted by applying a +0.078 m vertical datum correction to ensure consistency with the reference system adopted in the numerical model. This offset was determined by comparing the time series recorded at Ancona with those measured at a tide gauge installed in Senigallia by the Università Politecnica delle Marche, whose reference system is consistent with that adopted in the model.

The 2018 tidal time series was selected as representative input. The signal was processed in MATLAB by applying a low-pass filter to remove measurement noise, with the cutoff frequency selected based on the Fourier transform of the signal in order to preserve the dominant frequency components. Subsequently, local maxima and minima were identified, and their prominence was evaluated. Only peaks with a prominence greater than 0.15 m were retained to define the envelopes of maxima and minima.

Based on these envelopes, four characteristic tidal conditions were identified: maximum high tide (0.52 m), minimum high tide (−0.20 m), maximum low tide (0.14 m), and minimum low tide (−0.72 m). For each of these conditions, a time window of four days (two days before and two days after the selected peak) was extracted from the tidal time series. These time series were used as unsteady downstream boundary conditions, while the corresponding peak values were adopted as steady boundary conditions. As illustrated in Figure 13, these tidal signals capture the variability of sea levels at the river mouth and represent different boundary scenarios.

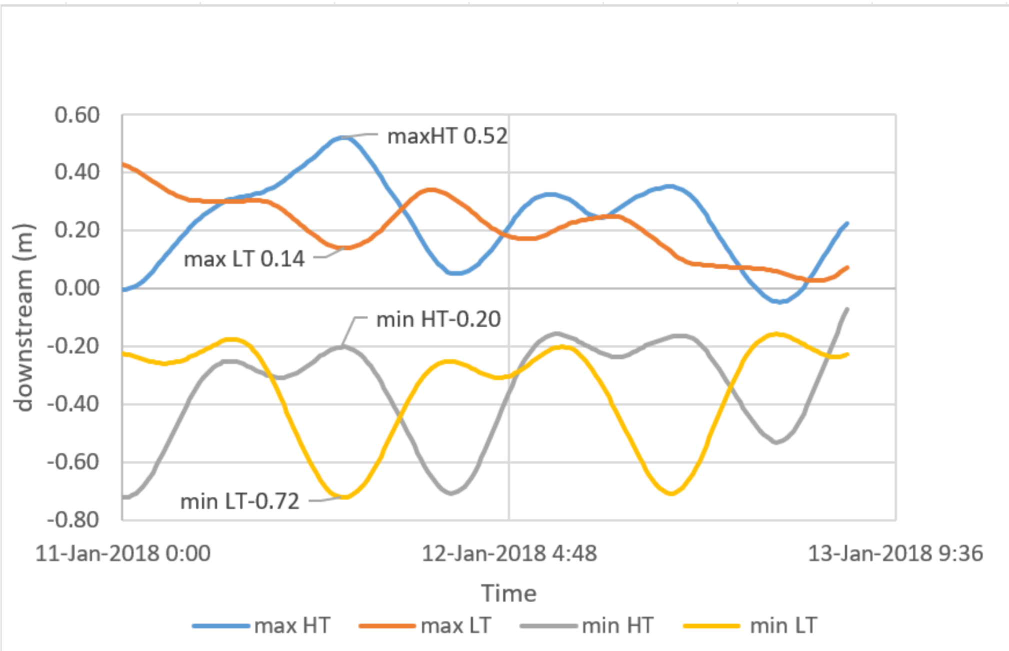

Figure 13. Tidal oscillations adopted as downstream boundary conditions for the unsteady simulations. The selected scenarios represent maximum high tide (maxHT), maximum low tide (maxLT), minimum high tide (minHT), and minimum low tide (minLT), referenced to mean sea level.

For the unsteady simulations, the selected tidal time series were combined with both upstream hydrographs (2018 and 2023). The upstream hydrographs were kept fixed in time, while the downstream boundary conditions were time-shifted so that the tidal peaks coincided with the arrival of the flood peak at the river mouth, accounting for an estimated travel time of approximately one hour from the upstream boundary. Only the portion of the tidal signal overlapping with the hydrograph duration was considered, ensuring consistent temporal boundary conditions for the simulations.

In addition to the tidal conditions derived from the analysis of the Ancona time series, further steady downstream boundary conditions were introduced to investigate the sensitivity of the model to simplified water level scenarios. In particular, constant water levels of −0.5 m, 0 m, and 1 m were considered as representative values to explore a wider range of possible hydraulic conditions at the downstream boundary. Unlike the tidal levels obtained from data analysis, these values do not correspond to specific observed events but were defined to provide a simplified and controlled assessment of the system response.

Moreover, additional steady boundary conditions were defined using representative extreme water level values (e.g., 1.609 m, 0.235 m, 1.591m, and −0.236 m), which are consistent with those reported in the literature for similar coastal environments and align with extreme water levels derived from statistical analyses of storm surge and tidal components (Baldoni et al., 2025).

The inclusion of these scenarios allows for a better understanding of the influence of downstream water levels on the overall hydraulic behaviour of the river, particularly in terms of backwater effects and flood propagation.

Based on the defined boundary conditions, a set of simulation scenarios was developed to analyze the system response under different hydraulic and tidal configurations, as explained in Table 2.

Table 2. Configuration of Model Runs: Topography and Boundary Condition Combinations

Scenarios	Topography	Upstream boundary condition	Downstream boundary condition	Downstream boundary condition type
1	2018	Stage 2018	Max high tide	Unsteady (hydrograph)
2	2018	Stage 2018	Max low tide	Unsteady (hydrograph)
3	2018	Stage 2018	Min high tide	Unsteady (hydrograph)
4	2018	Stage 2018	Min low tide	Unsteady (hydrograph)
5	2018	Stage 2023	Max high tide	Unsteady (hydrograph)
6	2018	Stage 2023	Max low tide	Unsteady (hydrograph)
7	2018	Stage 2023	Min high tide	Unsteady (hydrograph)
8	2018	Stage 2023	Min low tide	Unsteady (hydrograph)
9	2018	Stage 2018	Max high tide1.609	Steady (constant water level)
10	2018	Stage 2018	Max low tide 0.235	Steady (constant water level)
11	2018	Stage 2018	Min high tide 1.591	Steady (constant water level)
12	2018	Stage 2018	Min low tide -0.236	Steady (constant water level)
13	2018	Stage 2018	Max high tide 0.52	Steady (constant water level)
14	2018	Stage 2018	Max low tide 0.14	Steady (constant water level)
15	2018	Stage 2018	Min high tide -0.2	Steady (constant water level)
16	2018	Stage 2018	Min low tide -0.72	Steady (constant water level)
17	2018	Stage 2023	Max high tide 0.52	Steady (constant water level)
18	2018	Stage 2023	Max low tide 0.14	Steady (constant water level)
19	2018	Stage 2023	Min high tide -0.2	Steady (constant water level)
20	2018	Stage 2023	Min low tide -0.72	Steady (constant water level)
21	2018	Stage 2018	-0.5	Steady (constant water level)
22	2018	Stage 2018	1	Steady (constant water level)
23	2018	Stage 2023	-0.5	Steady (constant water level)
24	2018	Stage 2023	1	Steady (constant water level)
25	2018	Stage 2018	0	Steady (constant water level)
26	2018	Stage 2023	0	Steady (constant water level)

4.3. HEC-RAS Software

HEC-RAS is an open-source software developed by the US Army Corps of Engineers in 1995 at the Hydrologic Engineering Centre (HEC) in Davis, California, and it is one of the most famous software for the modelling of mono and bi-dimensional natural and anthropic channel networks (River Analysis System, RAS).

It allows to carry out simulations of different phenomena in different conditions, such as:

- Simulations in steady flow conditions, by considering either sub-critical and/or super-critical and/or mixed regimes. This tool is used to analyze mild slope flows in both single channels and channel networks;
- Simulations in unsteady flow conditions;
- Simulations devoted to the quantification and classification of solid transport hydrodynamic processes linked to either erosion and/or deposition phenomena;
- Water quality simulations, i.e. water temperature analysis and transported material such as dissolved oxygen and organic materials.

The employed version is the 6.6, which allows, in particular, to perform one-dimensional hydraulic simulations in unsteady flow environments, which are key aspect of this work.

4.3.1. Steady flow analysis

The software, performing a steady flow analysis, is able to return water profiles relative to steady or quasi-steady flow conditions: these results are elaborated by the software applying the law of conservation of energy to two consecutive cross-sections (Figure 14) through the “standard step method”, which consist of an iterative process.

The law of conservation of energy is represented by the following equation:

$$z_2 + Y_2 + \frac{a_2 v_2^2}{2g} = z_1 + Y_1 + \frac{a_1 v_1^2}{2g} + h_e \tag{1}$$

Where:

Z_1, Z_2 = thalweg of the two cross-sections;

Y_1, Y_2 = water depth (stage) at the two cross-sections;

V_1, V_2 = average velocity of the two cross-sections (total discharge/total flow area);

α_1, α_2 = velocity weighting coefficients of the two cross-sections:

g = gravitational acceleration;

h_e = energy head loss.

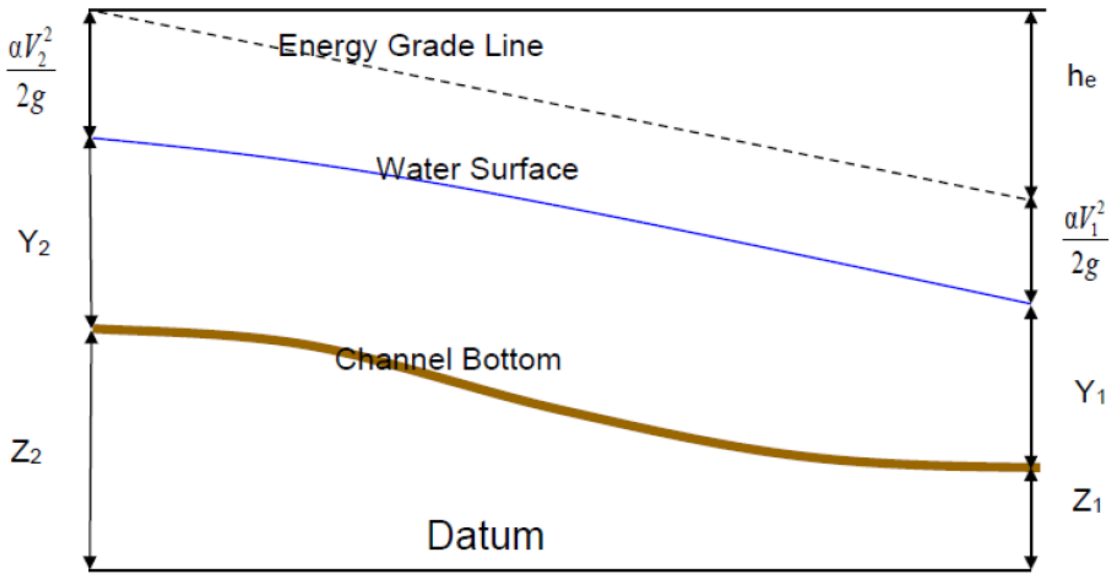

Figure 14. Representation of terms of the energy equation

More in details, the last term h_e, the head loss between the two cross-sections, takes into account both the friction losses due to roughness and contraction/expansion losses; it is calculated by the following equation:

$$h_e = L\bar{s}_f + C\left|\frac{a_2 v_2^2}{2g} - \frac{a_1 v_1^2}{2g}\right| \tag{2}$$

Where:

$\bar{Sf}$ = friction slope (slope of the energy grade line) between the two cross-sections.

C = expansion (or contraction) loss coefficient;

L = average length of the reach between the two cross-sections weighted with respect to the discharge distribution in the cross-sections, which is evaluated as:

$$L = \frac{L_{lob}Q_{lob} + L_{ch}\bar{Q}_{ch} + L_{rob}Q_{rob}}{Q_{lob} + Q_{ch} + Q_{rob}} \tag{3}$$

Where L_{lob}, L_{ch}, L_{rob} are referred to the cross-sections reach lengths specified for flow in the left overbank ("lob"), main channel ("ch"), and right overbank ("rob"), respectively, while $\bar{Q}_{lob}$, $\bar{Q}_{ch}$, $\bar{Q}_{rob}$ are the arithmetic averages of the flows between sections for the left overbank, main channel, and right overbank, respectively.

As natural stream channels are usually composed of very heterogeneous materials and different type of vegetation as well, the cross-sections are considered composed of different parts, each of them with a specific roughness coefficient, called Manning coefficient “n” (Figure 15).

Thus, the total conveyance (flow per unit of head loss per unit of length) is calculated, in order to determine the slope of the energy grade line **Sf**, through the use of Manning equation for each subdivision of the cross section:

$$Q = KS_f^{\frac{1}{2}} \tag{4}$$

$$K = \frac{1.486}{n} AR^{\frac{2}{3}} \tag{5}$$

Where:

K = conveyance for each subdivision;

n = Manning coefficient for each subdivision;

A = flow area for subdivision;

R = hydraulic radius for subdivision (A/P, with P = wet perimeter);

S_f = slope of the energy grade line.

These values of the conveyance factor are summed up by the software in order to get three final values for:

- K_{lob} = conveyance factor for the left overbank;
- K_{rob} = conveyance factor for the right overbank;
- K_{ch} = conveyance factor for the main channel, computed as a single element.

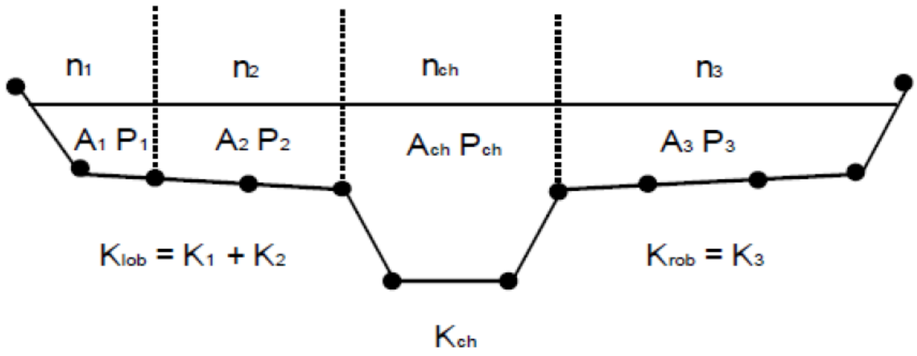

Figure 15. Default conveyance factor subdivision method

The total conveyance for the whole section is obtained by summing up all the three subdivision conveyances (K_{lob}, K_{rob}, and K_{ch}): this method is the default one in HEC-RAS for calculating the conveyances throughout the cross-sections.

An alternative procedure is also available, in which the conveyance is evaluated between every point in the overbanks, instead of calculating it within just the subdivision, as shown in Figure 16.

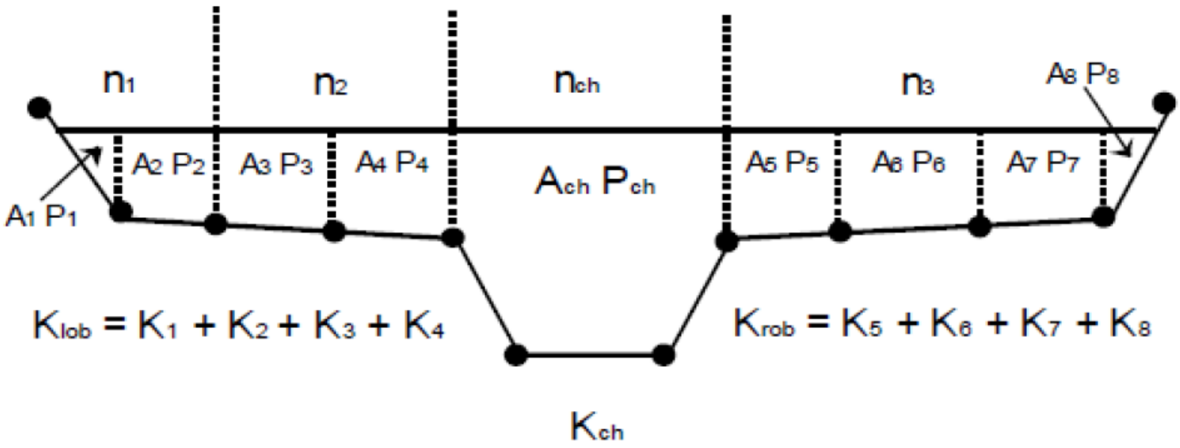

Figure 16. Alternative conveyance factor calculation method

With this method, the conveyance factors are summed up in order to get the total K_{lob} and K_{rob}. These two methods give different results whenever some portions of the overbanks have ground sections with significant vertical slopes: in general, the default approach provides a lower value for the total conveyance considering the same water surface elevation. On the other hand, the HEC-RAS default method is more consistent with the Manning equation and the concept of separate flow elements.

Then, the velocity weighting coefficient (α), is evaluated with respect to the conveyances of the left, right and main channel overbanks:

$$a = \frac{(A_t^2)\left[\frac{k_{lob}^3}{A_{tob}^2} + \frac{k_{ch}^3}{A_{ch}^2} + \frac{K_{rob}^3}{A_{rob}^2}\right]}{k_t^3} \tag{6}$$

where:

A_t = total flow area of cross section;

A_{lob}, A_{ch}, A_{rob} = flow areas of left overbank, main channel overbank and right overbank, respectively;

K_t = total conveyance of the cross-section;

K_{lob}, K_{ch}, K_{rob} = conveyances of left overbank, main channel overbank and right overbank, respectively.

The conveyance factor is used by the software to determine the friction loss, that is part of the total head loss h_e as mentioned before: it is a simple product of the slope of the energy grade line S_f and the average length of the reach between the two cross-sections weighted with respect to the discharge distribution in the cross-sections (L), which was determined previously. Regarding the first term S_f, it is calculated as an exploitation of the Manning equation:

$$s_f = \left(\frac{Q}{k}\right)^2 \tag{7}$$

In HEC-RAS there are four different alternatives for the estimation of Sf:

- Average Conveyance Equation

$$\bar{S}_f = -\left(\frac{Q_1 + Q_2}{k_1 + k_2}\right)^2 \tag{8}$$

- Average Friction Slope Equation

$$\bar{s}_f = \frac{s_{f1} + s_{f2}}{2} \tag{9}$$

- Geometric Mean Friction Slope Equation

$$\bar{s}_f = \sqrt{s_{f1} \times s_{f2}} \tag{10}$$

- Harmonic Mean Friction Slope Equation

$$\bar{s}_f = \frac{2(s_{f1} \times s_{f2})}{s_{f1} + s_{f2}} \tag{11}$$

Where the subscripts 1 and 2 refer to the two subareas the river cross-section is divided into.

Unless differently specified, the equation (8) is the default method used by the software.

The last contribute to be determined in the calculation of the total head loss h_e is the contraction/expansion coefficient (C), which represents the contraction or expansion to which the flow can be subjected, causing additional losses due to the changes in subsequent cross-sections.

Considering a sub-critical flow regime:

- With a mild change in cross section, values of 0.1 and 0.3 for the contraction/expansion coefficients, respectively, should be considered;
- in case of bridge section, with a sudden change in cross section, higher values should be assumed, i.e. 0.3 for the contraction and 0.5 for the expansion;
- in the presence of abrupt transitions, these values should be even higher, such as 0.6 for the contraction and 0.8 for the expansion.

In general, these coefficients are never greater than 1 and, on the other hand, if there is the presence of identic cross-section or anytime this further energy loss does not want to be taken into consideration, both coefficients can be set to 0.

In the case of super-critical flows, lower values of contraction/expansion coefficient should be adopted, because, since the dynamic head ($\alpha V^2/2g$) varies exponentially, to small stages variations correspond high variations of the total head, with the consequent overestimation of the head losses.

For this reason, considering super-critical flows:

- with a mild cross-section variation, suitable contraction/expansion coefficient values are 0.01 and 0.03, respectively.
- in case of sudden geometry variation, typically, values of 0.05 for the contraction coefficient and 0.2 for the expansion coefficient are usually recommended.

The software considers the presence of a contraction whenever the downstream flow velocity is higher than the upstream one. On the contrary, if the upstream velocity is greater than the downstream one, the program considers the presence of an expansion.

Then, in order to run the simulation, the boundary conditions must be introduced into the software, following these rules:

- downstream for sub-critical flow;
- upstream for super-critical flow;
- both upstream and downstream for mixed regime.

The software gives the possibility to select different types of boundary conditions, such as water surface elevation, critical depth, normal depth and rating curves.

The HEC-RAS computation procedure to evaluate the unknown water surface elevation is based on the following iterative procedure:

1. An initial water-surface elevation is assumed at the boundary cross-section, starting from the downstream boundary for subcritical flow conditions and from the upstream boundary for supercritical flow conditions;
2. determination of the corresponding total conveyance and velocity head;
3. calculation of the friction loss and development of the head loss equation h_e;
4. Once the values of the point 2 and 3 are known, these are used to find out a new value of the water surface elevation by using the law of conservation of energy equation;
5. The two values of the water surface elevations, the assumed one and the calculated one, are compared: if there is a difference between them less than 0.003 m, the iterative procedure ends up; on the other hand, if the difference is higher than 0.003 m, the iterative procedure continues until the latter value if satisfied.

Note that the law of conservation of energy is not applicable if the water surface elevation passes through the critical state (caused by, for example, a significant variation in the channel bed slope, a hydraulic jump, an overflow, the presence of bridge piers and junctions). In those cases, the momentum equation must be taken into account by the implementation of the unsteady flow analysis.

4.3.2. Unsteady flow analysis

As mentioned, the unsteady flow analysis takes into account both the principle of conservation of mass and the principle of conservation of momentum: the first one states that, for a control volume, the net rate of flow into the volume must be equal to the rate of change of storage inside the volume, whereas, the latter states that, for a control volume, the net rate of momentum entering the volume (momentum flux) plus the sum of all external forces acting on the volume must be equal to the rate of accumulation of momentum.

The relative equations are:

- Continuity equation:

$$\frac{\delta A_t}{\delta t} + \frac{\delta Q}{\delta x} - q_l = 0 \tag{12}$$

- Momentum equation:

$$\frac{\delta Q}{\delta t} + \frac{\delta Q v}{\delta x} - gA\left(\frac{\delta z}{\delta x} + S_{f0}\right) = 0 \tag{13}$$

where:

Q = channel flow;

A_T = total flow area (sum of the active area and the off-channel storage area);

q_l = lateral inflow per unit length;

A = cross-sectional area;

g = gravitational acceleration;

S_f = friction slope;

V = average flow velocity;

$\frac{\delta z}{\delta x}$ = water surface slope

These equations are solved by the software simultaneously, by means of “finite difference” method, i.e. transforming the partial derivatives into finite differences obtaining, as a result, an algebraic equation system.

4.3.3. Program interface

The U.S Army Corps of Engineers’ River Analysis System (HEC-RAS) is a software that was developed at the Hydraulic Engineering Center (HEC) as a part of the Hydrologic Engineering Center’s “Next Generation” (NexGen) of hydrologic engineering software.

The HEC-RAS main window (Figure 17) is structured in three sections, where at the top there is the menu bar, while moving downward there are the button bar and the part devoted to the project information.

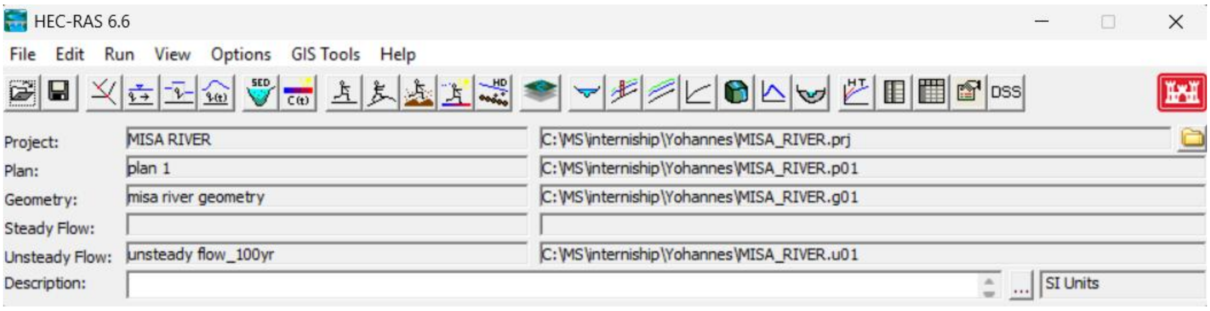

Figure 17. HEC-RAS main window

The menu bar, is essentially composed of the following options:

- File: option used for file management;
- Edit: option used for entering and editing data;
- Run: option used to perform hydraulic calculations;
- View: option containing a set of tools used to display the model output by means of graphs and tables;
- Options: menu item used to change program setup options;
- GIS tools: option used to enter the HEC-RAS Mapper tool, which allows the creation of terrain models with the subsequent visualization of inundations mapping and flood animations;
- Help: option used to get on-line help.

For what regards the main window button bar, all the functions are illustrated in Figure 18:

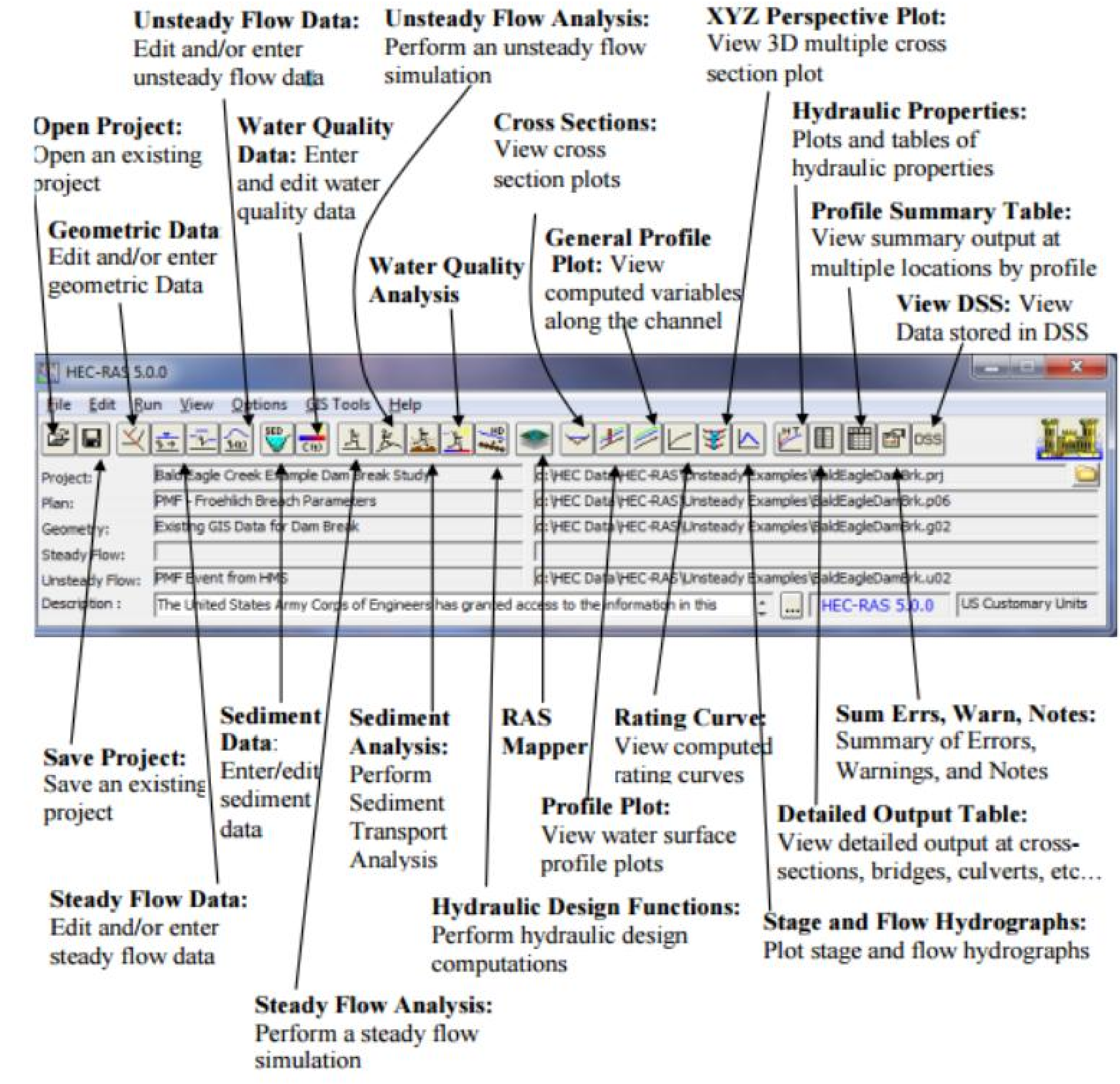

Figure 18. HEC-RAS main window button bar

The development of the hydraulic model in HEC-RAS follows five main steps:

1. Starting a new project
2. Entering geometric data
3. Entering flow data and boundary conditions
4. Performing the hydraulic calculations
5. Viewing and printing results

The geometrical configuration of the model can be accessed from the main window by selecting "Edit" and then "Geometric Data". As shown in Figure 19, the river reach is represented together with the cross-sections and their corresponding river stations, defining the spatial structure of the model used in the simulation.

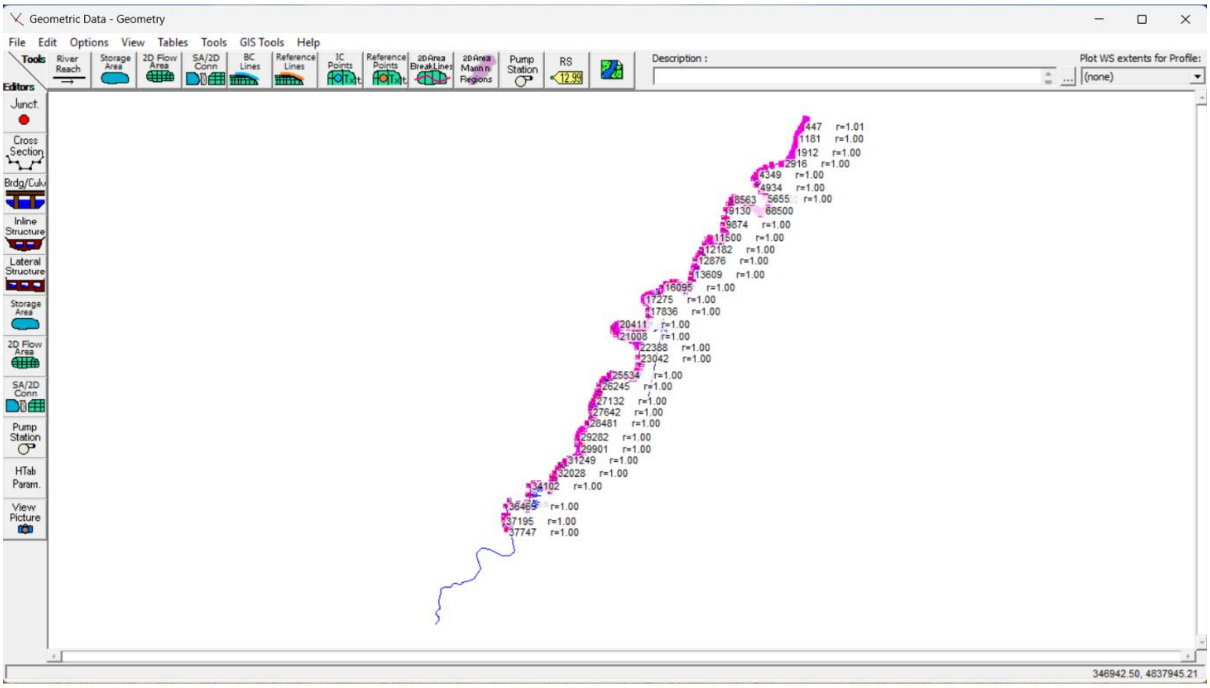

Figure 19. Geometric data window.

In this window, by selecting the “Cross Section” option, the individual cross-sections of the river can be visualized in detail. Each section is displayed separately, allowing a clearer understanding of the channel geometry and its spatial variation along the river reach.

Figure 20 shows the cross-section editor window in HEC-RAS, where the main geometric and hydraulic properties of a selected section are defined. In the upper part of the window, general information is provided, including the river and reach name, the river station (which decreases in the downstream direction), and a brief description of the cross-section.

The geometry of the cross-section is defined through a set of points listed in the “Cross Section Coordinates” table, where the station represents the horizontal distance along the section, and the elevation indicates the corresponding height above mean sea level. The spacing between consecutive cross-sections is specified in the “Downstream Reach Lengths” table, where LOB (Left Overbank), Channel, and ROB (Right Overbank) represent the distances between adjacent sections for different parts of the flow area.

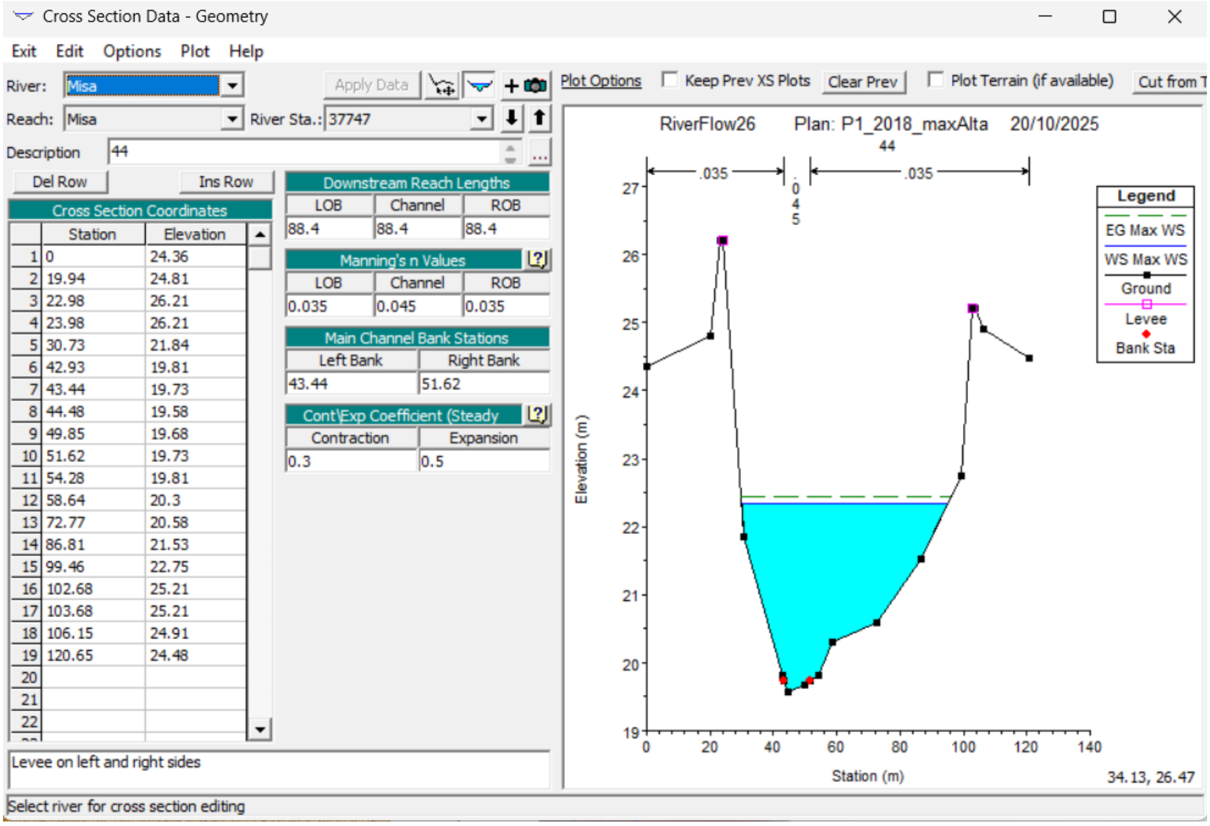

Figure 20. Example of river cross-section geometry in HEC-RAS

The “Main Channel Bank Stations” define the limits of the main channel within the cross-section, distinguishing it from the floodplain areas. Additionally, roughness coefficients are assigned through Manning’s values for the left overbank, main channel, and right overbank, depending on the characteristics of the channel and surrounding areas. Further options allow the inclusion of levees and ineffective flow areas, which represent portions of the section that do not actively convey flow.

4.3.3.1. Unsteady simulation

In the unsteady simulations, unlike the steady simulation, there are different boundary conditions, as shown below Figure 21, that must be assigned on both the most upstream section and the most downstream one.

The most used boundary conditions types are the following:

- Stage Hydrograph: where there is the possibility to add different water elevation values (referred to the average sea level) related to the considered time series;
- Flow Hydrograph: where there is the possibility to add different flow data for the considered time series;

- Stage/Flow Hydrograph: where it is possible to enter both values of stage and flow for the considered time series.

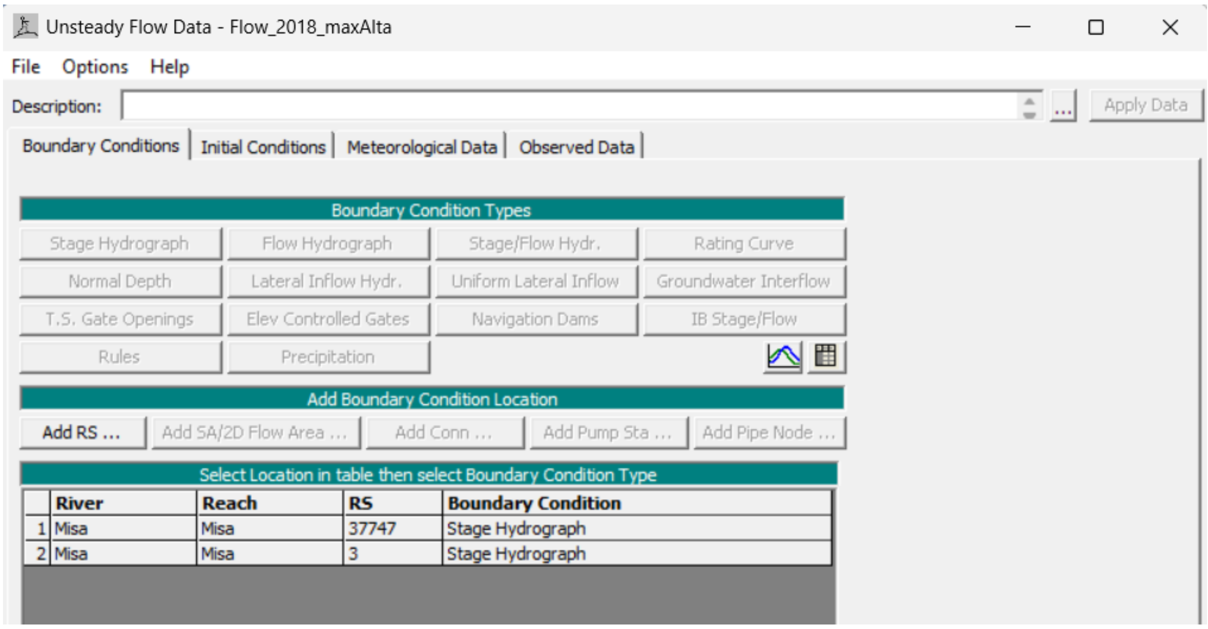

Figure 21. Unsteady flow data boundary conditions

In each of these types of boundary conditions, there is the possibility to set the period of analysis along with the "Data time interval", which is the interval of time over which the stage/flow data will be inserted into the software (Figure 22).

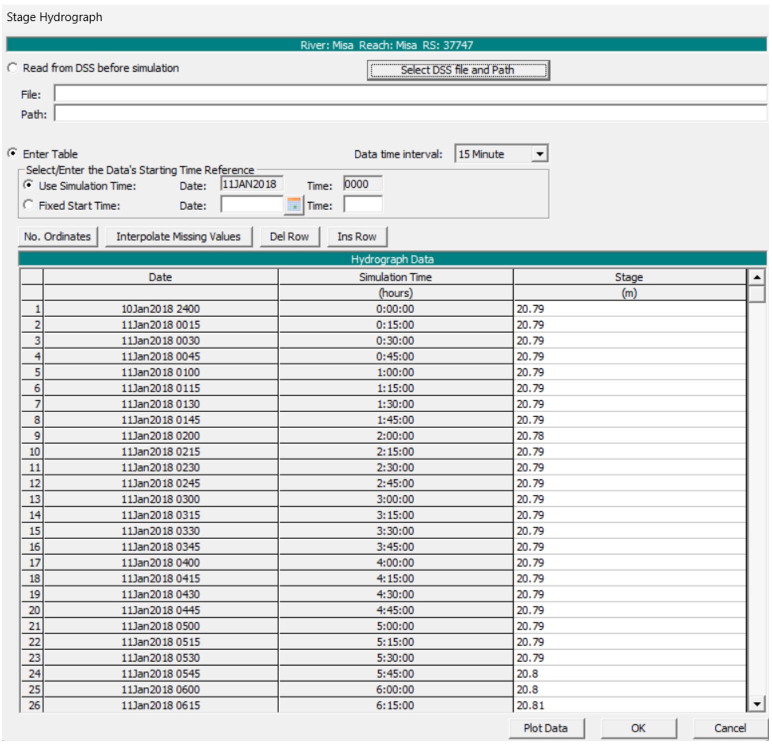

Figure 22 Stage hydrograph

Once the hydrograph is added, it is possible to plot it in order to visually check its correctness (Figure 23).

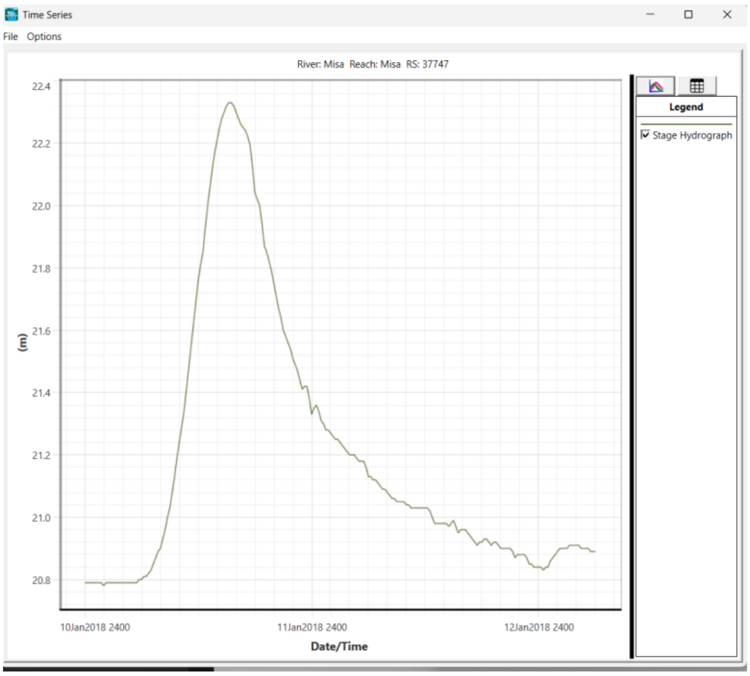

Figure 23. Stage hydrograph graph over time

There are also other types of boundary conditions that can be applied only as downstream boundary conditions:

- Rating Curve;
- Normal depth: it can be used only for open-ended reaches, and it requires to enter the slope of the energy grade line (the slope of the water surface can be used instead of the energy grade line since the two are similar).

In order to simulate an external inflow, that could be, for instance, a waste water treatment plant discharge (as it has been evaluated in this work), further boundary conditions can be applied on each cross-section of the river. In particular:

- Lateral Inflow Hydrograph: this option is used as an internal boundary condition to simulate an external inflow at a specific point along the stream. To implement this boundary condition, it is necessary to add a new river station (in the cross-section where the external inflow is supposed to be), then the flow hydrograph can be entered;
- Uniform Lateral Inflow Hydrograph: with this option a flow hydrograph can be added, and it will be uniformly distributed between two specified cross-sections along the river.

In addition to the already mentioned boundary conditions, other options concerning the groundwater (inflow or outflow depending on the water surface head), gate openings and navigation dams can be implemented into the software.

Once the boundary conditions are set, the unsteady flow data can be saved in order to be immediately recalled.

To run the unsteady simulation, the first step is the definition of a plan which defines both the geometry and the unsteady flow data to be analysed. Afterwards, it is possible to select the components which will be used for the unsteady flow analysis and that are: a geometric data pre-processor, the unsteady flow simulator and an output post-processor.

The geometric pre-processor is used to process the geometric data into a series of hydraulic properties tables, rating curves and family of rating curves. This option must be run at least once for the first time and it needs to be re-executed only if something in the geometric data changes. The cross-sections are processed into tables of elevation vs hydraulic properties of areas, conveyance and storage. The pre-processor creates hydraulic property tables for both the main channel and floodplain and, for what concerns the latter, differently from the steady simulation, they are worked out as combination of the left overbank and the right overbank properties, summed together in a single set of curves. The unsteady flow option utilizes an arithmetic average between the left and the right overbank reach lengths in order to compute a floodplain reach length. In order to correctly set the hydraulic property table, it is required to enter an interval which will be used for spacing the points in the cross-section table (Figure 24). In particular, this interval should be large enough to capture all possible water surface elevations that may be encountered during the unsteady flow simulations, because, in the case in which the water surface goes above these intervals, the model could be unstable. On the other hand, the interval should be also small enough in order to guarantee a sufficient level of detail to depict changes in area, conveyance, and storage with respect to elevation.

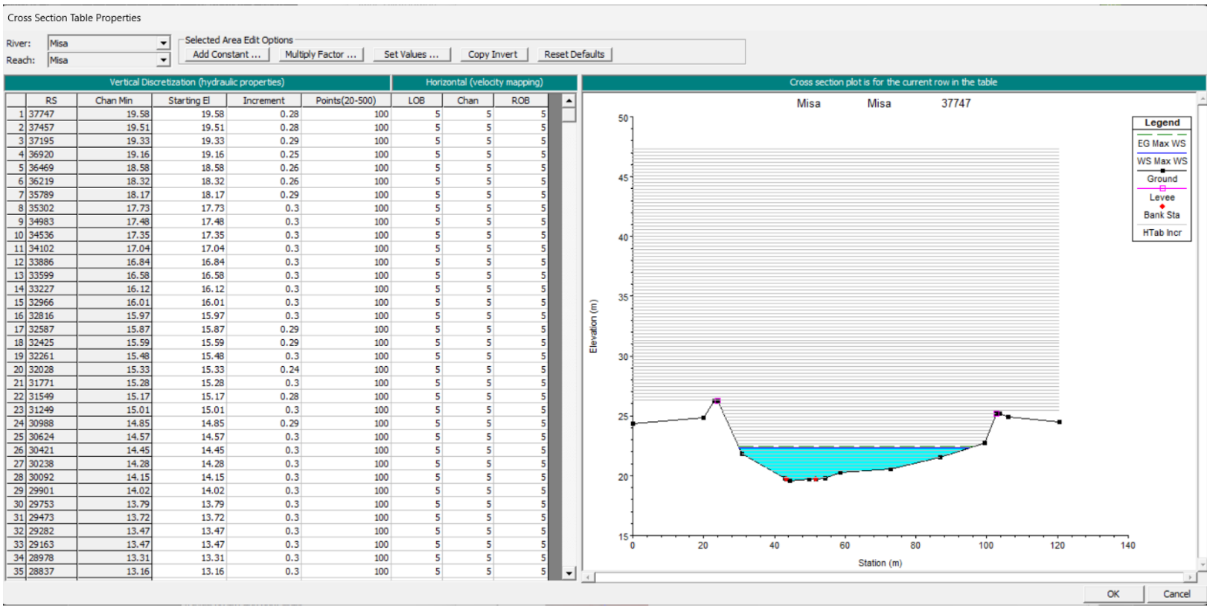

	RS	Chan Min	Starting El	Increment	Points(20-500)	LOB	Chan	ROB
1	37747	19.58	19.58	0.28	100	5	5	5
2	37457	19.51	19.51	0.28	100	5	5	5
3	37195	19.33	19.33	0.29	100	5	5	5
4	36920	19.16	19.16	0.25	100	5	5	5
5	36469	18.58	18.58	0.26	100	5	5	5
6	36219	18.32	18.32	0.26	100	5	5	5
7	35789	18.17	18.17	0.29	100	5	5	5
8	35302	17.73	17.73	0.3	100	5	5	5
9	34983	17.48	17.48	0.3	100	5	5	5
10	34536	17.35	17.35	0.3	100	5	5	5
11	34102	17.04	17.04	0.3	100	5	5	5
12	33886	16.84	16.84	0.3	100	5	5	5
13	33599	16.58	16.58	0.3	100	5	5	5
14	33227	16.12	16.12	0.3	100	5	5	5
15	32966	16.01	16.01	0.3	100	5	5	5
16	32816	15.97	15.97	0.3	100	5	5	5
17	32587	15.87	15.87	0.29	100	5	5	5
18	32425	15.59	15.59	0.29	100	5	5	5
19	32261	15.48	15.48	0.3	100	5	5	5
20	32028	15.33	15.33	0.24	100	5	5	5
21	31771	15.28	15.28	0.3	100	5	5	5
22	31549	15.17	15.17	0.28	100	5	5	5
23	31249	15.01	15.01	0.3	100	5	5	5
24	30988	14.85	14.85	0.29	100	5	5	5
25	30624	14.57	14.57	0.3	100	5	5	5
26	30421	14.45	14.45	0.3	100	5	5	5
27	30238	14.28	14.28	0.3	100	5	5	5
28	30092	14.15	14.15	0.3	100	5	5	5
29	29901	14.02	14.02	0.3	100	5	5	5
30	29753	13.79	13.79	0.3	100	5	5	5
31	29473	13.72	13.72	0.3	100	5	5	5
32	29282	13.47	13.47	0.3	100	5	5	5
33	29163	13.47	13.47	0.3	100	5	5	5
34	28978	13.31	13.31	0.3	100	5	5	5
35	28837	13.16	13.16	0.3	100	5	5	5

Figure 24. Hydraulic table parameters for cross-sections.

The post-processor provides further hydraulic information if compared to the unsteady flow computation. In general, the unsteady flow computation only calculates stage and flow at all the selected cross-sections, thus, if the post-processor is not run, the outputs of the simulation will only be the stage and flow hydrographs and the inundation mapping. On the other side, if the post-processor is run, all the available plots and tables can be interrogated as for the steady flow simulation.

In order to correctly set up the unsteady simulation, it is required entering both the start and the end of the simulation period from the "Simulation Time Window" in the "Unsteady Flow Analysis". This time interval can be either equal or less than the time period associated to the "Unsteady Flow Data".

For what regards the "Computation Setting" table, it is composed of different options such as:

- Computation Interval: this represents the simulation timestep. Firstly, it should be small enough to accurately describe both the rise and the fall of the hydrograph. Generally, a good estimate is to consider a computation interval which is equal or less than the time of rise of the hydrograph divided by 20. Secondly, it should follow the Courant condition criteria, i.e., the computation interval should be equal or less than the time required by water to travel from one cross-section to the next. Considering the latter time step, the model will have a high stability although it may require longer time to be run. Additional factors are linked to the presence of bridges and culverts, since the flow transition from unsubmerged to submerged flow within these structures can lead to an abrupt rise of the water surface upstream of the structure provoking a model instability;

- Mapping Output Interval: this field is used to enter the interval at which it is possible to visualize mapping output within HEC-RAS Mapper;
- Hydrograph Output Interval: this interval must be equal or large than the selected computation interval and is set in order to give a suitable number of points to define the shape of the computed hydrograph without losing information regarding the peaks or volume of the hydrograph;
- Detailed Output Interval: this option allows to set the time interval on which the simulation results will be shown. The selected time interval must always be equal or higher than the computational interval.

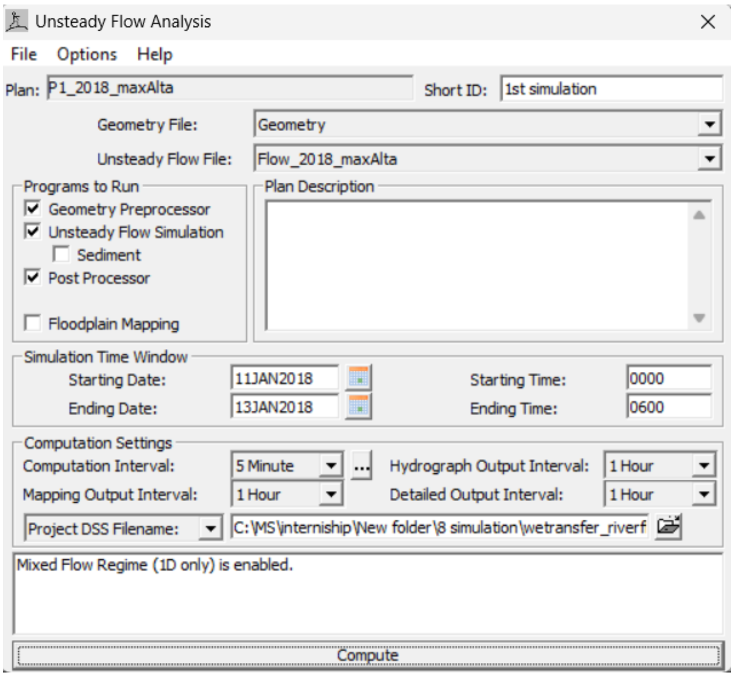

Figure 25. Unsteady flow analysis window

4.3.3.2. Unsteady simulation results

Once the simulation has been run, the obtained results can be consulted in different ways. One of these consists in the visualization of the results by means of a table which can be organized in relation to either the desired cross-sections and/or the desired profiles (Figures 26 and 27).

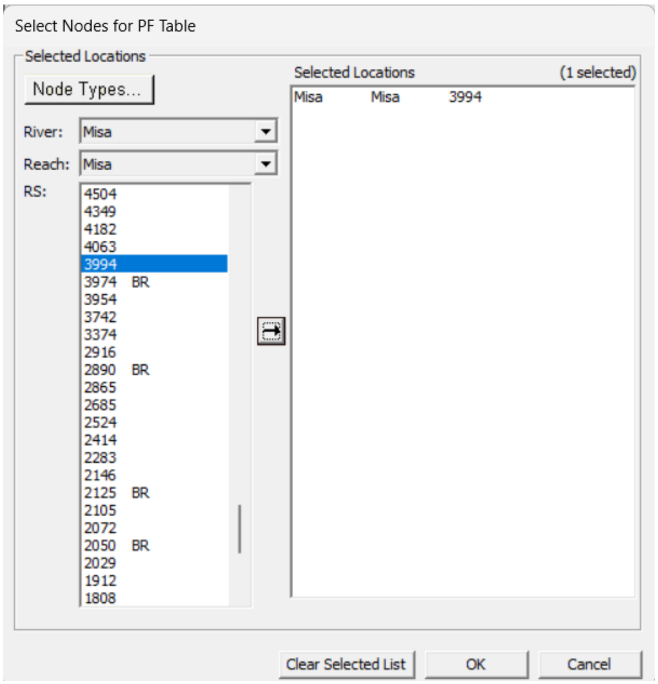

Figure 26. Selection of the cross-section upstream of bridges

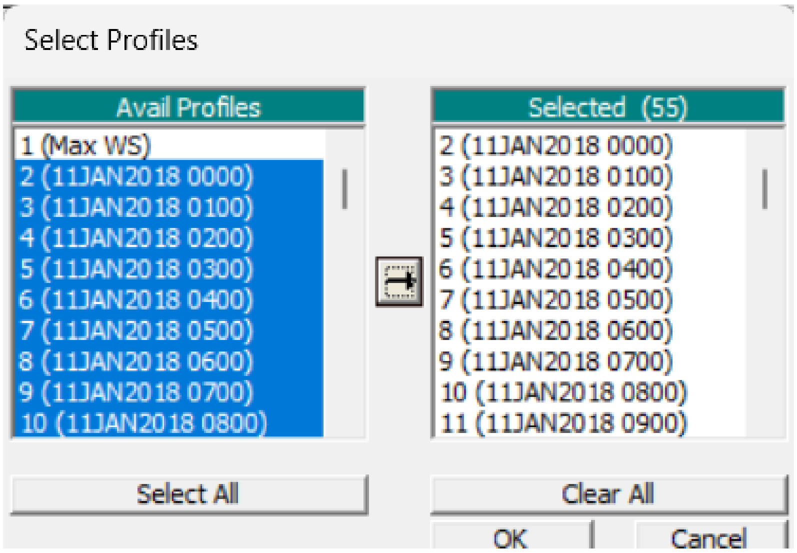

Figure 27. Selection of the profile

As both the cross-sections and the profiles are selected, all the information concerning the cross-sections, profiles, total flow, minimum channel elevation, water surface elevation, critical water surface, energy grade line elevation, energy grade line slope, channel velocity, flow area, top width and Froude number, are displayed as in Figure 28

Profile Output Table - Standard Table 1

File Options Std. Tables Locations Help

HEC-RAS Plan: 1st simulation Locations: User Defined

Reload Data

River	Reach	River Sta	Profile	Q Total	Min Ch El	W.S. Elev	Crit W.S.	E.G. Elev	E.G. Slope	Vel Chnl	Flow Area	Top Width	Froude # Chl
				(m3/s)	(m)	(m)	(m)	(m)	(m/m)	(m/s)	(m2)	(m)	
Misa	Misa	3994	11JAN2018 0000	1.00	-0.79	0.01	-0.50	0.01	0.000004	0.07	14.77	33.13	0.03
Misa	Misa	3994	11JAN2018 0100	1.07	-0.79	0.02	-0.50	0.02	0.000005	0.07	15.04	33.13	0.03
Misa	Misa	3994	11JAN2018 0200	1.19	-0.79	0.06	-0.49	0.06	0.000004	0.07	16.44	33.15	0.03
Misa	Misa	3994	11JAN2018 0300	15.90	-0.79	0.25	-0.16	0.28	0.000257	0.70	22.92	33.22	0.27
Misa	Misa	3994	11JAN2018 0400	17.60	-0.79	0.30	-0.14	0.32	0.000256	0.72	24.38	33.23	0.27
Misa	Misa	3994	11JAN2018 0500	17.71	-0.79	0.34	-0.14	0.36	0.000216	0.69	25.78	33.25	0.25
Misa	Misa	3994	11JAN2018 0600	17.69	-0.79	0.37	-0.14	0.39	0.000191	0.66	26.74	33.26	0.24
Misa	Misa	3994	11JAN2018 0700	17.79	-0.79	0.39	-0.14	0.41	0.000177	0.65	27.43	33.26	0.23
Misa	Misa	3994	11JAN2018 0800	18.10	-0.79	0.42	-0.13	0.44	0.000163	0.64	28.44	33.28	0.22
Misa	Misa	3994	11JAN2018 0900	19.44	-0.79	0.44	-0.12	0.46	0.000176	0.67	29.00	33.28	0.23
Misa	Misa	3994	11JAN2018 1000	23.02	-0.79	0.47	-0.07	0.50	0.000220	0.77	30.00	33.29	0.26
Misa	Misa	3994	11JAN2018 1100	30.63	-0.79	0.53	0.01	0.58	0.000312	0.96	32.09	33.31	0.31
Misa	Misa	3994	11JAN2018 1200	47.21	-0.79	0.67	0.15	0.76	0.000464	1.28	36.96	33.36	0.39
Misa	Misa	3994	11JAN2018 1300	76.77	-0.79	0.96	0.38	1.10	0.000578	1.66	46.39	33.46	0.45
Misa	Misa	3994	11JAN2018 1400	109.14	-0.79	1.26	0.60	1.45	0.000612	1.95	56.39	33.57	0.48
Misa	Misa	3994	11JAN2018 1500	138.18	-0.79	1.51	0.77	1.75	0.000612	2.14	65.05	33.65	0.49
Misa	Misa	3994	11JAN2018 1600	155.00	-0.79	1.65	0.87	1.91	0.000615	2.25	69.61	33.70	0.50
Misa	Misa	3994	11JAN2018 1700	154.56	-0.79	1.65	0.87	1.90	0.000615	2.24	69.51	33.70	0.50
Misa	Misa	3994	11JAN2018 1800	145.70	-0.79	1.58	0.82	1.82	0.000611	2.19	67.20	33.68	0.49
Misa	Misa	3994	11JAN2018 1900	127.01	-0.79	1.42	0.71	1.63	0.000612	2.07	61.82	33.62	0.49
Misa	Misa	3994	11JAN2018 2000	106.55	-0.79	1.23	0.58	1.42	0.000608	1.93	55.68	33.56	0.48
Misa	Misa	3994	11JAN2018 2100	90.13	-0.79	1.07	0.47	1.24	0.000611	1.81	50.25	33.50	0.47
Misa	Misa	3994	11JAN2018 2200	74.95	-0.79	0.92	0.37	1.06	0.000603	1.67	45.13	33.45	0.46
Misa	Misa	3994	11JAN2018 2300	64.66	-0.79	0.80	0.29	0.93	0.000609	1.58	41.16	33.41	0.45
Misa	Misa	3994	12JAN2018 0000	56.27	-0.79	0.70	0.23	0.81	0.000617	1.50	37.70	33.37	0.45
Misa	Misa	3994	12JAN2018 0100	51.38	-0.79	0.64	0.19	0.75	0.000604	1.44	35.92	33.35	0.44
Misa	Misa	3994	12JAN2018 0200	47.57	-0.79	0.60	0.16	0.70	0.000587	1.38	34.59	33.34	0.43
Misa	Misa	3994	12JAN2018 0300	43.57	-0.79	0.56	0.12	0.65	0.000567	1.32	33.16	33.32	0.42
Misa	Misa	3994	12JAN2018 0400	41.22	-0.79	0.54	0.10	0.63	0.000534	1.27	32.64	33.32	0.41
Misa	Misa	3994	12JAN2018 0500	39.04	-0.79	0.54	0.08	0.62	0.000485	1.21	32.53	33.32	0.39
Misa	Misa	3994	12JAN2018 0600	37.27	-0.79	0.55	0.07	0.61	0.000436	1.15	32.66	33.32	0.37

Total area of cross section active flow.

Figure 28. Profile output table

Another way to access the simulation results is by checking directly either each cross-section or the entire river profile (Figures 29 and 30), where it is even possible to see an animation of the water surface elevation trend over time.

In this study, water depth is considered as a key parameter for comparative analysis under different boundary condition scenarios. It is defined as the difference between the water surface elevation (WSE) and the main channel bed elevation at each cross-section. Depth values are extracted along the river reach, with particular focus on bridge locations, in order to assess the influence of varying upstream and downstream conditions on the hydraulic behaviour of the flow.

$$\text{Depth} = \text{Water Surface elevation} - \text{Main channel elevation}$$

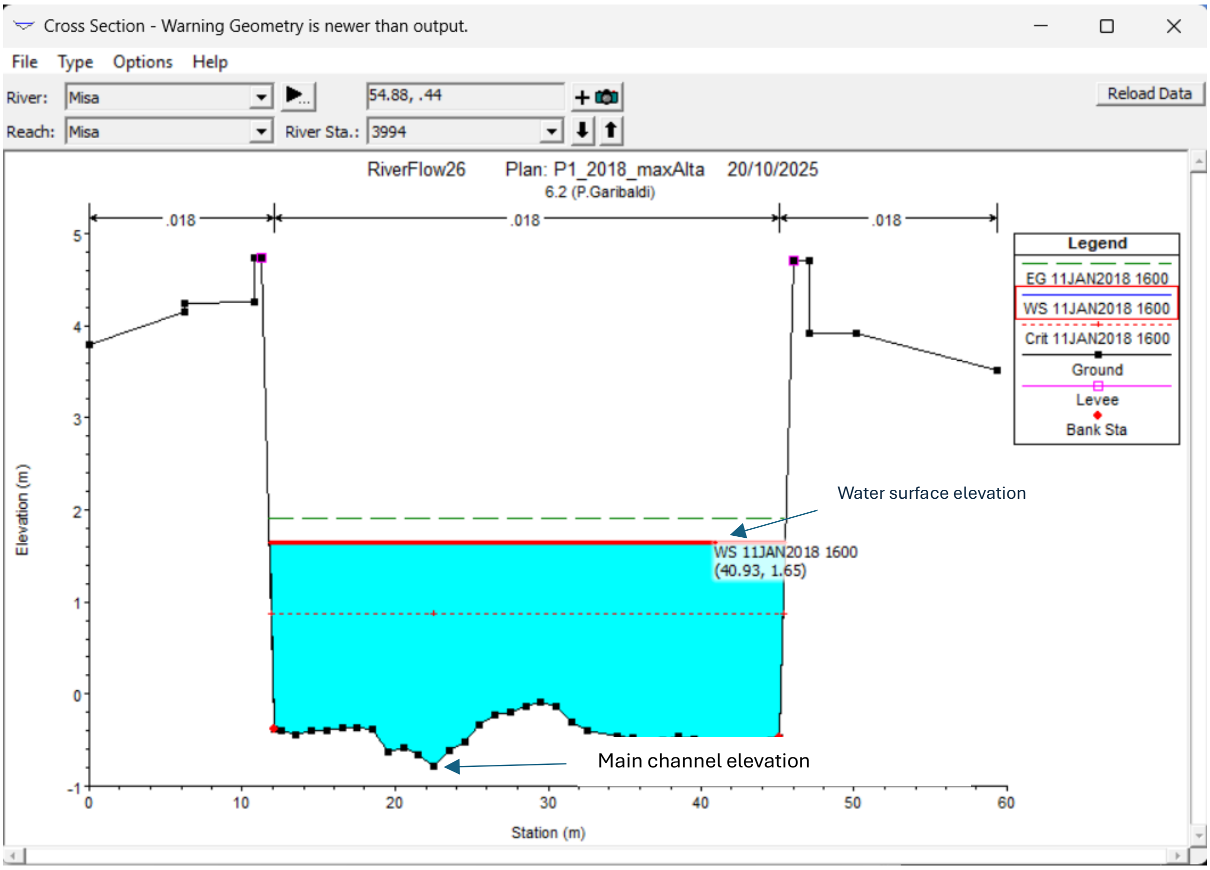

Figure 29. Water elevation at the river cross-section

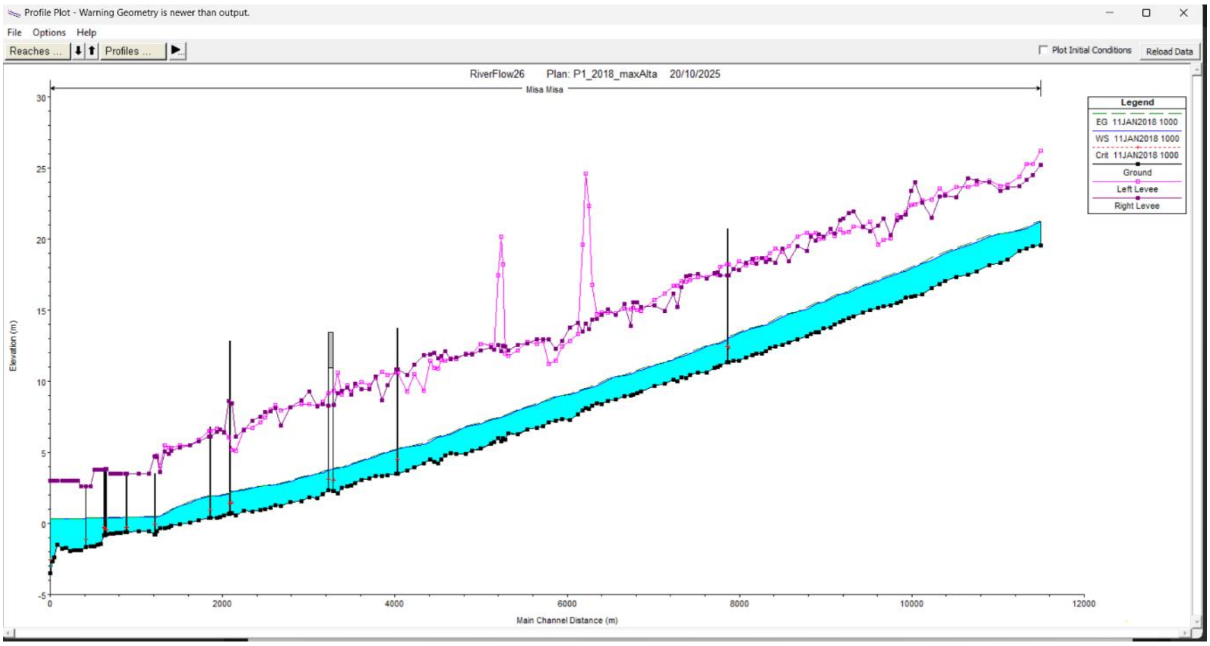

Figure 30. The black squares represent the thalweg points of each cross-section; the light and dark purple lines stand for the left and right levee, respectively; the vertical black lines display the bridges along the river profile; the light blue area represents the water-surface elevation.

4.3.4. Description and calibration of the adopted hydraulic model

The hydraulic simulations presented in this work were performed using an existing one-dimensional HEC-RAS model of the downstream reach of the Misa River. The model includes the river channel geometry, floodplain areas, and the three bridge crossings analysed in this study, namely Ponte Garibaldi, Ponte II Giugno, and Ponte Statale. The geometric data and model setup were derived from previous studies conducted on the Misa River (Rossetti, 2022).

The adopted model was previously calibrated and validated using field observations collected within the framework of monitoring activities carried out in the Misa River estuary. The calibration results, reported in Figure 31, show a clear improvement in the agreement between observed and simulated water levels after the model refinement. In particular, the updated configuration reproduces both the timing and magnitude of the main stage fluctuations more accurately than the baseline model, especially during the highest water-level peaks.

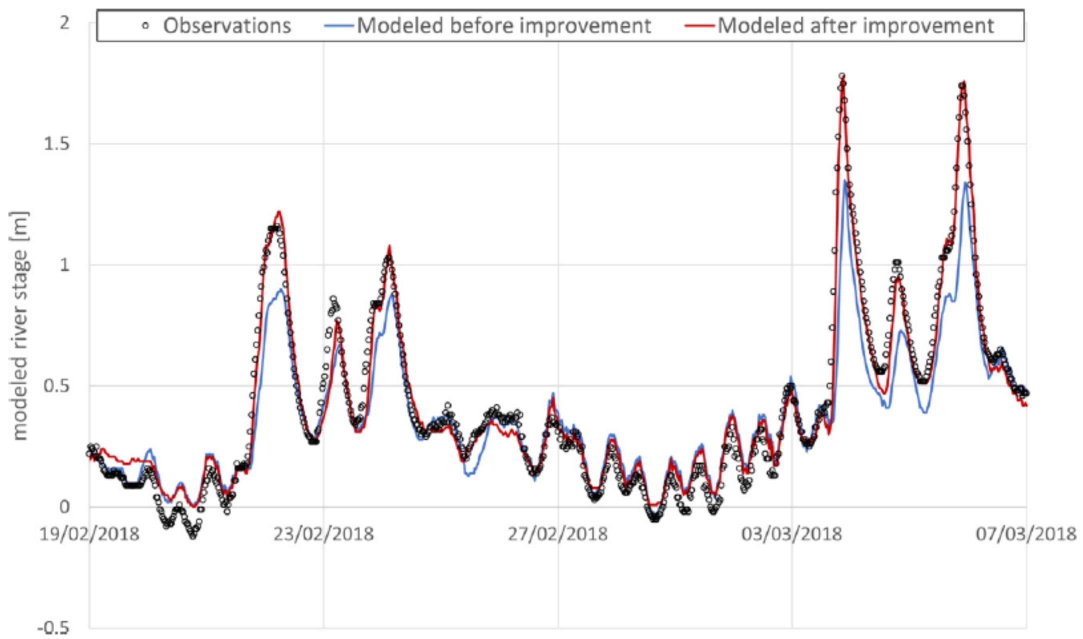

Figure 31. Time-series comparison at Ponte Garibaldi from 18 February to 07 March 2018 (calibration): stage observations (black dots) and numerical results for the baseline project (blue line) and after the improvement (red line) Postacchini el., 2025)

The reliability of the model is further confirmed by the validation results shown in Figure 32. The comparison between observed and simulated water levels for the entire year 2018 indicates a satisfactory agreement over a wide range of hydraulic conditions. The coefficient of determination ($R^2 = 0.919$) confirms the capability of the model to reproduce the observed hydraulic behaviour of the downstream reach of the Misa River.

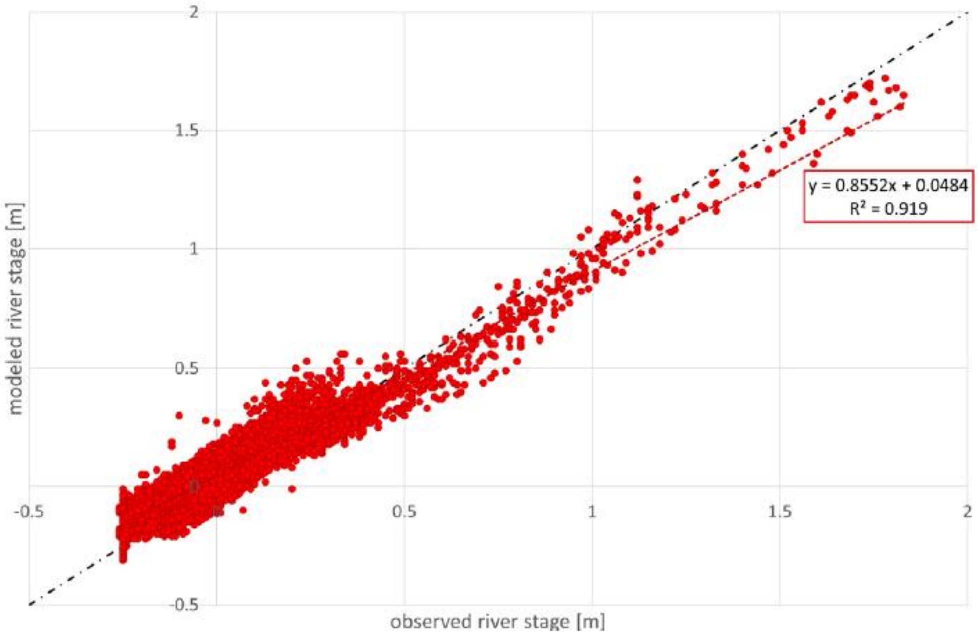

Figure 32. Scatter-plot comparison at Ponte Garibaldi during the whole 2018 (model validation): stage observations VS modelled results Postacchini el.,2025.

Based on these calibration and validation results, the model was considered sufficiently reliable and was therefore adopted to investigate the influence of different downstream boundary conditions on water depth and flow velocity along the downstream reach of the Misa River (Postacchini et al., 2025).

5. Results

The results of the hydraulic simulations are presented in terms of water depth (i.e., the distance between the water level and the talweg of the cross-section) and cross-section-averaged flow velocity at selected cross-sections located upstream of the Ponte Garibaldi, Ponte II Giugno, and Ponte Statale. The three bridges are located along the downstream urban reach of the Misa River, where the hydraulic response is influenced by the interaction between the upstream flood wave and the downstream tidal boundary condition.

As shown in Figure 33 below, the analysed bridge locations are situated within the final reach of the river. For each bridge, the results were extracted at the upstream cross-section in order to evaluate the local hydraulic response under the different downstream boundary condition scenarios.

Figure 33. Location of the Ponte Garibaldi, Ponte II Giugno, and Ponte Statale bridges along the downstream urban reach of the Misa River.

The results are organised according to the type of downstream boundary condition imposed at the river mouth. First, unsteady tidal boundary conditions are analysed. Then, steady downstream conditions are considered, including representative tidal levels, sensitivity scenarios, and additional extreme water-level cases.

For each group of simulations, the hydraulic response is compared for the two upstream hydrographs corresponding to the 2018 and 2023 flood events. Two reference instants are used throughout the analysis: XP, corresponding to the hydrograph peak, and h36, corresponding to 36 hours from the beginning of the simulation and representative of the recession limb. These instants are used to compare the system response during the flood peak and during moderate-flow conditions.

5.1. Unsteady downstream boundary conditions

A first set of analyses was carried out to investigate the hydraulic response of the Misa River under unsteady downstream boundary conditions. In these simulations, the upstream hydrographs were combined with time-varying tidal oscillations imposed at the downstream boundary, corresponding to the river mouth. A summary of the adopted simulation scenarios is provided in Table 2.

The analysed tidal conditions include maximum high tide (maxHT), maximum low tide (maxLT), minimum high tide (minHT), minimum low tide (minLT), and no tidal input (mean tide). The results are discussed at the three selected bridge sections, namely Ponte Garibaldi, Ponte II Giugno, and Ponte Statale, in order to evaluate the influence of the tidal signal on water depth and flow velocity along the downstream reach.

The section is organised according to the spatial sequence of the selected bridge sections along the analysed reach. The results are first presented for Ponte Garibaldi, followed by Ponte II Giugno and Ponte Statale. This comparison allows the spatial variation of the tidal influence to be assessed along the analysed river reach.

5.1.1. Ponte Garibaldi

The results obtained upstream of Ponte Garibaldi are presented in Figure 34, where the 2018 and 2023 events are compared in terms of water depth and cross-section-averaged velocity under unsteady downstream boundary conditions.

Around XP, the water-depth curves are almost overlapped for both events, indicating that the hydraulic response during the flood peak is mainly controlled by the upstream flood wave. A similar behaviour is observed for velocity, although the separation between tidal scenarios is slightly more visible, particularly during the 2018 event.

Before the flood peak and during the recession phase, the influence of the downstream tidal condition becomes clearer. Higher downstream water levels tend to maintain larger depths and lower velocities, whereas lower tidal levels are associated with slightly reduced depths and higher velocities. The separation between the curves becomes more evident around h36, when the upstream forcing decreases and the tidal contribution becomes relatively more significant.

The 2023 event produces higher depth and velocity values than the 2018 event because of the stronger upstream forcing. However, the relative influence of the tidal condition is more evident during the 2018 event, where the lower river forcing makes the downstream contribution easier to distinguish.

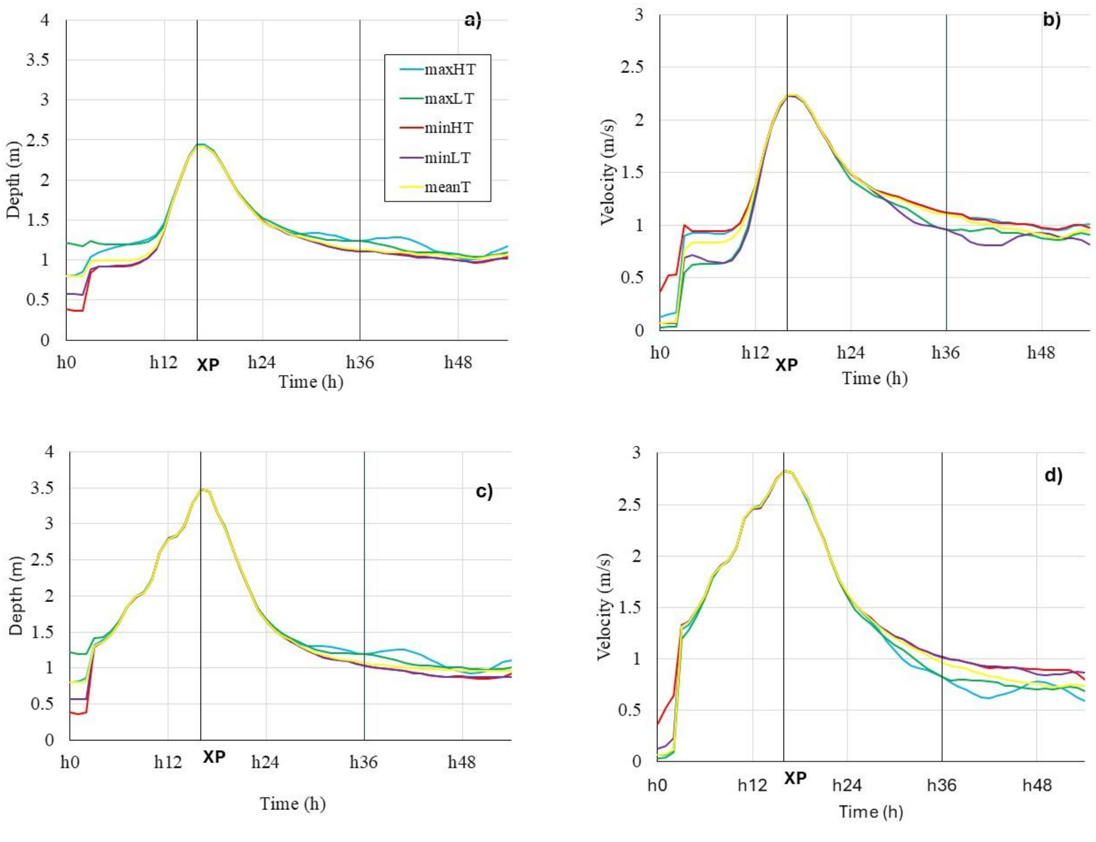

Figure 34. Temporal evolution of water depth and cross-section-averaged velocity upstream of the Ponte Garibaldi under unsteady downstream boundary conditions. Panels (a) and (b) refer to the 2018 event, while panels (c) and (d) refer to the 2023 event. The vertical lines indicate XP and h36. The legend shown in panel (a) applies to all panels.

As reported in Table 3, the influence of the unsteady tidal scenarios is limited at XP for both events. More evident differences occur at h36, where depth variations reach about 0.13 m in

2018 and 0.16 m in 2023, while velocity variations reach approximately 0.30 m/s and 0.20 m/s, respectively. These results indicate a stronger influence of the downstream boundary condition during the recession phase than at the flood peak.

Table 3 Water depth and cross-section-averaged velocity at the flood peak (XP) and along the recession limb (h36) for the unsteady downstream boundary condition scenarios at the Ponte Garibaldi section.

Scenarios	Downstream boundary condition	Event 2018				Event 2023			
		XP		36		XP		36	
		Depth (m)	Velocity (m/s)	Depth (m)	Velocity (m/s)	Depth (m)	Velocity (m/s)	Depth (m)	Velocity (m/s)
1 and 5	MaxHT	2.44	2.83	1.24	0.82	3.47	2.83	1.19	0.82
2 and 6	MaxLT	2.43	2.24	1.24	0.96	3.47	2.83	1.19	0.82
3 and 7	MinHT	2.42	2.24	1.11	1.12	3.47	2.83	1.04	1.01
4 and 8	MinLT	2.42	2.83	1.11	1.02	3.47	2.83	1.03	1.02
25 and26	0	2.42	2.24	1.13	1.1	3.47	2.83	1.07	0.96

5.1.2. Ponte II Giugno

The results obtained upstream of Ponte II Giugno are presented in Figure 35, where the 2018 and 2023 events are compared in terms of water depth and cross-section-averaged velocity under unsteady downstream boundary conditions.

Around XP, the water-depth curves are nearly superimposed for all tidal scenarios in both events, indicating that the hydraulic response is mainly controlled by the upstream flood wave. The same behaviour is observed for velocity, although a slightly larger separation among the tidal scenarios can be identified during the recession phase.

The influence of the downstream tidal condition becomes more evident after XP, particularly after h36. During this period, higher tidal levels tend to maintain slightly larger water depths and lower velocities, whereas lower tidal levels are associated with reduced depths and higher velocities. The effect is more pronounced for velocity than for water depth.

The 2023 event produces higher depth and velocity values than the 2018 event because of the stronger upstream forcing. Consequently, the relative influence of the tidal condition is less evident during the peak phase of the 2023 event and becomes distinguishable only during the recession period.

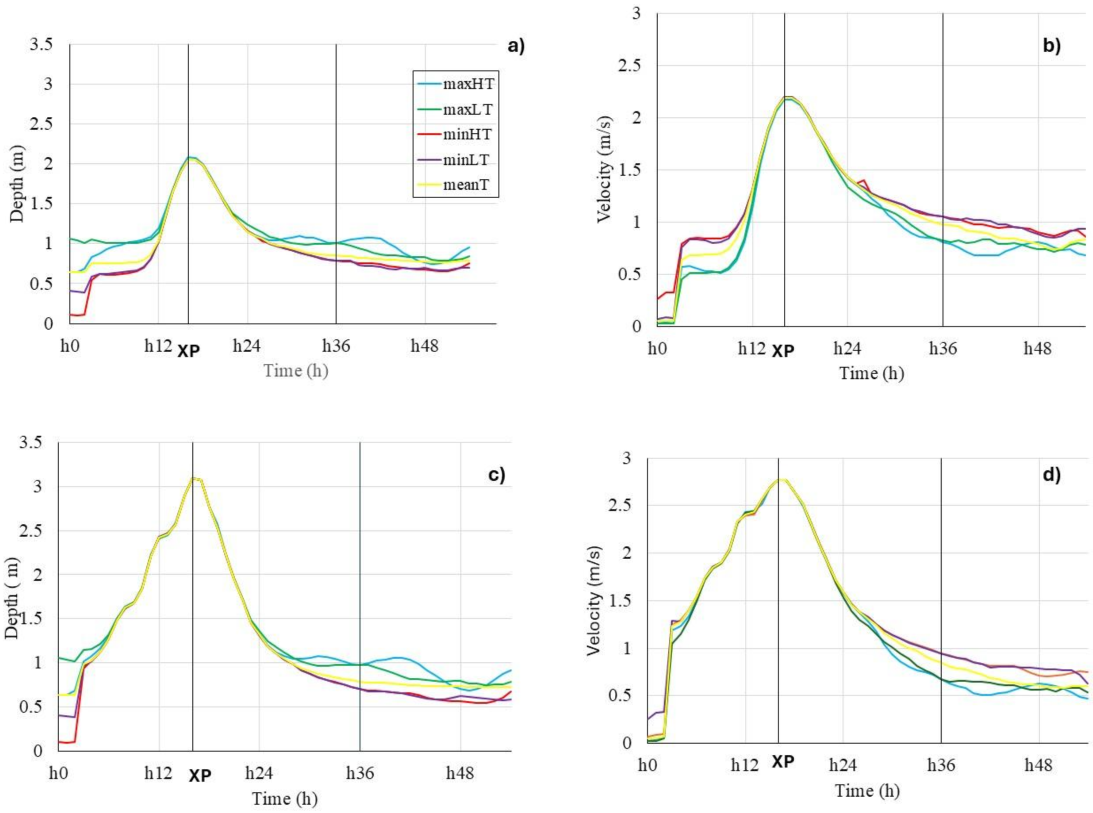

Figure 35. Water depth and cross-section-averaged velocity upstream of the Ponte II Giugno under unsteady downstream boundary conditions. Panels (a) and (b) refer to the 2018 event, while panels (c) and (d) refer to the 2023 event. The vertical lines indicate XP and h36. The legend shown in panel (a) applies to all panels.

As reported in Table 4, only minor differences are observed between the analysed scenarios at XP. At h36, depth variations increase to about 0.22 m in 2018 and 0.27 m in 2023, while velocity variations reach approximately 0.24 m/s and 0.27 m/s, respectively. This confirms the increasing effect of the downstream boundary condition during moderate-flow conditions.

Table 4 Water depth and cross-section-averaged velocity at the flood peak (XP) and along the recession limb (h36) for the unsteady downstream boundary condition scenarios at the Ponte II Giugno section.

Scenarios	Tide level (m)	Event 2018				Event 2023			
		XP		36		XP		36	
		Depth (m)	Velocity (m/s)	Depth (m)	Velocity (m/s)	Depth (m)	Velocity (m/s)	Depth (m)	Velocity (m/s)
1 and 5	MaxHT	2.08	2.17	1.01	0.81	3.09	2.77	0.98	0.68
2 and 6	MaxLT	2.05	2.19	1.01	0.82	3.09	2.77	0.98	0.68
3 and 7	MinHT	2.05	2.2	0.79	1.05	3.09	2.77	0.71	0.95
4 and 8	MinLT	2.05	2.2	0.79	1.05	3.09	2.77	0.71	0.95
25 and 26	0	2.05	2.19	0.85	0.98	3.09	2.77	0.79	0.85

5.1.3. Ponte Statale

The results obtained upstream of Ponte Statale are presented in Figure 36, where the 2018 and 2023 events are compared in terms of water depth and cross-section-averaged velocity under unsteady downstream boundary conditions.

Around XP, the water-depth and velocity curves remain largely controlled by the upstream flood wave, with only limited differences among the analysed tidal scenarios. However, after the flood peak, the influence of the downstream tidal condition becomes progressively more evident in both hydraulic variables.

The separation between the curves increases during the recession phase, particularly after h36. Higher tidal levels tend to maintain larger water depths and lower velocities, whereas lower tidal levels are associated with reduced depths and higher velocities. This behaviour is observed for both the 2018 and 2023 events and is more pronounced than at the upstream bridge sections.

As observed for the other locations, the 2023 event produces higher depth and velocity values because of the stronger upstream forcing. Nevertheless, the effect of the downstream tidal oscillations remains clearly visible during the later stages of the simulation, confirming the increasing influence of the river–sea interaction toward the downstream end of the analysed reach.

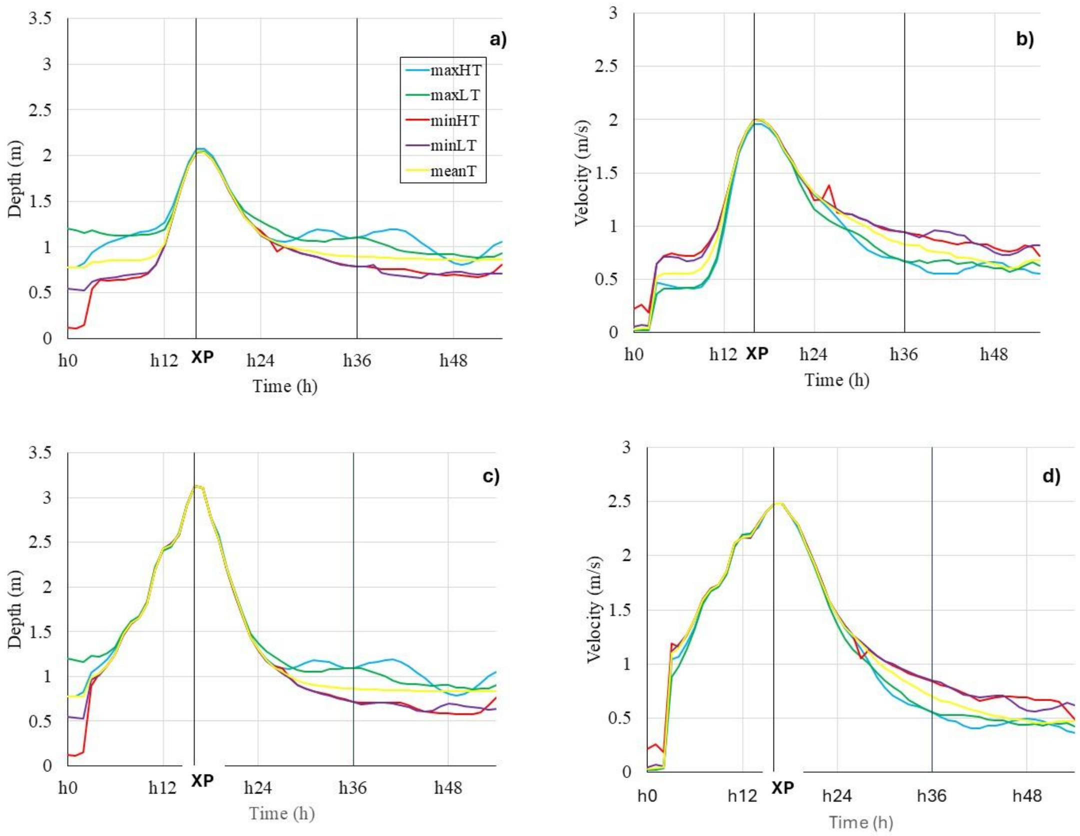

Figure 36. Water depth and cross-section-averaged velocity upstream of the Ponte Statale under unsteady downstream boundary conditions. Panels (a) and (b) refer to the 2018 event, while panels (c) and (d) refer to the 2023 event. The vertical lines indicate XP and h36. The legend shown in panel (a) applies to all panels.

As reported in Table 5, the analysed scenarios produce limited differences at XP, whereas a clearer separation is observed at h36. Depth variations reach about 0.32 m in 2018 and 0.37 m in 2023, while velocity variations reach approximately 0.27 m/s and 0.30 m/s, respectively. The results confirm the stronger influence of the downstream boundary condition during the recession phase.

Table 5 Water depth and cross-section-averaged velocity at the flood peak (XP) and along the recession limb (h36) for the unsteady downstream boundary condition scenarios at the Ponte Statale section.

Scenarios	Tide level (m)	Event 2018				Event 2023			
		XP		36		XP		36	
		Depth (m)	Velocity (m/s)	Depth (m)	Velocity (m/s)	Depth (m)	Velocity (m/s)	Depth (m)	Velocity (m/s)
1 and 5	MaxHT	2.07	1.96	1.11	0.67	3.13	2.48	1.09	0.55
2 and 6	MaxLT	2.04	1.99	1.11	0.67	3.13	2.48	1.09	0.55
3 and 7	MinHT	2.03	2	0.79	0.94	3.13	2.48	0.72	0.84
4 and 8	MinLT	2.03	2	0.79	0.94	3.13	2.48	0.72	0.85
25 and 26	0	2.04	2	0.89	0.83	3.13	2.48	0.87	0.7

5.1.4. Comparison between bridge sections

The results obtained at Ponte Garibaldi, Ponte II Giugno, and Ponte Statale are presented in Figures 34, 35, and 36, respectively. Comparing the three bridge sections makes it possible to evaluate how the influence of the unsteady downstream boundary condition changes along the analysed reach.

At all three bridge sections, the water-depth curves show limited differences between tidal scenarios around XP for both the 2018 and 2023 events, confirming the dominant role of the upstream flood wave during the peak phase. The separation between the curves becomes more

visible before the rising limb and during the recession phase, where positive tidal conditions produce a greater increase in water depth than the decrease associated with negative tidal conditions maintain slightly larger depths than lower tidal levels.

The velocity response highlights the tidal influence more clearly than the water depth. Lower tidal conditions are generally associated with higher velocities, whereas elevated downstream water levels produce lower values, particularly during the recession phase.

The comparison among the three bridge sections indicates that the hydraulic response at Ponte Garibaldi and Ponte II Giugno is very similar, with relatively limited differences between the tidal scenarios. At Ponte Statale, a clearer separation between the curves is observed, especially after h36, indicating a stronger influence of the downstream boundary condition. This behaviour is consistent with the location of Ponte Statale closer to the river mouth, where tidal forcing exerts a greater control on the hydraulic response.

To further evaluate the spatial variation of the tidal influence, Figures 37 and 38 compare the hydraulic response at the three bridge sections under the maximum high tide (maxHT) and minimum low tide (minLT) conditions, together with the corresponding no-tidal-input condition (meanT). These scenarios were selected because they represent the extreme positive and negative tidal conditions and therefore provide the clearest representation of the downstream boundary influence along the analysed reach.

For both flood events, the three bridge sections exhibit a similar temporal evolution. Under the maxHT condition, the largest water depths are generally observed at Ponte Garibaldi, while Ponte II Giugno and Ponte Statale show comparable values. In contrast, the minLT condition produces lower water depths and higher velocities, particularly during the recession phase. Around XP, the differences between the tidal and no-tidal-input conditions remain limited, whereas a clearer separation develops after the flood peak and around h36. The effect is most evident at Ponte Statale, confirming that the influence of the downstream boundary condition increases towards the river mouth and becomes more relevant during moderate-flow conditions than during the peak stage.

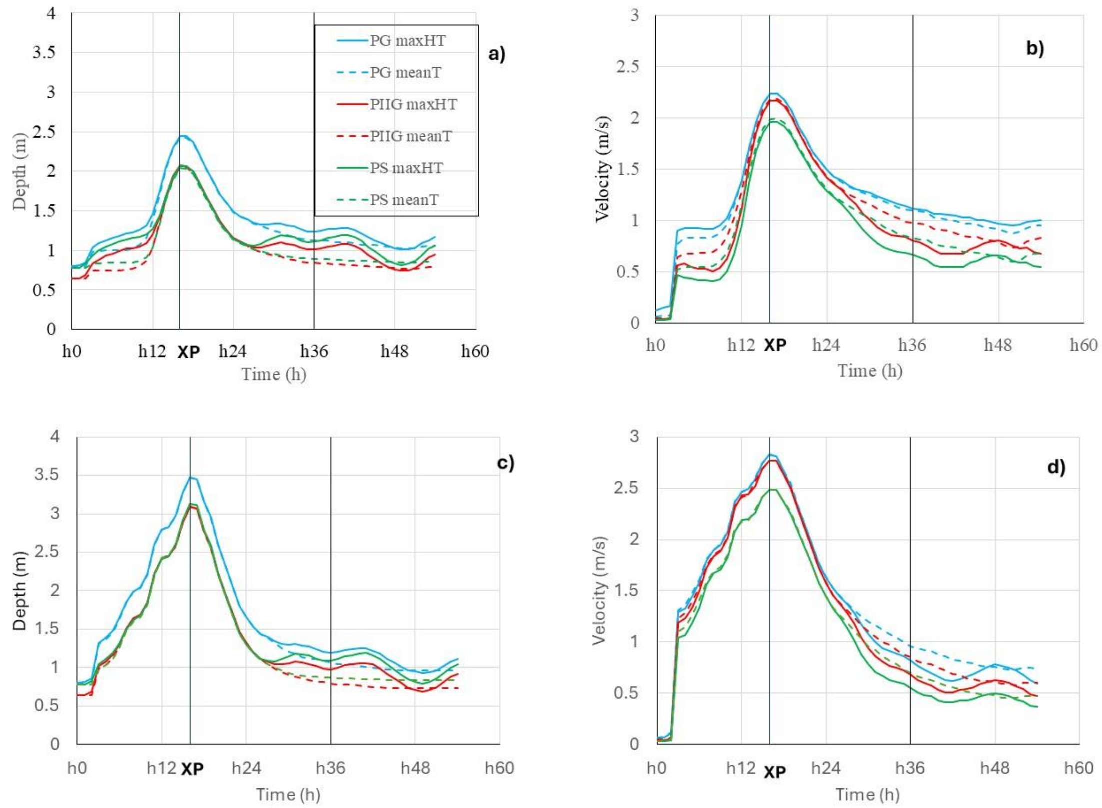

Figure 37 . Comparison of water depth and cross-section-averaged velocity at Ponte Garibaldi (PG), Ponte II Giugno (PIIG), and Ponte Statale (PS) under the maximum high tide (maxHT) and no-tidal-input (meanT) conditions. Panels (a) and (b) show water depth and velocity for the 2018 event. The vertical lines indicate the flood peak (XP) and the recession phase reference time (h36).

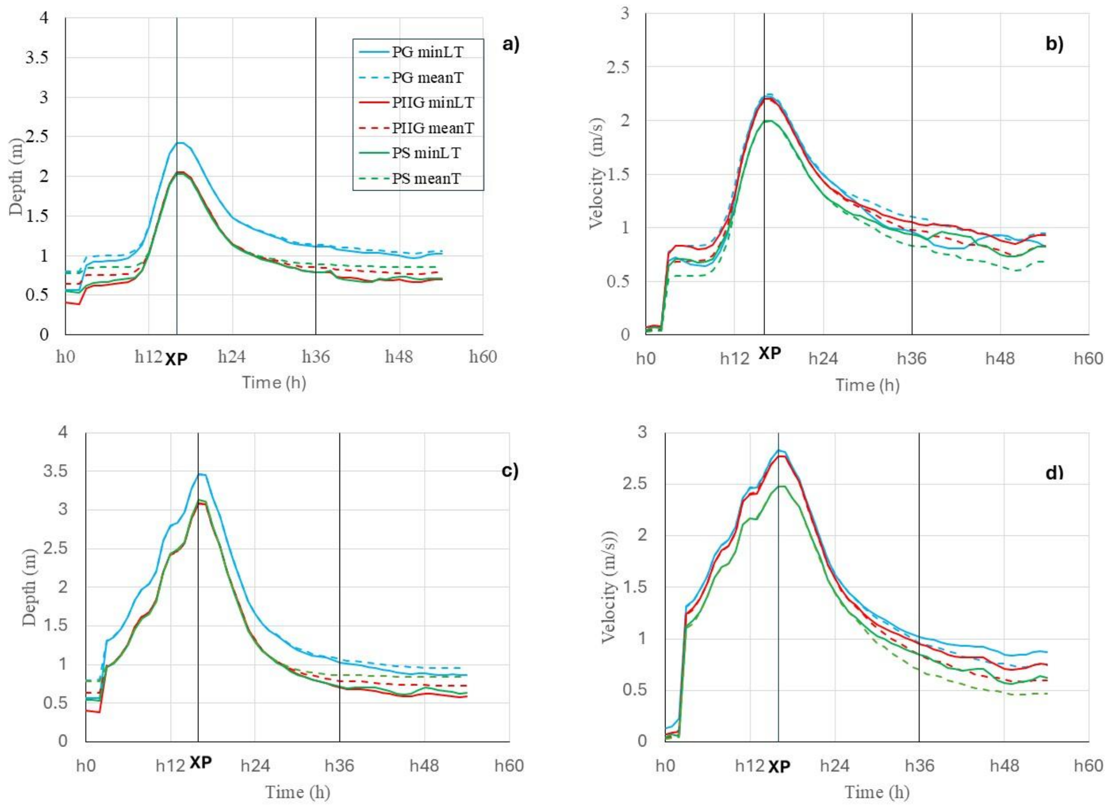

Figure 38. Comparison of water depth and cross-section-averaged velocity at Ponte Garibaldi (PG), Ponte II Giugno (PIIG), and Ponte Statale (PS) under the minimum low tide (minLT) and no-tidal-input (meanT) conditions. Panels (a) and (b) show water depth and velocity for the 2018 event, respectively, while panels (c) and (d) show the corresponding results for the 2023 event. The vertical lines indicate the flood peak (XP) and the recession phase reference time (h36).

To provide a concise quantitative summary of the analysed scenarios, Table 6 reports the water depth and cross-section-averaged velocity at XP and h36 for the 2018 event at Ponte Garibaldi. The selected section is representative of the overall trends observed at the other bridge sections and allows a direct comparison of the hydraulic response under the different downstream boundary conditions.

Table 6. Summary of water depth and cross-section-averaged velocity at XP and h36 for the 2018 event at Ponte Garibaldi under the analysed downstream boundary conditions. The selected section is representative of the trends observed at the other bridge sections.

Scenarios	Upstream boundary condition	Downstream boundary condition	Level at XP	Velocity at XP	Level at h36	Velocity at h36
1	Stage 2018	Max high tide	2.44	2.83	1.24	0.82
2	Stage 2018	Max low tide	2.43	2.24	1.24	0.96
3	Stage 2018	Min high tide	2.42	2.24	1.11	1.12
4	Stage 2018	Min low tide	2.42	2.83	1.11	1.02
5	Stage 2023	Max high tide	2.44	2.83	1.24	0.82
6	Stage 2023	Max low tide	2.43	2.24	1.24	0.96
7	Stage 2023	Min high tide	2.42	2.24	1.11	1.12
8	Stage 2023	Min low tide	2.42	2.83	1.11	1.02
9	Stage 2018	Max high tide1.609	2.76	1.93	2.46	0.4
10	Stage 2018	Max low tide 0.235	2.43	2.24	1.23	0.97
11	Stage 2018	Min high tide 1.591	2.74	1.94	2.44	0.4
12	Stage 2018	Min low tide -0.236	2.42	2.24	1.11	1.12
13	Stage 2018	Max high tide 0.52	2.44	2.22	1.43	0.79
14	Stage 2018	Max low tide 0.14	2.43	2.24	1.18	1.03
15	Stage 2018	Min high tide -0.2	2.42	2.24	1.11	1.12
16	Stage 2018	Min low tide -0.72	2.42	2.24	1.1	1.13
17	Stage 2023	Max high tide 0.52	2.44	2.22	1.43	0.79
18	Stage 2023	Max low tide 0.14	2.43	2.24	1.18	1.03
19	Stage 2023	Min high tide -0.2	2.42	2.24	1.11	1.12
20	Stage 2023	Min low tide -0.72	2.42	2.24	1.1	1.13
21	Stage 2018	-0.5	2.42	2.24	1.12	1.11
22	Stage 2018	1	2.5	2.16	1.87	0.56
23	Stage 2023	-0.5	2.42	2.24	1.12	1.11
24	Stage 2023	1	2.5	2.16	1.87	0.56
25	Stage 2018	0	2.42	2.24	1.13	1.1
26	Stage 2023	0	2.42	2.24	1.13	1.1

5.2. Steady downstream boundary conditions

After the unsteady tidal simulations, steady downstream boundary conditions were considered to examine the hydraulic response of the river under constant water-level conditions at the mouth. In this case, the downstream level was kept fixed throughout the event, making the effect of each imposed boundary condition easier to identify.

The steady simulations were organised into three groups: representative tidal levels, sensitivity scenarios, and additional extreme steady water-level conditions. The results for each group are presented in the following subsections.

5.2.1. Representative steady tidal levels and mean tide

The first group considers the representative tidal levels derived from the previous unsteady analysis: maximum high tide, maximum low tide, minimum high tide, and minimum low tide, together with the mean tide condition. These correspond to constant downstream water levels of 0.52 m, 0.14 m, −0.20 m, −0.72 m, and 0 m, respectively.

The results obtained at the three bridge sections are shown in Figures 39–41. In these simulations, the imposed downstream level produces a clear ordering of the hydraulic response. Higher downstream levels are associated with larger water depths and lower velocities, while lower levels lead to smaller depths and higher velocities. This separation is mainly visible before the rising limb and during the recession phase, whereas the curves tend to converge around **XP**, where the upstream flood wave controls the response.

Moving toward the downstream bridge sections, the separation between the steady tidal scenarios becomes more evident. At Ponte Garibaldi, the effect of the imposed downstream level is visible, especially during the recession phase. At Ponte II Giugno, the same pattern becomes clearer, while at Ponte Statale the separation is most pronounced, particularly in the velocity response. This suggests that the downstream boundary condition has a stronger influence toward the lower part of the analysed reach.

The comparison between the two events shows that the 2023 flood produces higher depths and velocities than the 2018 event. However, the relative effect of the imposed downstream level is easier to distinguish in the 2018 case, while the stronger 2023 flood wave reduces the separation between the curves near the peak. Around **h36**, the downstream effect becomes visible again, especially in the velocity plots.

These representative steady simulations show that the imposed downstream level has a limited effect during the flood peak but becomes more relevant under moderate-flow conditions. The physical interpretation of this behaviour and its comparison with the unsteady scenarios are discussed in Chapter 6.

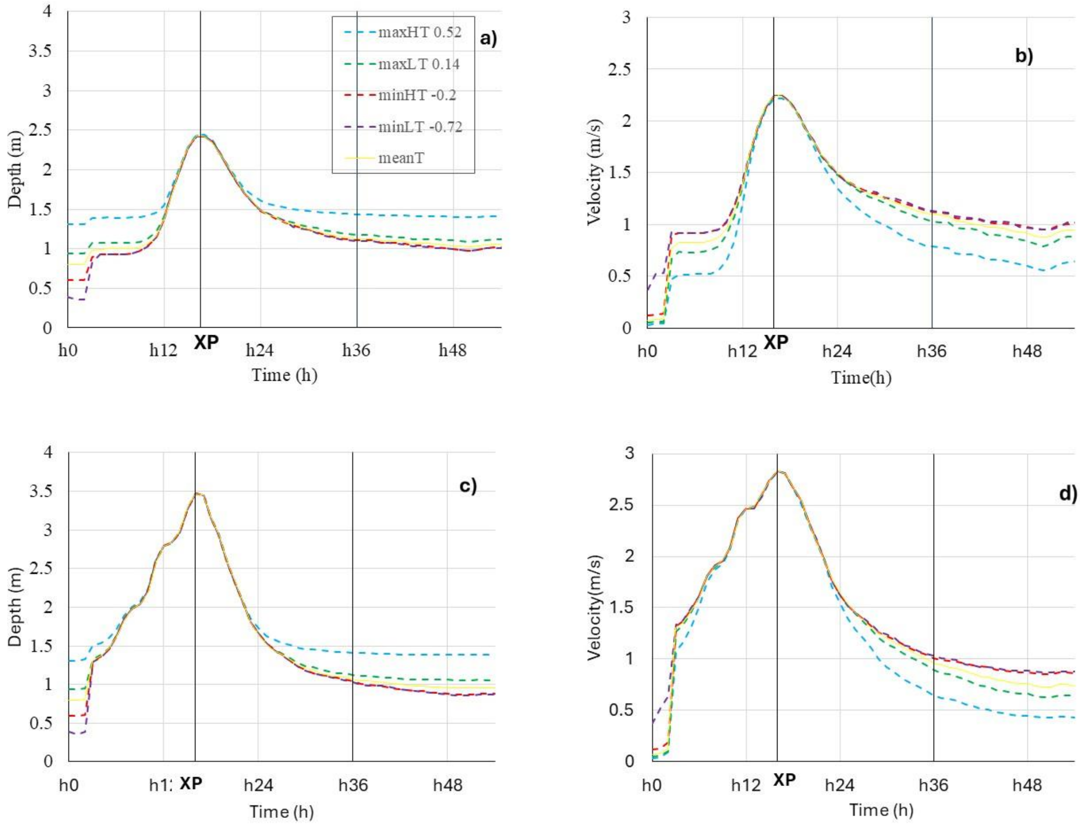

Figure 39. Water depth and cross-section-averaged velocity upstream of the Ponte Garibaldi under representative steady downstream tidal levels. Panels (a) and (b) refer to the 2018 event, while panels (c) and (d) refer to the 2023 event. The vertical lines indicate XP and h36. The legend shown in panel (a) applies to all panels.

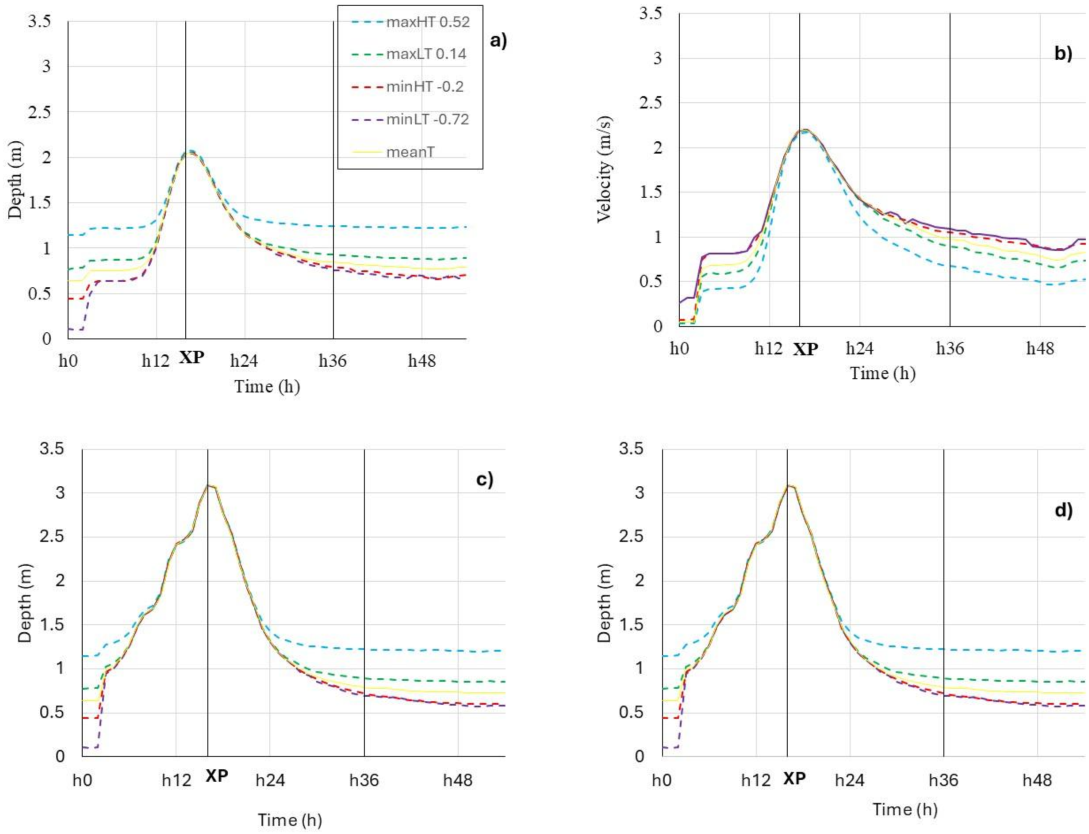

Figure 40. Water depth and cross-section-averaged velocity upstream of the Ponte II Giugno under representative steady downstream tidal levels. Panels (a) and (b) refer to the 2018 event, while panels (c) and (d) refer to the 2023 event. The vertical lines indicate XP and h36. The legend shown in panel (a) applies to all panels.

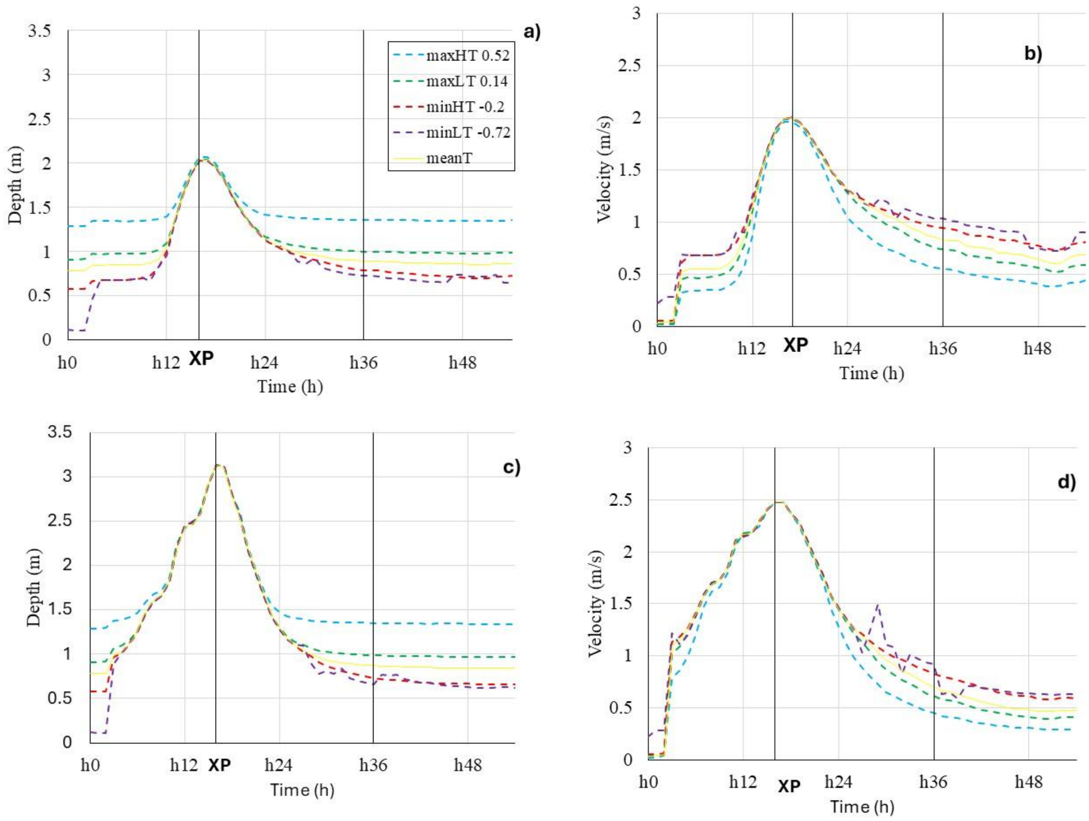

Figure 41. Water depth and cross-section-averaged velocity upstream of the Ponte Statale under representative steady downstream tidal levels. Panels (a) and (b) refer to the 2018 event, while panels (c) and (d) refer to the 2023 event. The vertical lines indicate XP and h36. The legend shown in panel (a) applies to all panels.

A quantitative summary of the hydraulic response is reported in Tables 7–9 for Ponte Garibaldi, Ponte II Giugno, and Ponte Statale, respectively. At the flood peak (XP), the effect of the imposed downstream water level is limited at all three bridge sections. For the 2018 event, water-depth variations range from approximately 0.08 m at Ponte Garibaldi to 0.17 m at Ponte Statale, while velocity variations remain below 0.16 m/s. For the 2023 event, both water depth and velocity are almost unchanged among the analysed scenarios, indicating that the hydraulic response during peak-flow conditions is primarily governed by the upstream flood wave.

Table 7. Water depth and cross-section-averaged velocity at the flood peak (XP) and along the recession limb (h36) for the representative steady tidal levels and sensitivity scenarios at the Ponte Garibaldi section.

Scenarios	Tide level (m)	Event 2018				Event 2023			
		XP		36		XP		36	
		Depth (m)	Velocity (m/s)	Depth (m)	Velocity (m/s)	Depth (m)	Velocity (m/s)	Depth (m)	Velocity (m/s)
22 and 24	1	2.5	2.16	1.87	0.56	3.47	2.82	1.86	0.46
13 and 17	0.52	2.44	2.22	1.43	0.79	3.47	2.83	1.41	0.65
14 and 18	0.14	2.43	2.24	1.18	1.03	3.47	2.83	1.12	0.9
15 and 19	-0.2	2.42	2.24	1.11	1.12	3.47	2.83	1.04	1.01
21 and 23	-0.5	2.42	2.24	1.12	1.11	3.47	2.83	1.04	1.01
16 and 20	-0.72	2.42	2.24	1.1	1.13	3.47	2.83	1.03	1.03
25 and 26	0	2.42	2.24	1.13	1.1	3.47	2.83	1.07	0.96

Table 8. Water depth and cross-section-averaged velocity at the flood peak (XP) and along the recession limb (h36) for the representative steady tidal levels and sensitivity scenarios at the Ponte II Giugno section.

Scenarios	Tide level (m)	Event 2018				Event 2023			
		XP		36		XP		36	
		Depth (m)	Velocity (m/s)	Depth (m)	Velocity (m/s)	Depth (m)	Velocity (m/s)	Depth (m)	Velocity (m/s)
22 and 24	1	2.17	2.07	1.69	0.49	3.09	2.77	1.69	0.39
13 and 17	0.52	2.08	2.17	1.24	0.67	3.09	2.77	1.23	0.55
14 and 18	0.14	2.05	2.19	0.93	0.89	3.09	2.77	0.89	0.75
15 and 19	-0.2	2.05	2.2	0.79	1.05	3.09	2.77	0.72	0.94
21 and 23	-0.5	2.05	2.2	0.78	1.09	3.09	2.77	0.71	0.94
16 and 20	-0.72	2.05	2.2	0.76	1.09	3.09	2.77	0.69	0.98
25 and 26	0	2.05	2.19	0.85	0.98	3.09	2.77	0.78	0.85

Table 9. Water depth and cross-section-averaged velocity at the flood peak (XP) and along the recession limb (h36) for the representative steady tidal levels and sensitivity scenarios at the Ponte Statale section.

Scenarios	Tide level (m)	Event 2018				Event 2023			
		XP		36		XP		36	
		Depth (m)	Velocity (m/s)	Depth (m)	Velocity (m/s)	Depth (m)	Velocity (m/s)	Depth (m)	Velocity (m/s)
22 and 24	1	2.2	1.84	1.83	0.41	3.12	2.48	1.83	0.33
13 and 17	0.52	2.07	1.96	1.36	0.55	3.13	2.48	1.35	0.45
14 and 18	0.14	2.04	1.99	1	0.74	3.13	2.48	0.99	0.61
15 and 19	-0.2	2.03	2	0.79	0.94	3.13	2.48	0.73	0.83
21 and 23	-0.5	2.03	2	0.73	1.08	3.13	2.48	0.72	0.85
16 and 20	-0.72	2.03	2	0.73	1.04	3.13	2.48	0.66	0.92
25 and 26	0	2.04	2	0.89	0.83	3.13	2.48	0.87	0.7

5.2.2. Sensitivity scenarios

A further set of steady simulations was carried out by imposing simplified constant downstream water levels of −0.5 m, 0 m, and 1 m. These scenarios were introduced to test the sensitivity of the hydraulic response to controlled variations in the downstream water level.

The results obtained at Ponte Garibaldi, Ponte II Giugno, and Ponte Statale are shown in Figures 42–44. Compared with the representative tidal levels, these scenarios provide a clearer indication of how the model responds to simplified changes in the imposed downstream condition.

The response follows the expected hydraulic pattern. The **1 m** condition produces the largest water depths for both events, especially before the rising limb and during the recession phase, while also causing a marked reduction in velocity. Conversely, the **−0.5 m** condition generally produces lower water depths and higher velocities, with the mean tide condition lying between the two sensitivity levels.

Around **XP**, the differences between the three scenarios remain small, particularly for the 2023 event, confirming that the flood peak is mainly governed by the upstream hydrograph. The imposed downstream level becomes more influential during the recession phase, especially around **h36**, where the separation between the curves is more evident.

Along the analysed reach, the effect of the sensitivity scenarios increases moving downstream. At Ponte Garibaldi, the separation between scenarios is visible mainly after the peak. At Ponte II Giugno, the same pattern becomes clearer, while at Ponte Statale the response is the most pronounced, particularly during moderate-flow conditions and in the velocity curves. This confirms that velocity is generally more sensitive than water depth to variations in the imposed downstream level.

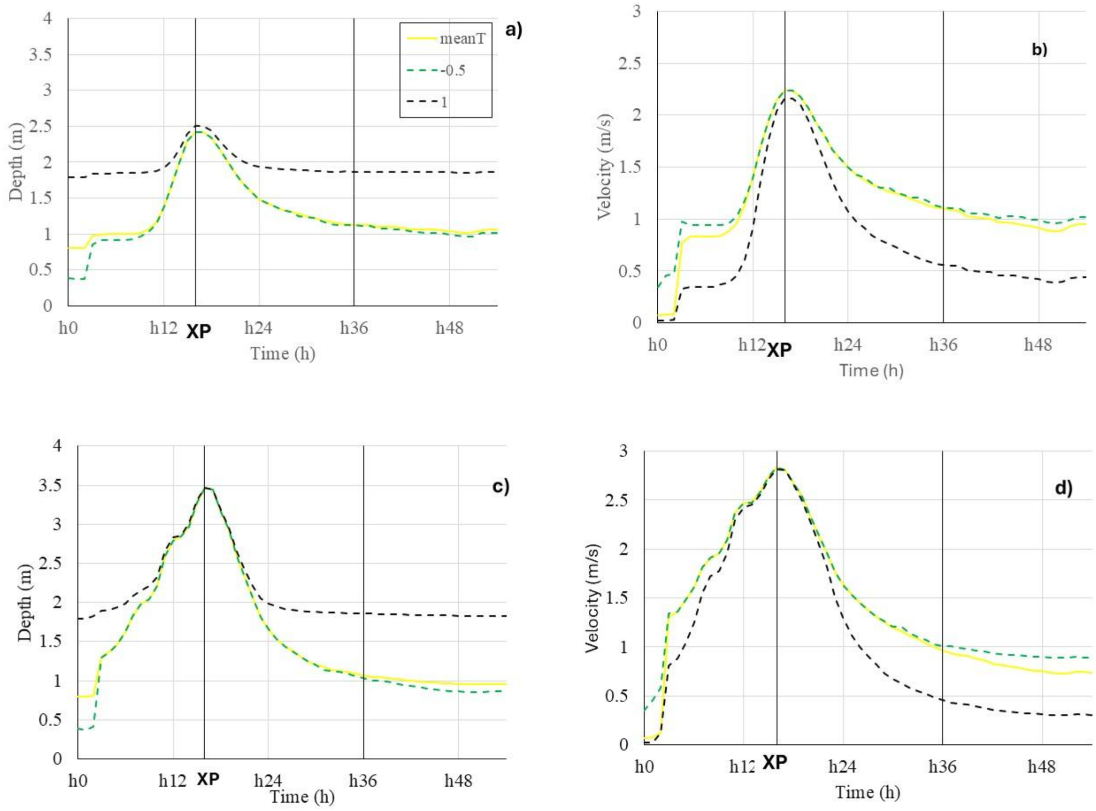

Figure 42. Water depth and cross-section-averaged velocity upstream of the Ponte Garibaldi under steady sensitivity scenarios. Panels (a) and (b) refer to the 2018 event, while panels (c) and (d) refer to the 2023 event. The imposed downstream water levels are −0.5 m, 0 m, and 1 m. The vertical lines indicate XP and h36. The legend shown in panel (a) applies to all panels.

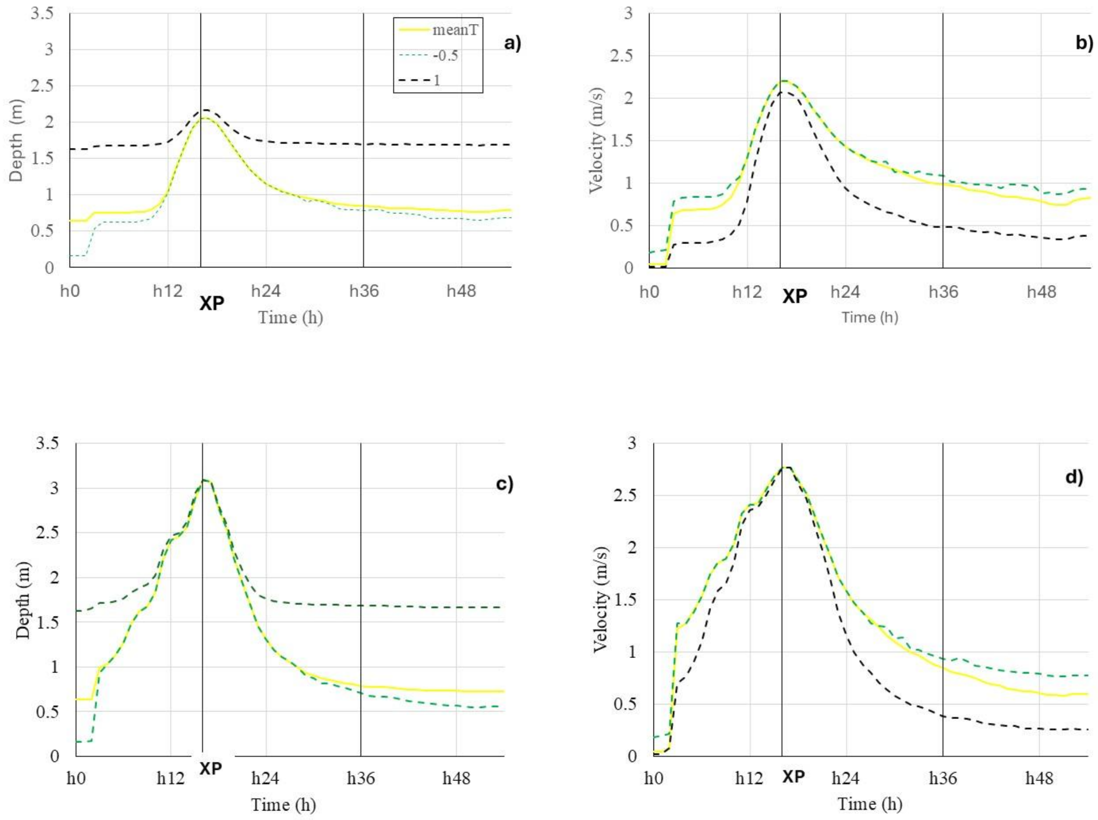

Figure 43. Water depth and cross-section-averaged velocity upstream of the Ponte II Giugno under steady sensitivity scenarios. Panels (a) and (b) refer to the 2018 event, while panels (c) and (d) refer to the 2023 event. The imposed downstream water levels are −0.5m,0 m, and 1 m. The vertical lines indicate XP and h36. The legend shown in panel (a) applies to panels.

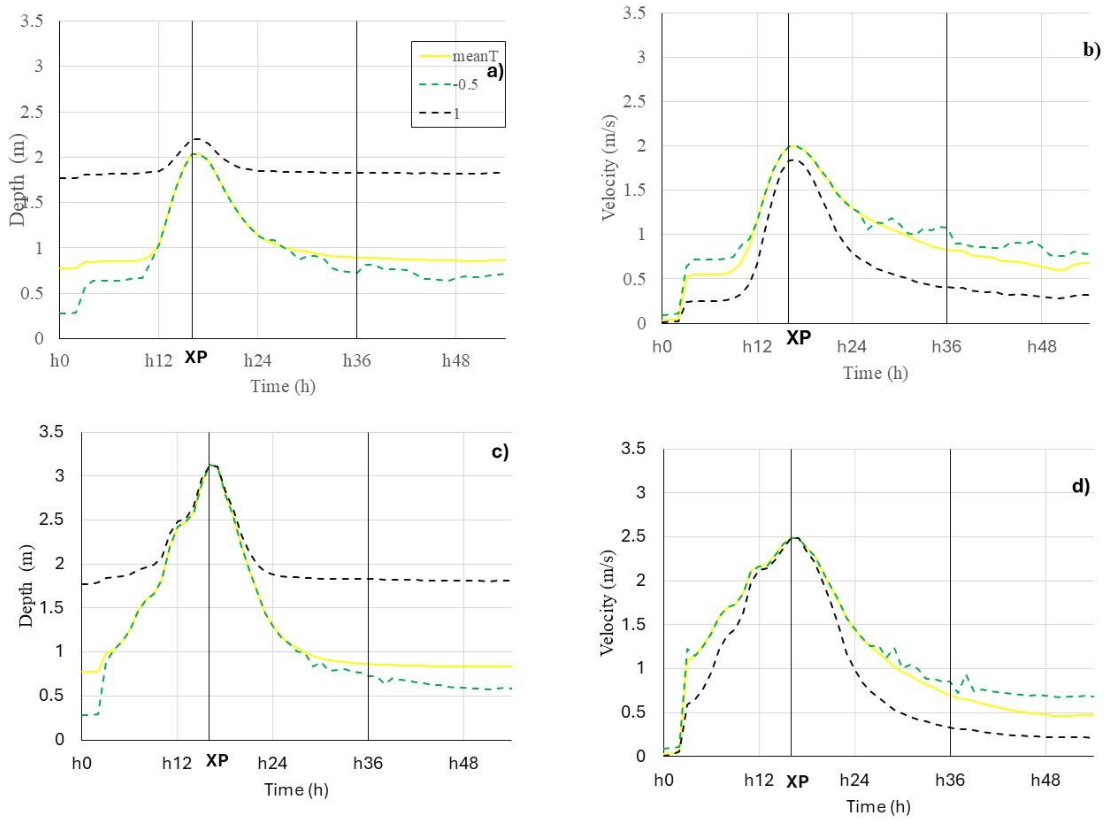

Figure 44. Water depth and cross-section-averaged velocity upstream of the Ponte Statale under steady sensitivity scenarios. Panels (a) and (b) refer to the 2018 event, while panels (c) and (d) refer to the 2023 event. The imposed downstream water levels are −0.5 m, 0 m and 1 m. The vertical lines indicate XP and h36. The legend shown in panel (a) applies to all panels.

As reported in Tables 7–9, a different behaviour emerges during the recession phase (h36), when the influence of the downstream boundary condition becomes progressively more evident. In all sections, higher tidal levels are associated with larger water depths and lower velocities, whereas lower tidal levels result in reduced depths and increased velocities. The magnitude of these differences increases from the upstream to the downstream bridge sections. For the 2018 event, water-depth variations increase from approximately 0.77 m at Ponte Garibaldi to 1.10 m at Ponte Statale, while velocity variations range between about 0.57 and 0.67 m/s. A similar trend is observed for the 2023 event, with depth variations increasing from approximately 0.83 m to 1.17 m and velocity variations remaining close to 0.60 m/s.

The comparison among the three bridge sections highlights a gradual increase in the influence of the downstream boundary condition towards the river mouth. While the flood peak remains largely controlled by the upstream discharge, the recession phase is increasingly affected by tidal forcing, resulting in a clearer separation between the analysed scenarios at the downstream sections.

5.2.3. Extreme steady conditions

The final group of steady simulations considers additional downstream water-level conditions applied to the 2018 event. These scenarios include **1.609 m, 0.235 m, 1.591 m, and −0.236 m**, together with the mean tide condition. The results obtained at Ponte Garibaldi, Ponte II Giugno, and Ponte Statale are shown in Figures 45–47.

Compared with the previous steady cases, these simulations produce a stronger contrast between the highest downstream levels and the remaining scenarios. The two high-water-level conditions, **1.609 m** and **1.591 m**, maintain water depths well above the mean tide case over a large part of the simulation. Their effect is visible before the rising limb, around XP, and during the recession phase, indicating that sufficiently high downstream levels can influence a wider portion of the hydrograph.

The velocity response follows the same pattern, but in the opposite direction. Under the highest downstream levels, velocity is strongly reduced, especially after the peak and around **h36**. In contrast, the lower downstream levels, **0.235 m** and **−0.236 m**, remain closer to the mean tide response and produce more limited changes in both depth and velocity.

This behaviour is observed at all three bridge sections, although the response becomes clearer toward the downstream part of the analysed reach. At Ponte Garibaldi, the separation between scenarios is visible mainly during the recession phase. At Ponte II Giugno, the effect becomes more pronounced, while at Ponte Statale the high downstream levels produce the strongest separation from the remaining cases, particularly in the velocity response. These simulations show that, under sufficiently high steady downstream levels, the downstream boundary condition can affect not only the recession limb but also the hydraulic response near the flood peak.

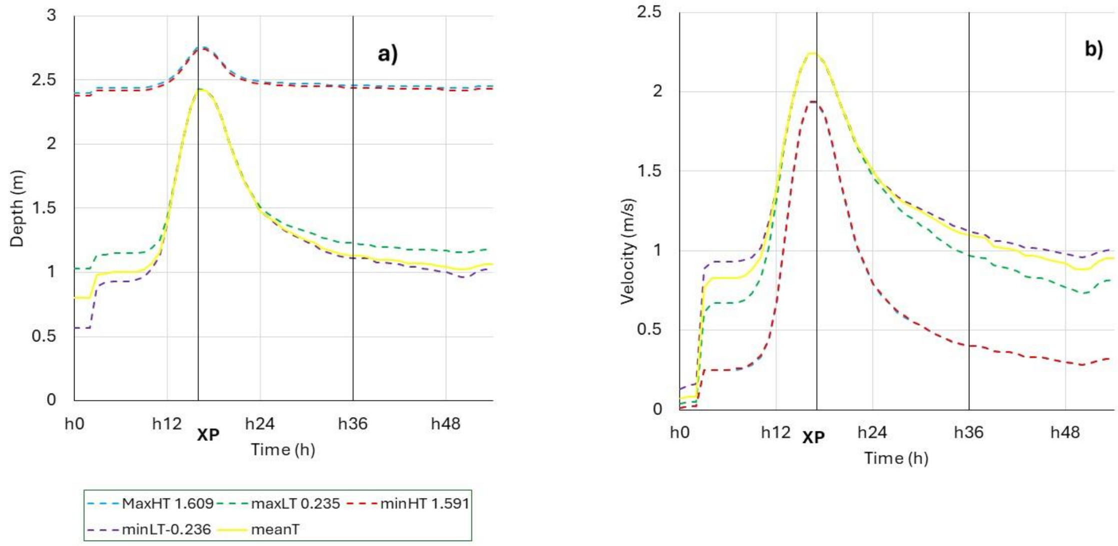

Figure 45. Water depth and cross-section-averaged velocity upstream of the Ponte Garibaldi under additional extreme steady downstream conditions for the 2018 event. The imposed downstream water levels are 1.609 m, 0.235 m, 1.591 m, and −0.236 m, together with the mean tide condition. The vertical lines indicate XP and h36. The legend applies both panels.

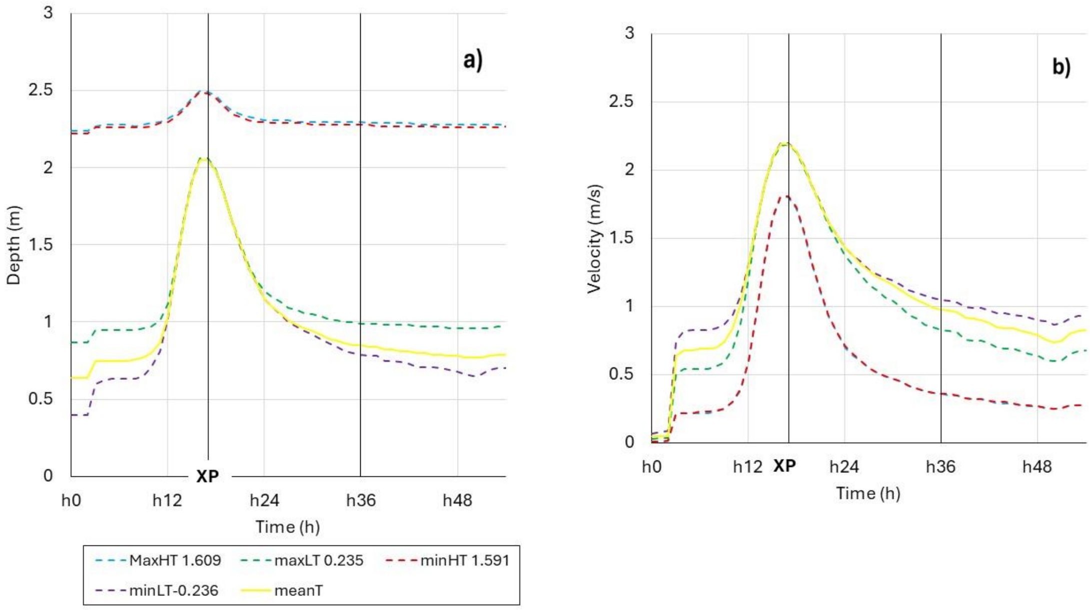

Figure 46. Water depth and cross-section-averaged velocity upstream of the Ponte II Giugno under additional extreme steady downstream conditions for the 2018 event. The imposed downstream water levels are 1.609 m, 0.235 m, 1.591 m, and −0.236 m, together with the mean tide condition. The vertical lines indicate XP and h36. The legend applies to both panels.

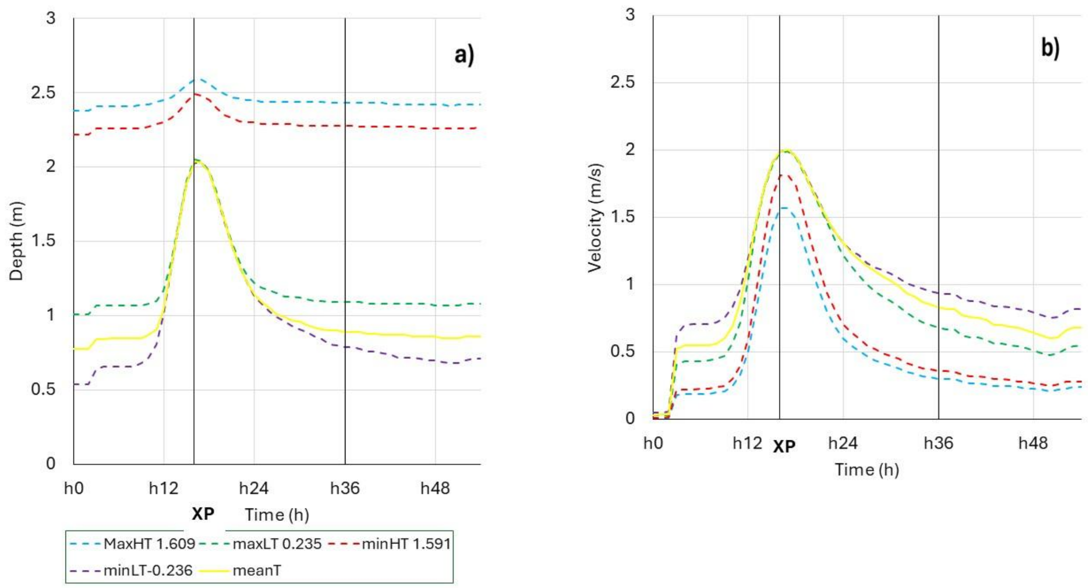

Figure 47. Water depth and cross-section-averaged velocity upstream of the Ponte Statale under additional extreme steady downstream conditions for the 2018 event. The imposed downstream water levels are 1.609 m, 0.235 m, 1.591 m, and −0.236 m, together with the mean tide condition. The vertical line indicates XP and h36. The legend applies to both panels.

A quantitative summary of the hydraulic response under the extreme steady tidal level scenarios is reported in Tables 10–12 for Ponte Garibaldi, Ponte II Giugno, and Ponte Statale, respectively. Compared with the representative steady scenarios, the extreme tidal levels produce a more pronounced hydraulic response at all bridge sections. At the flood peak (XP), water-depth variations range from approximately 0.34 m at Ponte Garibaldi to 0.56 m at Ponte Statale, while velocity variations range between about 0.31 and 0.43 m/s. The influence of the downstream boundary condition becomes substantially stronger during the recession phase (h36), where water-depth variations reach approximately 1.35 m, 1.51 m, and 1.64 m at Ponte Garibaldi, Ponte II Giugno, and Ponte Statale, respectively. The corresponding velocity variations reach about 0.72 m/s, 0.69 m/s, and 0.64 m/s. These results confirm that extreme sea-level conditions substantially amplify the influence of the downstream boundary condition, particularly at the downstream bridge sections.

Table 10 Water depth and cross-section-averaged velocity at the flood peak (XP) and along the recession limb (h36) for the extreme steady tidal level scenarios at the Ponte Garibaldi section.

Scenarios	Tide level (m)	Event 2018			
		XP		36	
		Depth (m)	Velocity (m/s)	Depth (m)	Velocity (m/s)
9	1.609	2.76	1.93	2.46	0.4
10	0.235	2.43	2.24	1.23	0.97
11	1.591	2.74	1.94	2.44	0.4
12	-0.236	2.42	2.24	1.11	1.12

Table 11 Water depth and cross-section-averaged velocity at the flood peak (XP) and along the recession limb (h36) for the extreme steady tidal level scenarios at the Ponte II Giugno section.

Scenarios	Tide level (m)	Event 2018			
		XP		36	
		Depth (m)	Velocity (m/s)	Depth (m)	Velocity (m/s)
9	1.609	2.5	1.8	2.3	0.36
10	0.235	2.06	2.18	0.99	0.83
11	1.591	2.49	1.81	2.28	0.36
12	-0.236	2.05	2.2	0.79	1.05

Table 12 Water depth and cross-section-averaged velocity at the flood peak (XP) and along the recession limb (h36) for the extreme steady tidal level scenarios at the Ponte Statale section.

Scenarios	Tide level (m)	Event 2018			
		XP		36	
		Depth (m)	Velocity (m/s)	Depth (m)	Velocity (m/s)
9	1.609	2.59	1.57	2.43	0.3
10	0.235	2.05	1.99	1.09	0.68
11	1.591	2.49	1.81	2.28	0.36
12	-0.236	2.03	2	0.79	0.94

6. Discussion

In general, the results show that the influence of the downstream boundary condition is limited during the flood peak, when the hydraulic response is mainly controlled by the upstream river forcing. Around XP, water depth and cross-section-averaged velocity show only small variations between the analysed scenarios, especially for the 2023 event, where the stronger flood wave reduces the relative effect of the downstream water level, as expected in a microtidal environment.

However, during the rising and recession stages of the hydrograph, the response becomes more sensitive to the downstream condition. Higher downstream water levels tend to increase water depth and reduce flow velocity, while lower downstream levels generally produce lower depths and higher velocities. This behaviour is evident around hour 36, where the river forcing is weaker and the effect of the tidal boundary becomes clearer.

This behaviour is consistent with previous studies on estuarine hydraulic response, where tidal effects were found to be limited near the flood peak and more relevant during the rising and recession phases. In the present work, the same approach is extended to the three selected bridge sections, allowing the spatial variation of the downstream influence along the final reach of the Misa River to be examined.

The following sections discuss the main similarities and differences between the simulations, the role of steady and unsteady downstream boundary conditions, and the influence of river–sea interaction on hydrograph propagation. Finally, the possible impact on bridge sections is evaluated using the dimensionless depth–velocity relationship and the specific hydraulic force, following the approach adopted by (Perugini et al**.,** 2026).

6.1. Role of river–sea interaction

The role of river–sea interaction was further investigated by analysing the hydraulic response at the selected bridge sections under different downstream boundary conditions. To quantitatively compare the simulations, water depth and cross-section-averaged velocity were extracted at two reference instants: the flood peak (XP) and the recession limb (h36).

As shown in Section 5.1, the influence of the downstream boundary condition is limited around the flood peak but becomes more evident during the recession phase, when larger differences in both water depth and velocity are observed. This behaviour indicates that the relative importance of tidal forcing increases as river discharge decreases. The corresponding results for the representative steady, sensitivity, and extreme steady scenarios are discussed in Sections 5.2.1–5.2.3.

6.2. Steady versus unsteady downstream conditions

Although the unsteady downstream boundary condition represents the more realistic configuration, the tidal oscillation makes the combined effect of river discharge and sea level more difficult to interpret throughout the event, especially along the recession limb. In the unsteady simulations, the downstream water level varies continuously with time, so the hydraulic response depends not only on the magnitude of the tide but also on its timing relative to the flood hydrograph.

The steady simulations, on the other hand, allow the role of each downstream water level to be isolated more clearly. By keeping the tidal level constant during the simulation, it becomes easier to identify how increasing or decreasing downstream levels affect water depth and cross-section-averaged velocity at the selected bridge sections. For this reason, the steady cases are useful for interpreting the influence of the tidal boundary condition, while the unsteady cases provide a more realistic representation of the river–sea interaction.

A representative comparison between unsteady and steady downstream boundary conditions is shown in Figure 48 and Table XX for the 2018 event at the Ponte Garibaldi section. The results indicate that both approaches produce a similar hydraulic response around the flood peak (XP), where the flow is primarily controlled by the upstream flood wave. However, clearer differences emerge during the recession phase (h36), when the influence of the downstream boundary condition becomes more significant. The steady simulation highlights more clearly the effect of the imposed downstream water level, whereas the unsteady simulation reflects the temporal variability of the tidal signal. Similar behaviour is observed at the remaining bridge sections and events, as presented in Chapter 5.

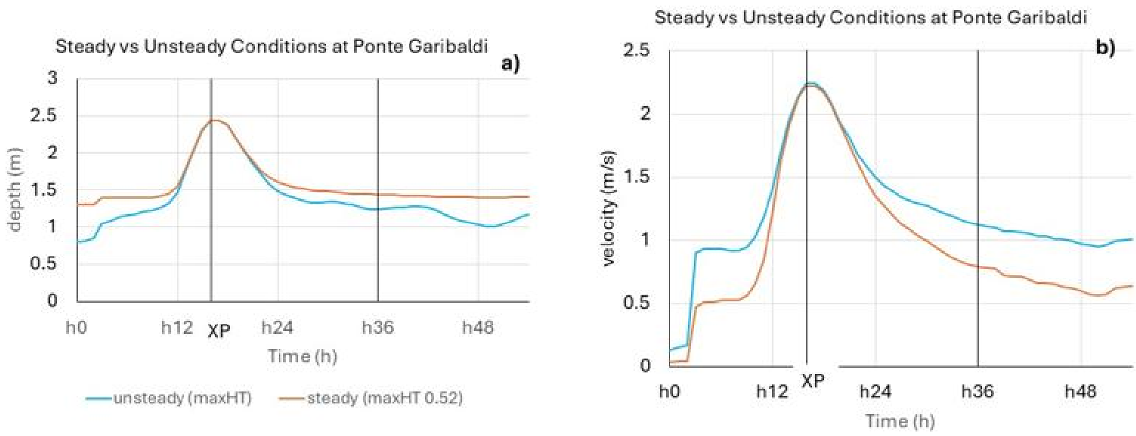

Figure 48. comparison between representative unsteady (MaxHT) and steady (MaxHT, 0.52 m) downstream boundary conditions for the 2018 event at Ponte Garibaldi. Panels (a) and (b) show water depth and cross-section-averaged velocity, respectively. Vertical lines indicate XP and h36.

Table 13. comparison between representative unsteady (MaxHT) and steady (MaxHT, 0.52 m) downstream boundary conditions for the 2018 event at Ponte Garibaldi. Panels (a) and (b) show water depth and cross-section-averaged velocity, respectively. Vertical lines indicate XP and h36.

Scenarios	Tide level (m)	Event 2018			
		XP		36	
		Depth (m)	Velocity (m/s)	Depth (m)	Velocity (m/s)
1 and 5	MaxHT	2.07	1.96	1.11	0.67
13 and 17	0.52	2.44	2.22	1.43	0.79

6.3. Impact on bridge piers

The hydraulic response at the analysed bridge sections was further investigated in order to evaluate the possible impact of the downstream boundary conditions on bridge hydraulic loading. Since the previous analyses showed that the influence of the downstream tidal forcing becomes more evident during the recession phase, the values extracted at hour 36 were used for the present assessment. The analysis was based on two complementary indicators: the dimensionless relationship between water depth and cross-section-averaged velocity, and a specific hydraulic force parameter combining momentum flux and hydrostatic pressure contributions. The assessment was carried out for the unsteady, representative steady, sensitivity, and extreme steady scenarios at the Ponte Garibaldi, Ponte II Giugno, and Ponte Statale bridge sections.

6.3.1. Dimensionless depth–velocity relationship

The dimensionless analysis was performed by normalizing the water depth and cross-section-averaged velocity of each simulation with respect to the corresponding mean tide values for each bridge section and event. The resulting relationships are reported in Figures 49 for the unsteady scenarios, the representative steady and sensitivity scenarios, and the extreme steady scenarios, respectively.

h/h_0 and V/V_0 represent the normalized water depth and normalized cross-section-averaged velocity, respectively, where h_0 and v_0 correspond to the values obtained under the mean tide condition.

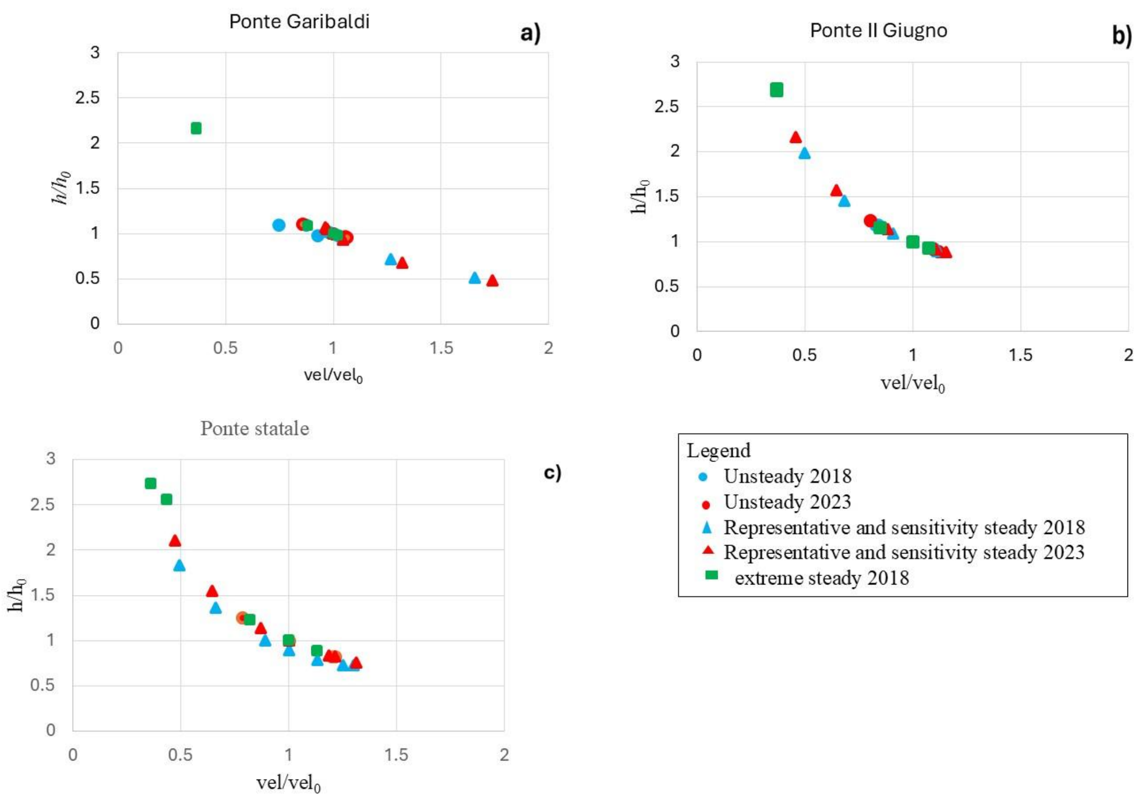

Figure 49. Dimensionless depth–velocity relationship at h36 for the analysed downstream boundary conditions: (a) Ponte Garibaldi, (b) Ponte II Giugno, and (c) Ponte Statale. Unsteady scenarios, representative steady and sensitivity scenarios, and extreme steady scenarios are shown together. Water depth and cross-section-averaged velocity were normalized with respect to the corresponding mean tide condition for each bridge section and event.

Figure 49 shows a consistent inverse relationship between normalized water depth and normalized velocity under all analysed downstream boundary conditions. The unsteady simulations remain relatively concentrated around the reference condition ((h/h_0 = 1), (V/V_0 = 1)), indicating limited variations induced by downstream tidal oscillations. In contrast, the representative steady, sensitivity, and extreme steady scenarios produce progressively larger deviations from the unitary state. Higher downstream water levels are generally associated with increased relative depths and reduced relative velocities, whereas lower downstream levels produce the opposite response.

At Ponte Garibaldi (Figure 49a), most of the dimensionless points remain clustered around the reference condition, indicating a relatively limited influence of the downstream boundary condition. At Ponte II Giugno (Figure 49b), a wider spread of the points is observed, reflecting a stronger hydraulic response to variations in downstream water level. The largest deviations occur at Ponte Statale (Figure 49c), where both the increase in normalized depth and the reduction in normalized velocity become more pronounced, particularly for the extreme steady scenarios.

In general, the dimensionless analysis confirms a consistent inverse relationship between normalized water depth and normalized velocity under all the analysed downstream boundary conditions. While the unsteady simulations remain relatively concentrated around the reference condition, the representative steady, sensitivity, and extreme steady scenarios produce progressively larger deviations from the unitary state. In all cases, higher downstream tidal levels are associated with increased relative depths and reduced relative velocities, whereas lower downstream levels produce the opposite response. Furthermore, the hydraulic response becomes progressively more pronounced from Ponte Garibaldi to Ponte Statale, highlighting the increasing influence of river–sea interaction toward the downstream reach of the study area.

6.3.2. Specific hydraulic force parameter

To understand the combined action of water depth and flow velocity, a specific hydrodynamic force parameter was estimated, including both momentum flux and hydrostatic pressure contributions. Following Perugini et al. (2026), this parameter was plotted against the tidal level imposed at the downstream boundary and was defined as:

$$S = V^2 D + \frac{1}{2} g D^2$$

where V is the cross-section-averaged velocity, D is the water depth, and $g$is the gravitational acceleration.

The parameter S was used as a hydraulic indicator to compare the possible impact of the different downstream boundary conditions at the bridge sections. Positive tidal levels increase the hydraulic force parameter mainly through the increase in water depth, whereas negative tidal levels tend to reduce the overall force. Therefore, the analysis provides a useful comparison of the hydraulic loading conditions around the bridge piers, without representing a full structural force assessment.

The specific hydrodynamic force analysis was carried out only for the representative steady tidal levels, sensitivity scenarios, and extreme steady scenarios, for which a fixed downstream boundary level is imposed during the simulation.

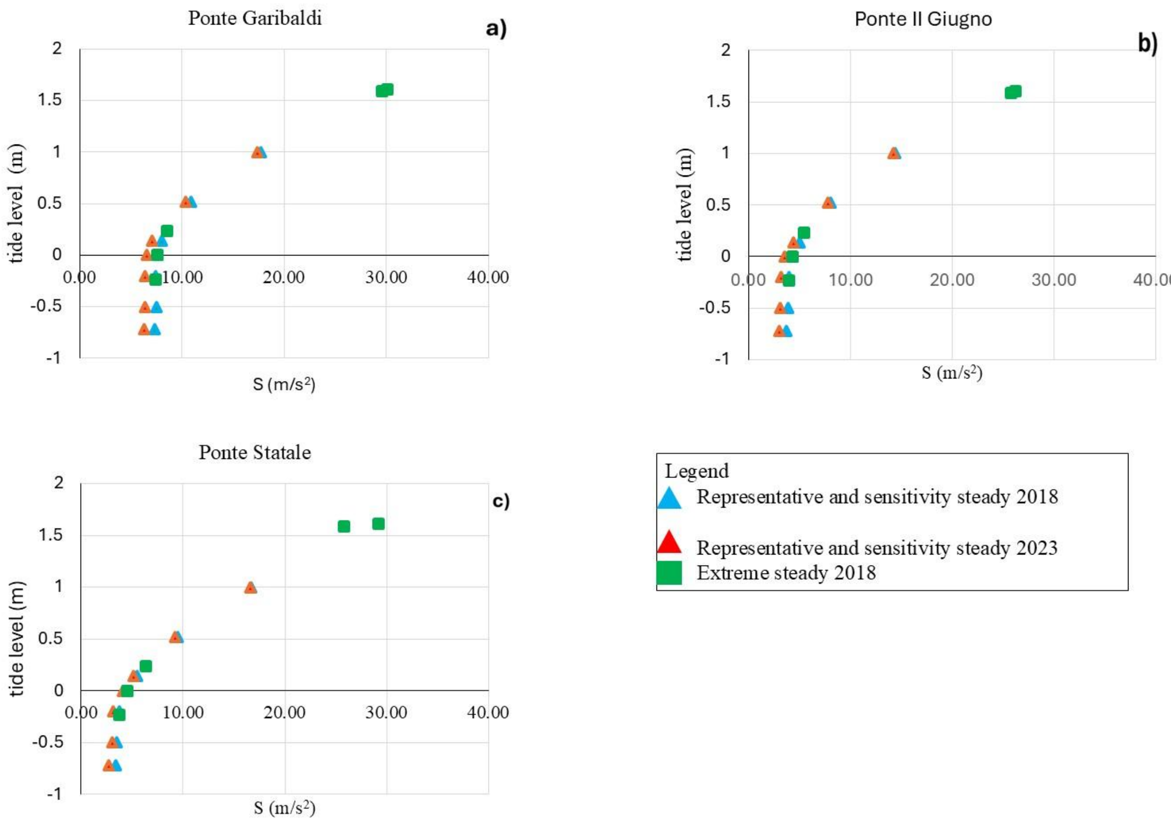

Figure 50.. Specific hydrodynamic force parameter evaluated at h36 for the representative steady tidal levels, sensitivity scenarios, and extreme steady scenarios: (a) Ponte Garibaldi, (b) Ponte II Giugno, and (c) Ponte Statale.

The results are reported in Figure 50. The specific hydrodynamic force parameter increases progressively with increasing downstream tidal level at all the analysed bridge sections. The results indicate that positive downstream levels generate larger hydraulic loading conditions, whereas negative levels are associated with lower force values despite the corresponding increase in velocity. This behaviour highlights the dominant role of the hydrostatic pressure contribution under elevated water levels, where the increase in water depth compensates for the simultaneous reduction in cross-section-averaged velocity.

At Ponte Garibaldi (Figure 50a) and Ponte II Giugno (Figure 50b), the relationship between imposed downstream level and hydraulic force parameter is regular and progressively increasing for both the 2018 and 2023 events. The same tendency becomes evident at Ponte Statale (Figure 50c), where the increase in force values associated with high downstream levels confirms the stronger influence of river–sea interaction approaching the river mouth. These results suggest that, although high-tide conditions generally reduce flow velocities, the simultaneous increase in water depth produces larger overall hydraulic loading conditions around the bridge sections. Conversely, low-tide conditions are characterized by reduced force values but relatively higher velocities, which may favour erosive processes and local scour development around bridge foundations.

The extreme steady scenarios show the largest variation among all the analysed downstream boundary conditions. At all bridge sections, the highest downstream tidal levels (approximately 1.6 m) produce a substantial increase in the hydraulic loading indicator, whereas the negative and near-zero levels are associated with significantly lower force values. This behaviour confirms that extreme high-tide conditions strongly amplify the hydrostatic pressure contribution through the increase in water depth. Consequently, the combined hydraulic loading acting on the analysed bridge sections becomes considerably higher under elevated downstream water levels.

At Ponte Garibaldi, Ponte II Giugno, and Ponte Statale, the increase in the force parameter between low- and high-tide conditions is particularly pronounced, with the highest tidal levels producing force values several times larger than those observed under negative downstream levels. These results indicate that extreme downstream tidal levels may substantially modify the hydraulic response during moderate-flow conditions, increasing the potential loading conditions around bridge sections and highlighting the importance of considering river–sea interaction effects in estuarine hydraulic assessments.

Overall, the obtained results demonstrate that downstream tidal forcing plays a relevant role in the hydraulic response of the lower Misa River, particularly during moderate-flow conditions and in the downstream bridge sections. The combined effects of water depth increase and flow velocity variation influence the hydraulic loading conditions associated with the analysed bridge sections, confirming the importance of considering river–sea interaction in estuarine hydraulic modelling.

.

7. Conclusion

The results of this thesis show that the downstream boundary condition plays an important role in the hydraulic response of the final reach of the Misa River, although its influence depends strongly on the stage of the flood event and on the relative intensity of river and tidal forcing. The analysis was carried out using a one-dimensional HEC-RAS model, in which upstream water-level hydrographs recorded at the Bettolelle hydrometric station and obtained through the SIRMIP database were combined with downstream tidal levels derived from the Ancona tide gauge managed by ISPRA. The upstream water levels were referred to the model vertical datum by adding the Bettolelle hydrometer-zero elevation of 19.18 m above mean sea level, while the downstream tidal series were corrected using an offset of +0.078 m to ensure consistency with the same reference system. The 2018 event, characterized by a peak discharge of approximately 158 m^3/s, and the 2023 event, characterized by a peak discharge of approximately 300 m^3/s, were combined with unsteady tidal oscillations, representative steady tidal levels, sensitivity scenarios, and additional extreme steady water-level conditions, for a total of 26 numerical simulations. The results indicate that, during the flood peak identified as XP, the main role in relation to water depth and cross-section-averaged velocity is played by the upstream river forcing, while the contribution of the downstream tidal forcing remains limited, as expected in a microtidal environment. This behaviour is particularly evident for the 2023 event, where the stronger upstream flood wave reduces the relative influence of the downstream boundary condition. Conversely, during moderate-flow conditions, especially around h36 along the recession limb, the effect of the downstream water level becomes much clearer. Higher downstream levels tend to maintain larger water depths and lower velocities, while lower downstream levels produce smaller depths and higher velocities. Under the representative steady and sensitivity scenarios, the largest response was observed at Ponte Statale, where water-depth variations reached about 1.10 m for the 2018 event and about 1.17 m for the 2023 event, while velocity variations reached approximately 0.67 m/s and 0.59 m/s, respectively. Under the extreme steady conditions, the response was even stronger: at h36, water-depth variations reached approximately 1.35 m at Ponte Garibaldi, 1.51 m at Ponte II Giugno, and 1.64 m at Ponte Statale, with corresponding velocity variations of approximately 0.72 m/s, 0.69 m/s, and 0.64 m/s.

These results confirm that, even in microtidal areas, the combined effects of river and tidal forcing should be carefully considered. Although all cases are characterized by small differences during the flood peak and in the hours close to the peak, clear differences appear during the recession phase, when the relative role of tidal action increases. The comparison among Ponte Garibaldi, Ponte II Giugno, and Ponte Statale showed that the influence of the downstream boundary condition is not uniform along the analysed reach, becoming more evident toward the downstream part of the river, especially in the velocity response. This spatial behaviour confirms the increasing relevance of river–sea interaction approaching the river mouth. From an engineering point of view, the results also show that high- and low-tide conditions may lead to different hydraulic implications. During high-tide conditions, critical water levels can be reached earlier or persist beyond the peak flow passage, creating prolonged adverse conditions and making the assessment of hydraulic clearance at bridges particularly important. At the same time, high tide tends to reduce flow velocities, thereby decreasing sediment transport and the risk of scour at the base of structures. Conversely, during low tide, although water levels slightly decrease, flow velocities are higher than they would be if tidal effects were neglected. Increased velocities can enhance sediment transport and erosion, raising the potential risk of scour around bridge foundations. If this occurs during the rising limb or near the peak of a flood, it may not only advance but also amplify the potential for bridge-bed erosion; after the flood passage, low-tide conditions can sustain elevated velocities for a longer duration, prolonging erosive action and delaying sediment deposition and the refilling of scour holes. The dimensionless depth–velocity relationship and the specific hydrodynamic force parameter confirmed this interpretation: higher downstream levels increase the hydraulic loading indicator mainly through the increase in water depth and hydrostatic contribution, while lower downstream levels are associated with relatively higher velocities and therefore with a greater potential for erosion processes.

Hence, moderate-flow conditions are critical and may have significant implications for sediment transport and bridge stability in the Misa River estuary. In this thesis, the analysis was conducted at the three selected bridge sections along the downstream urban reach, providing a broader assessment of the spatial variability of the hydraulic response. The work focused on hydraulic modelling and therefore provides an assessment of flow conditions under different tidal and riverine influences, without directly simulating sediment transport, bed evolution, or local scour around bridge piers and abutments. Nevertheless, the results show that even a relatively small increase in the tidal level at the downstream boundary may produce a relevant increase in the dynamic action on structures and infrastructures affected by river–sea flows, with possible implications for erosion, scouring processes, and bridge stability. Further studies are therefore required to investigate the morphodynamic behaviour of the river. Future research should consider coupled hydro-morphodynamic three-dimensional modelling, parametric scenario analyses, the identification of relevant hydraulic and morphodynamic indices, and a comprehensive evaluation of their effects on sediment transport and bridge safety. Such developments would allow the interactions between hydrodynamics, sediment dynamics, and infrastructure stability to be better understood, supporting more effective management and design strategies for microtidal estuarine systems.

8. References

Baldoni A., Perugini E., Soldini L., Calantoni J., Brocchini M., 2021. *Long-term evolution of an inner bar at the mouth of a microtidal river*. Estuarine, Coastal and Shelf Science.

Bevacqua E., Maraun D., Vousdoukas M. I., Voukouvalas E., Vrac M., Mentaschi L., Widmann M., 2019. *Higher probability of compound flooding from precipitation and storm surge in Europe under anthropogenic climate change*. Science Advances.

Brocchini M., Calantoni J., Postacchini M., Sheremet A., Staples T., Smith J., Reed A., Edwards F., Braithwaite III E., Lorenzoni C., Russo A., Corvaro S., Mancinelli A., Soldini L., 2017. *Comparison between the wintertime and summertime dynamics of the Misa River estuary*. Marine Geology.

Camus P., Haigh I. D., Nasr A., Wahl T., Darby S. E., Nicholls R. J., 2021. *Regional analysis of multivariate compound flooding potential: sensitivity analysis and spatial patterns*. Natural Hazards and Earth System Sciences.

Carnacina I., Pagliara S., Leonardi N., 2019. *Bridge pier scour under pressure flow conditions*. River Research and Applications.

Gaiolini M., Colombani N., Mastrocicco M., Postacchini M., 2023. *Seawater intrusion assessment along the Volturno River (Italy) via numerical modeling and spectral analysis*. Journal of Hydrology.

Hydrologic Engineering Center, 2024. *HEC-RAS River Analysis System: Hydraulic Reference Manual, Version 6.6*. U.S. Army Corps of Engineers, Davis, California.

Hydrologic Engineering Center, 2024. *HEC-RAS River Analysis System: User's Manual, Version 6.6*. U.S. Army Corps of Engineers, Davis, California.

ISPRA, n.d. *Servizio Mareografico Nazionale: Rete Mareografica Nazionale*. Istituto Superiore per la Protezione e la Ricerca Ambientale.

Lu Z., Gao Z., Huang J., 2004. *Local scour around large bridge piers in an estuary*. Proceedings of the 9th International Symposium on River Sedimentation, IAHR, Yichang, China.

Melito L., Postacchini M., Sheremet A., Calantoni J., Zitti G., Darvini G., Penna P., Brocchini M., 2020. *Hydrodynamics at a microtidal inlet: analysis of propagation of the main wave components*. Estuarine, Coastal and Shelf Science.

Perugini E., Postacchini M., Getachew Y. A., Darvini G., Melito L., Brocchini M., 2026. *Impact of river-sea interactions on bridges at a microtidal estuary: moderate sea forcing*. River Flow 2026 – 13th International Conference on Fluvial Hydraulics, IAHR.

Postacchini M., Manning A. J., Calantoni J., Smith J. P., Brocchini M., 2023. *A storm driven turbidity maximum in a microtidal estuary*. Estuarine, Coastal and Shelf Science.

Postacchini M., Zitti G., Perugini E., Rossetti R., Brocchini M., 2025. *Application of hydrokinetic turbines in microtidal rivers: the Misa River test site*. Renewable Energy.

Pritchard D. W., 1967. *What is an estuary: physical viewpoint*. In: Lauff G. H. (Ed.), Estuaries. American Association for the Advancement of Science.

Regione Marche – Autorità di Bacino Regionale, 2016. *Piano di Assetto Idrogeologico del bacino del fiume Misa*. Regione Marche.

SIRMIP, n.d. *Sistema Informativo Regionale Meteo-Idro-Pluviometrico*. Centro Funzionale Multirischi, Protezione Civile Regione Marche.

U.S. Army Corps of Engineers, 2020. *HEC-RAS River Analysis System: Hydraulic Reference Manual*. Hydrologic Engineering Center, Davis, California.

Valle-Levinson A., 2011. *Classification of estuarine circulation*. Treatise on Estuarine and Coastal Science, Academic Press.

9. Acknowledgements

I would like to express my sincere gratitude to my supervisor, Professor Matteo Postacchini, for his guidance, support, and valuable advice throughout the development of this thesis. His expertise and constructive feedback were fundamental to the completion of this work. I am also deeply grateful to Professor Eleonora Perugini for her continuous support, patience, and technical assistance. Her suggestions, comments, and availability greatly contributed to improving both the quality of the analyses and the presentation of the results. I would like to thank the Department of Civil, Building and Architectural Engineering of Università Politecnica delle Marche for providing the academic environment and resources necessary for this research.

A special thanks goes to my family for their constant encouragement, understanding, and unconditional support throughout my studies. Their confidence in me has always been a source of motivation during both the most challenging and rewarding moments of this journey. Finally, I would like to thank all the colleagues, friends, and researchers who, directly or indirectly, contributed to this work and to my academic experience in Italy. This thesis represents the conclusion of an important stage of my personal and professional growth, and I am grateful to everyone who has been part of this journey.